ABSTRACT

Title of Document: ARCING FAILURE OF ROHS COMPLIANT ELECTROMAGNETIC RELAYS

Robert Donald Boettcher, Master of Science, 2012

Directed By: Associate Professor F. Patrick McCluskey
Department of Mechanical Engineering

Electronic relay contacts have traditionally been made of materials, primarily Ag/CdO, which are resistant to welding under short, high power pulses. However, since 2006, RoHS prohibits the use of cadmium in electronics, driving the elimination of Ag/CdO and its replacement with Ag/SnO_2. The reliability of relays made with Ag/SnO_2 contacts has been shown to be vendor specific. This thesis focuses on developing an understanding of the metallurgical and design factors that vary by manufacturer and their effect on welding susceptibility of Ag/SnO_2 electromagnetic relay contacts and other related relay failure mechanisms. In addition, it aims to predict a safe operating area of power and energy over which specific relay contacts will not weld under high power DC conditions.

Relays from various manufacturers were subjected to capacitor discharge pulses of 250 V at 10-80 μF to characterize relay reliability. Failure analysis was then conducted on the welded contacts using scanning electron microscopy (SEM) and wavelength-dispersive spectroscopy (WDS) in order to address material properties and design

variations that affect the welding susceptibility of relays. The incidence and extent of degradation is correlated to material characteristics including contact composition, oxide content, hardness, contact geometry, and surface roughness using a physics of failure approach. The relays with a higher percent content of indium oxide exhibited a greater reliability than those without. Both power and energy were then varied to further investigate the one cycle to failure boundary region and a failure map is presented.

ARCING FAILURE OF ROHS COMPLIANT ELECTROMAGNETIC RELAYS

By

Robert Donald Boettcher

Thesis submitted to the Faculty of Graduate School of the
University of Maryland, College Park in partial fulfillment
Of requirements for the degree of
Master of Science
2012

Advisory Committee:

Dr. F. Patrick McCluskey, Chair, Associate Professor of Mechanical Engineering
Dr. Michael Azarian, Assistant Research Scientist of Mechanical Engineering
Dr. Hugh Bruck, Professor of Mechanical Engineering & Director of Graduate Studies

Dedication

To my parents, Brian and Janet.

Acknowledgements

I would first like to thank Dr. McCluskey for accepting me into his research group and providing me the means to finish my Master's studies and research in one year. Without your keen sense of timing I may have been without funding or without a thesis while trying to pursue a Master's as part of the BS/MS program, so your willingness to take me into the group and your mentorship along the way has been greatly appreciated.

I would also like to say thank you to all of the members of Dr. McCluskey's research group for all that they have done. You have been there to provide advice, support, and friendship over the past year, and I will always remember that as we move on to new things. Hannes, thanks for all the "office hours" and political discussions – we'll see which was more helpful as time goes on. Also thanks to Rayhoo for helping with the countless relays that needed to be soldered. Lastly, thanks to Chandra, Ali, Thomas and Shahin for your feedback as well.

Many thanks to CALCE as well for the use of their facilities and equipment.

Finally, I would like to thank my loving parents that have made everything up until now possible. Through your support through undergrad I was able to focus on my studies full time without having to worry about a second job to support myself, so I thank you for that. Also, many thanks to my two sisters Vicky and Kathy for being there and my brother-in-law Mike for being the closest thing to a brother I have ever had.

Table of Contents

Dedication ii
Acknowledgements iii
Table of Contents iv
Table of Figures vi
Table of Tables vii
Chapter 1: Introduction 1
1.1 Electromagnetic Relay Operation 2
1.2 Types of Relays 3
1.3 Contact Materials 7
1.4 Relay Failure Mechanisms 9
1.5 Research Motivation 13
Chapter 2: Literature Review 15
2.1 Arc Erosion Degradation 15
2.1.1 Arc Erosion Physics 16
2.1.2 Arc Erosion Modeling 17
2.2 Relay Dynamics 18
2.2.1 Bounce Duration and its Effect on Welding 19
2.2.2 Make and Break Operation Welding Mechanisms 19
2.3 Electrical Contact Resistance: Fundamental Principles 21
2.4 Silver/ Tin Oxide as a Replacement to Ag/CdO 23
2.5 Electrical Testing 26
2.6 Experimental Selection 27
Chapter 3: Preliminary Testing in the Standby Power Supply 28
3.1 SPS Preparation 28
3.2 Experimental Setup 32
3.3 High Speed Video Clips 34
3.3.1 Relay 102 switching from DC to AC, or NO to NC contact position. 34
3.3.2 Relay 102 switching from AC to DC, or NC to NO contact position. 35
3.4 Discussion of Results 36
Chapter 4: Automated Test Circuit Setup and Sample Preparation 38
4.1 Test Circuit Design 38
4.2 Circuit Construction 39
4.2.1 Ribwound Resistors 40
4.2.2 Arduino UNO Microcontroller 40
4.2.3 Failure Sensing Method 41
4.2.4 Power Supplies and Curve Characterization 42
4.3 Relay Sample Preparation 44
4.4 Conclusion 45
Chapter 5: Comparison of Relay Reliability 46
5.1 Constant Power Test 46
5.2 Constant Power Results 46
5.3 Discussion and Analysis of Results 49
5.4 Conclusion 53
Chapter 6: Physics of Failure Analysis of Manufacturer Dependent Relay Reliability 54
6.1 Relays Investigated in This Study 54

6.2 Contact Size 55
6.3 Contact Geometry 56
6.4 Contact Area 60
6.5 Contact Resistance 62
6.6 Contact Material 63
6.7 Contact and Spring Hardness 67
6.8 Failure Analysis 68
6.8.1 10μF 68
6.8.2 50μF 71
6.8.3 70μF 72
6.8.4 EPMA Line Scan Across Weld Interface 74
6.9 Correlations to Welding 75
6.10 Conclusion 77
Chapter 7: One Cycle Weld Failure Interface 79
7.1 Test Methodology 79
7.2 Test Results 82
7.2.1 250V Test –1.5MW Power 83
7.2.2 350V – 3.0MW 84
7.2.3 450V – 5MW 84
7.2.4 100V 0.11Ω – 1.7kW 85
7.2.5 Constant Energy 86
7.2.6 Power-Law Model Comparison 88
7.3 Conclusion 89
Chapter 8: Conclusions and Contributions 91
8.1 Conclusions 91
8.2 Contributions 94
8.3 Future Works 94
Appendix A: Automated Test Circuit Arduino C++ Code 96
Appendix B: RC Circuit Theory 98
Appendix C: MATLAB Code for Contact Radius of Curvature Image Analysis 99
Appendix D: MATLAB Code for Contact Area Image Analysis 99
Appendix E: XRD Material Analysis Raw Data 100
Appendix F: One Cycle Weld Interface Test Results 101
References 102

Table of Figures

Figure 1: Electromagnetic Relay Parts Layout. 2
Figure 2: Relay Contact Positions. 3
Figure 3: (a) Relay with Contacts; (b) Relay without contacts; (c) Hybrid relay 4
Figure 4: Hinged Relay Schematic 4
Figure 5: A plunger relay schematic 5
Figure 6: A reed relay schematic 5
Figure 7: Circuit diagram of relay poles and throws. 6
Figure 8: A chart showing desirable relay properties 7
Figure 9: (a) Tin whiskers inside on insulator guide hole; (b) Whisker growth between contact support arms 11
Figure 10: (a) Arc erosion process; (b) High speed sequence of arc formation 12
Figure 11: (a) A pip and crater formation; (b) Contact material loss due to arc erosion 12
Figure 12: Reference Frame for Relay Contact Theory 21
Figure 13: Cross-section after deformation. 22
Figure 14: Weld break force vs. oxide % in silver tin indium oxide contacts tested for 16,000 operations of lamp load. 24
Figure 15: Weld break force quartiles of different Ag-SnO_2 compositions 25
Figure 16: Underside of PCB when first opening SPS. 28
Figure 17: Removal of top PCB. 29
Figure 18: PCB with relays and power electronics. 29
Figure 19: Soldering the pin connector to the additional wire lengths. 30
Figure 20: Fully reconnected SPS. 31
Figure 21: Opened relays on PCB. 32
Figure 22: High speed camera setup. 33
Figure 23: Relay 102 switching from NO to NC. 34
Figure 24: Relay 102 switching from NC to NO. 36
Figure 25: Automated relay test circuit. 38
Figure 26: Automated test circuit. 40
Figure 27: Arduino UNO. 41
Figure 28: Failure sensing circuit. 42
Figure 29: Low voltage power supplies and DMM. 43
Figure 30: High voltage power supply and oscilloscope. 43
Figure 31: Relay pin layout. 44
Figure 32: Constant Power Test - Capacitance vs. Average CTF. 47
Figure 33: CTF vs. Energy semi-log scale. 49
Figure 34: CTF vs. Energy log-log scale. 49
Figure 35: Power-Law vs. Exponential Comparison. 51
Figure 36: Relay A, B, and C from left to right. 54
Figure 37: Relay contacts A (left), B (middle), and C (right). 55
Figure 38: Relay A main contact where NO is the top side and NC is the bottom side. 57
Figure 39: Relay A secondary contact. 57
Figure 40: Relay B main contact with NO side on top and NC on bottom. 58
Figure 41: Relay B secondary contact. 58
Figure 42: Relay C main contact with the NO side on top and NC on bottom. 59
Figure 43: Relay C secondary contact. 59
Figure 44: Pressure film results. 60
Figure 45: SEM image of Cu / AgSnO2 interface and EDS analysis point in relay C. 63
Figure 46: Ka peaks in EDS analysis of relay C. 64
Figure 47: EPMA used in material analysis. 65
Figure 48: New/unused contact images. 68
Figure 49: Main and secondary contact after welding. 69

Figure 50: Weld region and splash area. *70*
Figure 51: Overview of weld section. *71*
Figure 52: Close up of weld at 20X. *72*
Figure 53: Contact and weld overview. *72*
Figure 54: Weld interface at 20X and 100X. *73*
Figure 55: Test points used in one cycle to failure testing. *81*
Figure 56: Test results. *82*
Figure 57: CTF vs. Energy for 250V, 1.5MW. *83*
Figure 58: CTF vs. Energy for 350V, 3.0 MW. *84*
Figure 59: CTF vs. Energy for 450V, 5.0MW. *85*
Figure 60: CTF vs. Energy for 100V, 0.11Ω, 1.7kW. *86*
Figure 62: Constant energy CTF vs. Power. *87*

Table of Tables

Table 1: Characteristics of common contact materials *8*
Table 2: Contact failure modes *9*
Table 3: Physical effects on contact reliability *9*
Table 4: Inrush current by load type *13*
Table 5: Material Components *25*
Table 6: Constant Power Test Results. *47*
Table 7: Test Parameter Power and Energy Levels. *48*
Table 8: Power and Exponential Law Constants. *52*
Table 9: Contact diameter. *56*
Table 10: Contact radius of curvature. *56*
Table 11: Results from MATLAB code. *61*
Table 12: Contact radius and area. *62*
Table 13: Contact resistance. *62*
Table 14: Element type and % weight from EDS analyis. *63*
Table 15: XRD results in phase weight %. *65*
Table 16: WDS average weight %. *66*
Table 17: Contact and spring hardness. *67*
Table 18: EPMA line scan of relay A weld region. *74*
Table 19: EPMA line scan of relay B weld region. *75*
Table 20: EPMA line scan of relay C weld region. *75*
Table 21: Test point parameters used in one cycle failure testing. *81*

Chapter 1: Introduction

Electromagnetic relays (EMR) are used in a variety of applications where a low voltage input signal is used to control a much higher power circuit. They play an important role in communication switching as well as in automotive, aerospace, and industry automation where reliability of the relay is critical.

In 2006, the Restriction of Hazardous Substances Directive (RoHS) eliminated the use of cadmium in electromagnetic relays – cadmium had been the preferred material for many contact applications because of its resistance to welding at high power levels. In place of Cd, the industry adopted silver tin oxide and other cadmium free contacts for electrical power switching devices [1]. Silver-tin oxide based contact materials can have different compositions, impurities, levels of porosity, grain structures, and surface roughness, and these influence contact properties such as arc erosion resistance, welding resistance, arc mobility, and contact resistance. At the same time, the performance of the contacts is also dependent on numerous factors other than the contact material itself, including opening speed, closing speed, contact pressure, and contact bounce [2]. Since these design parameters vary between manufacturers, the performance and reliability of relay contacts is expected to differ between manufacturers. The reliability in relays used in power electronics is critical when used in such applications as system backup or control systems, and this has led to the focus of this work: relay susceptibility to welding under high power conditions. The remainder of this section will provide the necessary background information on relays while giving an overview of relay operation, types of relays, contact materials in use, failure mechanisms, and the research motivation.

1.1 Electromagnetic Relay Operation

An electromagnetic relay is an electrically operated mechanical switch that uses a low voltage input signal to control a much higher power circuit. For this reason, relays are used in such applications as starting a car, opening and closing circuit breakers in power transmission lines, and switching to a standby power supply.

Relays consist of an electromagnetic coil (inductor), a spring, a metal plate, and switch contacts as seen in Figure 1. In order to switch, a low power circuit, typically 12 VDC, energizes an inductor coil that creates a magnetic field. The magnetic field attracts the metal plate towards the magnetic coil and overcomes the spring force, thus closing the circuit between the contacts on the side that is normally open. When the control signal falls below the lower threshold voltage, the spring force overcomes the now weaker magnetic force and the contact switch returns to its position on the side that is normally closed.

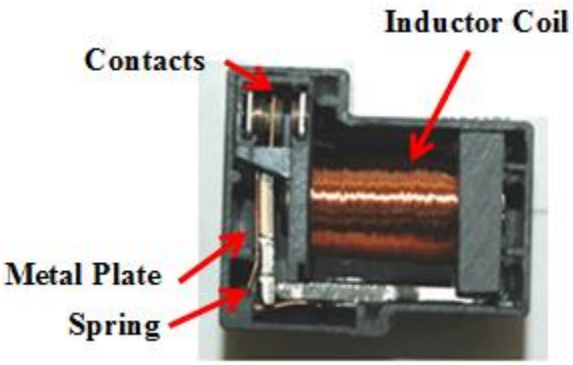

Figure 1: Electromagnetic Relay Parts Layout.

An explanation of the normally closed and normally open contact positions in a single pole double throw (SPDT) relay can be seen in Figure 2 where the top represents the

normally closed side which is in contact when the coil is de-energized, and the bottom contact is normally open. The primary contact seen in the middle has two sides and moves to the normally open side when the coil is energized.

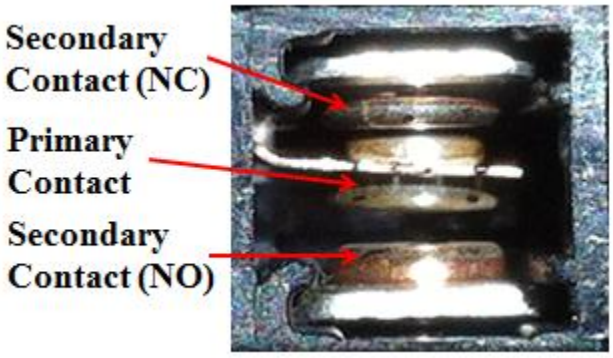

Figure 2: Relay Contact Positions.

1.2 Types of Relays

There are many types of relays that fit a variety of applications. The three main types are relays with contacts, relays without contacts, and hybrid relays. As the name indicates, a relay with contacts uses an electromagnetic operation to mechanically open and close the contacts (Figure 3a). Relays without contacts, or solid state relays (SSR), do not have moving mechanical parts, but are instead comprised of triacs, resistors, or semiconductor devices (Figure 3b). Last is the hybrid relay which combines the two aforementioned types (Figure 3c)**.** This paper will focus on the electromechanical relay (relay with contacts) since the other two types behave like semiconductor devices and are outside the scope of this work.

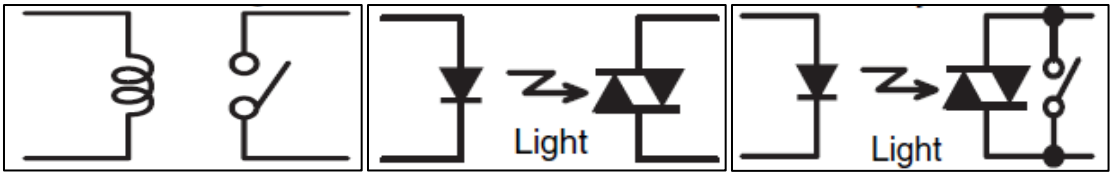

Figure 3: (a) Relay with Contacts; (b) Relay without contacts; (c) Hybrid relay [3].

Within electromechanical relays, there are three main types: hinged relays, plunger relays, and reed relays. There are also other types that involve permanent magnets; however, they are less common than the traditional hinged relay. A hinged relay operates by an armature pivoting about a fulcrum. The electromagnet attracts the armature and directly opens and closes a contact. This type of relay is the most common in use today as seen in Figure 1 & Figure 4.

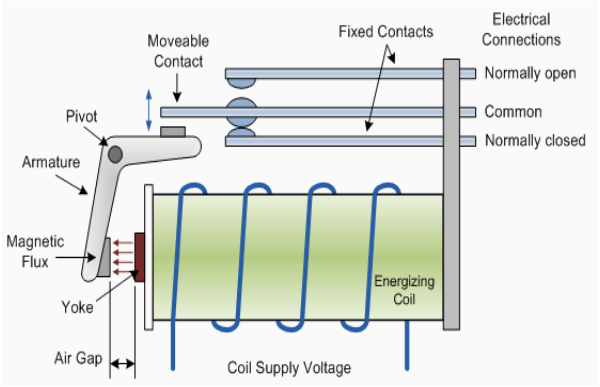

Figure 4: Hinged Relay Schematic [4].

A plunger relay uses the plunger-shaped electromagnet as the armature section to open and close the contacts as shown in Figure 5. When the coil is energized, it pulls on the metal rod and the shorting bar attached to the end of the plunger which closes the contacts. This type of relay has a much greater travel distance between contacts, and the contacts are typically much larger, allowing plunger relays to be used with higher voltages and currents.

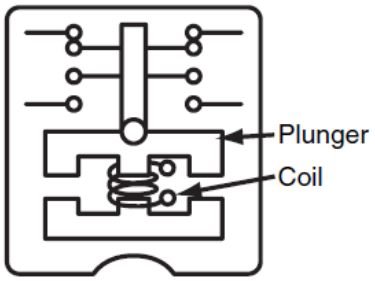

Figure 5: A plunger relay schematic [3].

Reed relays (Figure 6) are the third typical mechanical relay. They consist of a pair of thin metal strips (reeds) that are hermetically sealed in a glass tube. A magnetic coil surrounds the tube and when activated causes the reeds to attract each other and close the contacts. When the coil is de-energized, the spring tension from the reed separates the contacts. Reed relays are no longer used by the telephone companies for switching, but they are still used for test equipment and electronic instrumentation due to their fast switching characteristics, extended life (to 10^9 operations), and their hermetic seal [5]. Because the contacts are hermetically sealed, they can switch signals as low as femtoamps and nanovolts. Other electromechanical relays cannot switch such low signals because they are not hermetically sealed and a polymer film builds up on the contacts which requires sufficient voltage to break through before conduction can take place.

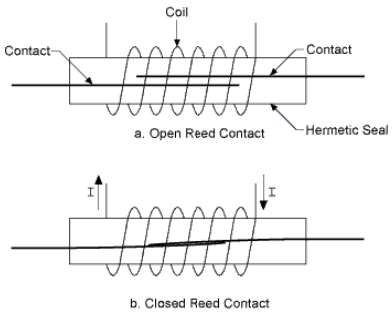

Figure 6: A reed relay schematic [6].

Within all types of relays, there are multiple classifications: single pole single throw (SPST), single pole double throw (SPDT), double pole single throw (DPST), and double pole double throw (DPDT) (Figure 7). A relay will switch one or more poles, and each pole's contacts can be thrown by energizing the coil. A normally-open (NO) contact is open when the coil is not energized, and closes when the coil is energized. Vice versa, a normally-closed (NC) contact is disconnected when the coil is energized. The nomenclature of poles and throw can be seen in Figure 7 and contact classification is shown previously in Figure 2.

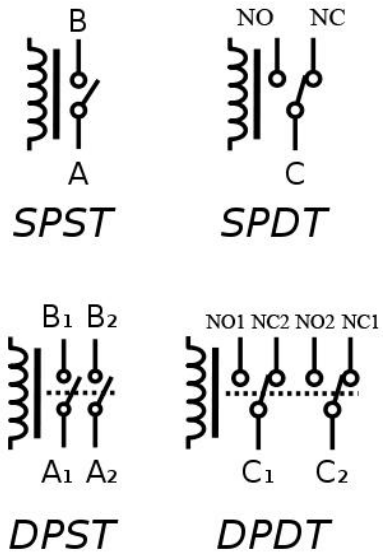

Figure 7: Circuit diagram of relay poles and throws [7].

The relays studied in this project are single pole double throw (SPDT) hinged-type relays as seen in Figure 1. While the research on the contact button material composition and geometry may be applied to other relay types, the other relays are considered outside the scope of this project.

1.3 Contact Materials

Contact material has a major influence on the performance of a relay, affecting maximum inrush current, maximum switching current, contact resistance, contact reliability and electrical life. The selection of poor contact materials can lead to increased arc erosion, increased contact resistance, susceptibility to contact welding, and increased bounce time.

The properties required by contact material for the switching phase are [8]:

- Elasticity/softness to absorb kinetic energy to reduce bouncing
- High thermal conductivity to maintain a low temperature at the contact surface
- High melting temperature to avoid material migration, evaporation, sputtering, and welding

More general contact material property requirements can be seen below in Figure 8.

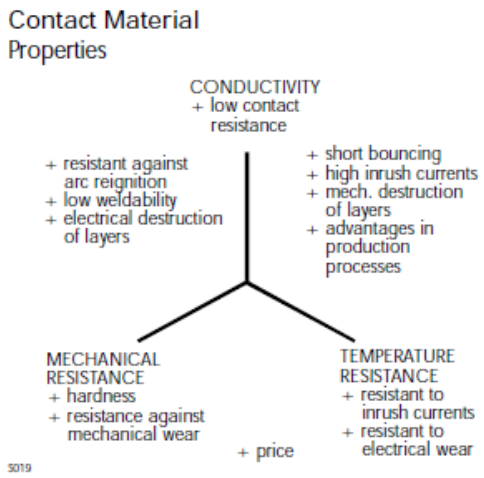

Figure 8: A chart showing desirable relay properties [8].

The most common material used in relay contacts is silver due to its high electrical conductivity and thermal conductivity; however, by itself it is susceptible to contact welding. For this reason, silver alloys and silver-ceramic composites dominate the relay industry today. A table showing common contact materials and their properties is shown below in Table 1. Silver Cadmium Oxide is not shown in the table because it is being phased out by RoHS, but it has good wear resistance, arc extinguishing properties, and has very little tendency to weld. Silver tin oxide is the most popular replacement for AgCdO, since RoHS took effect in 2006, because of its superior welding resistance.

Table 1: Characteristics of common contact materials [9].

Contact Material	Ag (silver)	Electrical conductivity and thermal conductivity are the highest of all metals. Exhibits low contact resistance, is inexpensive and widely used. A disadvantage is it easily develops a sulfide film in a sulfide atmosphere. Care is required at low voltage and low current levels.
	$AgSnO_2$ (silver-tin)	Exhibits superior welding resistance characteristics equal or better than AgCdO. Like silver, it easily develops a sulfide film in a sulfide atmosphere.
	AgW (silver-tungsten)	Hardness and melting point are high, arc resistance is excellent, and it is highly resistant to material transfer. However, high contact pressure is required. Furthermore, contact resistance is relatively high and resistance to corrosion is poor. Also, there are constraints on processing and mounting to contact springs.
	AgNi (silver-nickel)	Equals the electrical conductivity of silver. Excellent arc resistance.
	AgPd (silver-palladium)	At standard temperature, good corrosion resistance and good sulfidation resistance. However, in dry circuits, organic gases adhere and it easily develops a polymer. Gold clad is used to prevent polymer buildup. Expensive.
Surface Finish	Rh plating (rhodium)	Combines perfect corrosion resistance and hardness. As plated contacts, used for relatively light loads. In an organic gas atmosphere, care is required as polymers may develop. Therefore, it is used in hermetic sealed relays (reed relays, etc.) . Expensive.
	Au clad (gold clad)	Au with its excellent corrosion resistance is pressure welded onto a base metal. Special characteristics are uniform thickness and the nonexistence of pinholes. Greatly effective especially for low level loads under relatively adverse atmospheres. Often difficult to implement clad contacts in existing relays due to design and installation.
	Au plating (gold plating)	Similar effect to Au clad. Depending on the plating process used, supervision is important as there is the possibility of pinholes and cracks. Relatively easy to implement gold plating in existing relays.
	Au flash plating (gold thin-film plating) 0.1 to 0.5μm	Purpose is to protect the contact base metal during storage of the switch or device with built-in switch. However, a certain degree of contact stability can be obtained even when switching loads.

The relays under investigation in this project are all of the silver/tin oxide type; however, the composition of each contact varies significantly between manufacturer which will be shown to greatly affect contact performance and relay reliability. While other material types may also be used in power electronics, they are not compared in the scope of this project. A more detailed explanation on how material type affects $AgSnO_2$ relay performance and reliability is provided in the literature review section.

1.4 Relay Failure Mechanisms

Reliability is the ability of a product to function properly under a certain set of conditions for a defined period of time. For relays, the reliability is often expressed in terms of the number of switching operations, and the principal requirement is consistency of contact resistance [8]. Relays are relatively simple in design compared to other electronic devices, and for this reason they have only a few failure modes. The most common failure modes are latch-up and bridging of contacts, and high contact resistance due to erosion and contamination. Other modes include wear-out of structural parts such as the spring, failure to make contact closure, and damage to the enclosure. Table 2 shows a list of these failure modes and mechanisms and Table 3 lists influences on relay degradation.

Table 2: Contact failure modes [8].

CONTACT FAILURE MODE		
Arc discharge	Surface layer	Particle
• contact welding • contact erosion • material transfer	• inorganic layer (oxide, sulphide) • organic layer (oil, grease, vapour)	• abrasion (plastics) • dust
influence of contact material	influence on contact resistance	influence on contact reliability

Table 3: Physical effects on contact reliability [8].

INFLUENCE ON ELECTRICAL CONTACTS		
Influences	Parameters	Effect
electrical	• current • voltage	heating, melting, material migration, chemical reactions, fritting, electrical discharge, contact resistance
thermal	• arc	melting of contact material, material migration
mechanical	• friction • pressure	deformation, wear, cold welding, contact resistance
ambient conditions	• dust • gases	increased wear, particles, formation of chemical layers and corrosion
chemical	• oxidation	contact resistance, inorganic and organic layers, corrosion

Latch-up and Bridging of Contact

The failure mechanism of contact latch-up is the welding of contacts due to high current and voltage. Welding of contacts occurs at the instant of closing by a large current arc discharge that accompanies the bounce of the contact. When the temperature is hot enough, the contacts become soft at the surface and stick together upon contact. Contacts may fail to open if the force to break the weld is higher than the maximum opening force provided by the spring. The strength of a weld is determined by the electrical/thermal stress on the contact spot caused by the amperage and duration of the arc immediately preceding contact impact; and the mechanical stress on the contact spot caused by the spring or magnetic coil. Kinetic parameters that affect the stress include impact velocity, contact mass, and static contact force [10]. It was found by Neuhaus that both the frequency and strength of welds increase proportionally with the arc current while the influence of increasing the arc time attains a saturation value as the molten pools surrounding the arc roots approach their state of thermal equilibrium. Also, supply voltage values higher than the minimum arc voltage cause stable bounce arcs lasting the total bounce period, while at lower values the bounce arc may lose current before reclosure, thus lowering the weld force.

As for bridging of contacts, tin whiskers have been a problem in tin-plated finishes on relay contacts. In the 1990's and early 2000's, many satellites failed due to the growth of tin whiskers in pure tin plated electromagnetic relays [11]. The satellites were designed with a primary and redundant satellite control processor (SCP) but the tin whisker induced short circuits took out both, resulting in a complete loss of the satellite's primary

mission. As a result, pure tin-plated components have been prohibited by the Military and NASA to prevent future failures, and as a result the industry has moved away from tin-plated relays. A study by the Foxboro Company attributes the tin whiskers to stress and electromigration, and found growth on the NC terminal and inside an insulator guide hole [12]. The images can be seen below in Figure 9**.**

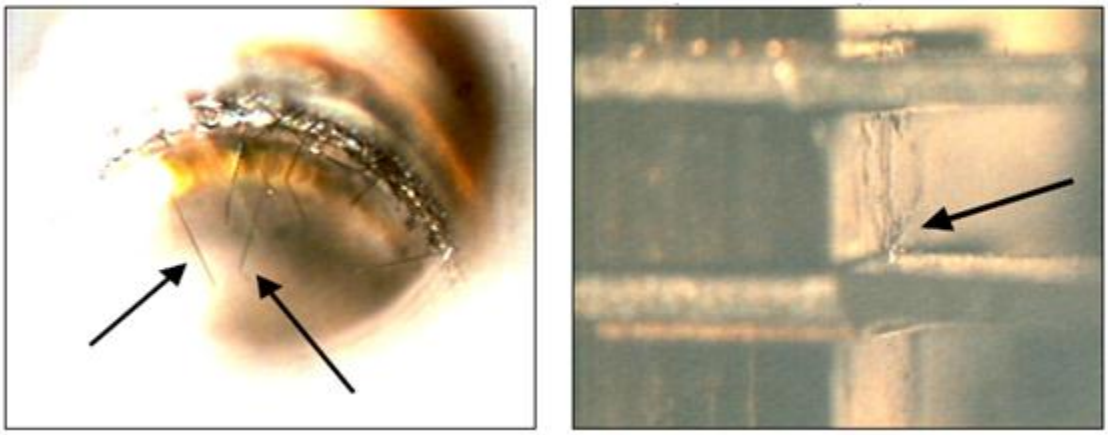

Figure 9: (a) Tin whiskers inside on insulator guide hole; (b) Whisker growth between contact support arms [12].

Contact Failure

Contact failure can be classified as a reduction in contact force due to contact erosion, and the deposition of contaminants onto the contact surface. The arc erosion process can be best described as a three part process: first the metallic arc phase where material is vaporized, secondly the gaseous phase arc where material is ejected, and third the redeposition of vaporized and ejected material [13]. A depiction of the arc formation and

erosion process can be seen on the next page in Figure 10 while the arcing process and material sputtering can be seen in Figure 10**.**

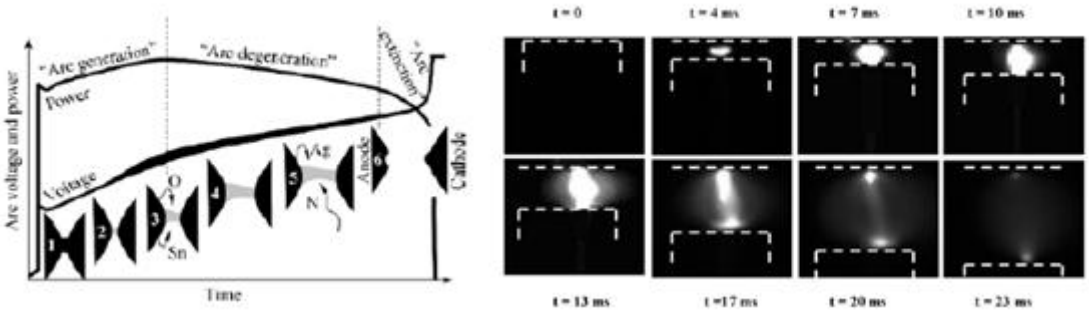

Figure 10: (a) Arc erosion process [13]; (b) High speed sequence of arc formation [14].

As the metals erode from the anode, they deposit on the cathode and a pit and crater condition is formed as seen in Figure 11a**.** This typically occurs at lower load voltages. During other conditions seen at higher voltages, symmetrical mass transfer occurs, and over time both contacts lose mass as metal is ejected at high temperatures. This leads to an open circuit where the contacts fail to electrically close the load circuit (Figure 11b).

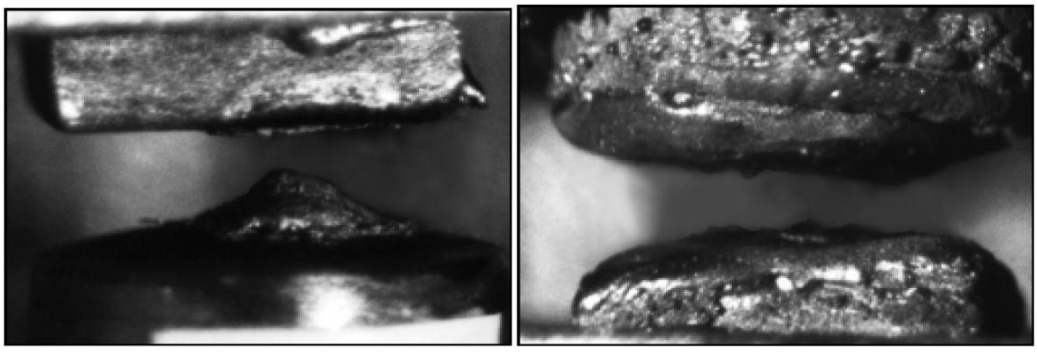

Figure 11: (a) A pip and crater formation; (b) Contact material loss due to arc erosion [15].

It is important to note that voltage and current are the most important criteria for arc formation and degradation. A secondary effect of the arcs is extremely high temperatures – between 6000°C and 10,000°C – causing the surface of the contacts to melt. The primary cause of the high inrush current is the lower resistance values during the switching to the load as seen in Table 4. Capacitive loading is capable of producing inrush currents as high as 20 to 40 times the steady state current which can be very damaging during the switching process.

Table 4: Inrush current by load type [16].

Type of Load	Inrush Current
Resistive	Steady state current
Motor	5 to 10 times the steady state current
Incandescent lamp	10 to 15 times the steady state current
Mercury lamp	Up to 3 times the steady state current
Sodium vapor lamp	1 to 3 times the steady state current
Capacitive	20 to 40 times the steady state current
Transformer	5 to 10 times the steady state current

Arc erosion leads to contact degradation and can eventually result in relay failure through either a significant change in relay resistance if signal attenuation is considered a failure mode, or by welding, since arc erosion can degrade a contact to a point where it is possible to latch-up even at low power conditions.

1.5 Research Motivation

The research presented in this thesis is motivated by manufacturer dependent differences in relay reliability. The relays studied in this project are SPDT silver/tin-oxide relays used in power electronic applications (standby power supplies) rated for 250VDC, and it was

noted that one relay was experiencing latch-up/welding failure whereas the other two manufacturers' relays under the same loading conditions performed without failure. The objectives of this project were then to validate the differences in relay reliability, address the manufacturer dependent differences in relay reliability by assessing material properties and design variations that cause welding and latch-up failure in relay contacts when subjected to short pulses of high voltage and high current, and lastly to determine the safe operating areas for the relays by investigating the power and energy relationship that result in first cycle weld failure. It should be noted that the relay failure occurs in the normally open contacts during the switchover to DC backup when the relay is energized. For this reason, the project focuses on the closing of the relay (NO contacts) and considers the NC contacts outside the scope of this work.

Chapter 2: Literature Review

In this chapter, the results of previous work regarding arc erosion degradation, relay dynamics, predictive reliability techniques, contact materials, and silver tin oxide relay contacts are reviewed. This chapter will be divided into those sections knowing that the studies on relay dynamics, contact material performance, and silver/tin oxide contacts will relate back to the relay's susceptibility to weld and how resistant it is to arc erosion.

2.1 Arc Erosion Degradation

Arcing phenomena is the main cause of erosion, transfer, and migration of contact material in switches and relays [17]. Arcing can occur between the opening contacts during a "break" operation, as well as during the contact bounce period in the "make" operation. It can be said that contact erosion is the most important factor when determining the life and reliability of a relay [18]. Since the amount of erosion is directly related to arc energy, and the arc energy is also proportional to the arc duration, the DC arc duration has an important effect on the life and the reliability of contacts [19].

Many studies look at the arcing process during the opening phase, and of these, most studies on dc arcing have concentrated on the influence of contact opening velocity on arc duration and energy [20]. In a study by Teste, contact opening under DC voltage in the case of high-intensity currents for Ag and $AgSnO_2$ contacts is investigated [14]. The influence of several parameters on contact opening is studied such as opening velocity, arc current intensity, nature of the circuit load, and material type. These will be covered in greater detail in the next subsection: relay dynamics. With regards to contact erosion and degradation, the study proposed a qualitative approach by means of a 3D

profilometer. This allows the measurement of displaced matter instead of solely relying on a change in mass to determine contact erosion and degradation.

2.1.1 Arc Erosion Physics

As shown in Figure 10 in the introduction section, there are three distinct stages during the complex arcing phenomenon. The initial stage of drawing the arc is described as the "metallic ion stage" and results in material transfer from the anode to the cathode [21]. It is believed that during this stage the Ag^+ and Sn^+ (M^+) ions are attracted to the cathode and deposit there with a net flow of material from the anode to the cathode. The second stage is called the "gaseous ion stage" where material is transferred from the cathode to the anode. When the arc lengthens as the contacts continue to separate, gas molecules have a higher probability of entering the discharge, when are then ionized to g^+. These gaseous ions are attracted to the cathode, sputter, and then erode the cathode surface [13]. The third and final stage is the redeposition of material back onto the contacts.

In more detail, the process is described by Swingler as follows [13]: The arc generation regime consists of the rupture of the molten metal bridge of the separating contact pair and is indicated by the sudden rise in voltage as the arc discharge is initiated (Figure 10). Material is removed from both the anode and cathode to form the bridge which is then used in the metallic ion arc [22]. Once the bridge is ruptured, material is removed from the anode and deposited on the cathode and follows the model proposed by Chen et al. [23]. The metallic ion arc then grows resulting in increased anode erosion and cathode deposition. Once the arc voltage reaches a trigger level, in this study 14 to 15 volts, the surface analysis data shows a decrease in the rate of cathode deposition and anode erosion. The relative amount of Sn and O has started to decrease whereas at the beginning

of this state there are high amounts of Sn andO which dominate the arc when compared to Ag due to the lower heat of vaporization. At the end of this stage, the surface is depleted of SnO_2 so less is present in the arc. Next, at higher trigger values between 16-20V, or 1.6 to 2.6 ms into the arcing process, instabilities in the arc conductance cause the voltage characteristic to show increased levels of fluctuations. Also, the affected area of the contact surface has enlarged to its maximum due to mobility of the arc roots. By this point, the arc is considered to transition into to the arc degeneration regime. This regime begins with gaseous ions forming in the arc, but it was found that there is little transfer of mass from the anode to cathode during the discharge process. Lastly, the arc extinguishes around 28-38V or 7.5ms into the arcing process as the arc is no longer able to support itself. It is important to note that the before mentioned voltages are for the study loading conditions which used three 12V lead-acid batteries and allowed a 24A current loading when the contacts were closed [13].

2.1.2 Arc Erosion Modeling

There have been several studies on arc erosion modeling. One of the first was a one-dimensional contact model proposed by Nakagawa that split the contact into thin disks represented by a numbered lattice. The computer program written performed an energy balance based on the input energy, energy loss by conduction, energy of joule heating, and stored energy. This study was performed on Cu-W alloy contacts, but the underlying concepts can be applied to other metal combinations such as AgCdO and $AgSnO_2$. From this study, it was demonstrated that one can calculate the transient temperature rise as well as show the domain of melting and evaporation within the contact material due to energy input from the electrode surface. It was also made clear that the latent heat of

evaporation of Cu played an important role in suppressing the temperature rise of W and in reducing the amount of erosion – the calculated results show that a Cu-W electrode with 40-50% Cu and 50-60% W erodes less than a pure Cu or W electrode, agreeing well with experimental results [24].

A more recent electrical arc erosion model for high current derived by Pons combined three different models: an arc energy transport model [25] to get the energy brought by the electrical arc at time t, a thermal model to get the arc erosion due to vaporization, and a magneto-hydrodynamic model to get the arc erosion due to splash erosion [26]. It calculates the amount of contact material removed after one electrical arc breaking operation; however, it does not take into account deposition mechanisms. This information is useful for the arc erosion process if failure can be correlated to loss of mass versus cycles at a certain current intensity, but at this time the loss of mass from arc erosion is not correlated to welding failure.

2.2 Relay Dynamics

In relay reliability and performance, the relay parameters such as opening velocity, spring stiffness, contact hardness, contact geometry, bounce behavior, and breakaway force are each important. It has been studied by Huimin et al. that increasing the contact breakaway initial velocity from 0.08 m/s to 0.3 m/s decreases the bridge duration, the metallic phase arc duration, the gaseous phase arc duration, and the total arc duration under a resistive load. As such, Huimin concludes that increasing the contact breakaway initial velocity by design will help to improve life and reliability of a relay [27].

2.2.1 Bounce Duration and its Effect on Welding

Other studies have focused on the dynamic welding properties of hard silver and silver metal oxides [28],[29]. The results show that strong welds were always associated with very short bounces during make or break, normally less than 100 μs [30]. The arc during bounce melts the silver at the arc roots and a weld can form when the contacts close on an area of molten silver. As the amount of silver on the surface becomes greater, the probability of closing on molten silver becomes greater thus forming stronger welds. It is also reported that for longer duration bounces (typically over 300 μs), the bounce height becomes significantly greater which has two effects: 1) an increase in impact splash during contact closing, and 2) a reduction of material transfer efficiency due to the larger gap and arc area involved. What this means is there is a reduction in the amount of silver in the actual contact spot, so the weld strength of longer bounces is generally weak. Conversely, short bounces (typically 40 to 100 μs) are very efficient in producing a concentrated silver spot on the cathode with much less impact splash at closure thus resulting in a strong weld. Also mentioned in the paper by Witter and Chen is the improved resistance to welding and erosion for higher levels of oxide content which will be reviewed later in this section.

2.2.2 Make and Break Operation Welding Mechanisms

A more recent study by Zhao et al. investigated the existence of relationships between the series of arc duration characteristics and the occurrence of contact welding [31]. Welding can occur on both the make and break operation; however, it is more typical for welding to occur on the make than during break operation. Out of 29 incidents of welding in the study, 27 occurred during make operations while only 2 were during break. It is generally

considered that increasing the number of operations will result in increased contact erosion, a decrease in contact force and overtravel. This may cause a marked increase in arc duration which could be used as an indication of imminent welding; however, the experimental results did not show a strong relationship between make/break arc duration, the number of operations, and the occurrence of welding. This suggests randomness to the mechanism behind welding and is described as follows.

The occurrence of welding depends on whether the weld force is greater than the break force of the relay spring. While the spring force can be considered a constant, the weld force varies considerably with each operation and cannot be easily predicted since it is a product of the welded area and welding strength. The area and strength are strongly dependent on the number of contact spots, the spot size, the volume of the melted pool, and its material composition. It also depends on the cooling/solidification rate of the melted pool, making it difficult to predict the occurrence of welding.

This demonstrates that welding sometimes occurs suddenly or randomly in the electrical lifetime test without any previous signs or changes in the make and break arc durations. It may be possible with more research to predict the occurrence of welding based on the welded area and the weld strength in each break operation.

It is important to note that the contact closing velocity, closing force, bounce height, and arc duration are all dependent on such relay parameters as inductor coil force, spring force, material hardness, contact geometry, and contact material. The inductor coil and spring force as well as contact mass affect the closing and opening velocity. The hardness and geometry will affect the bounce due to their relationship to coefficient of restitution,

and the contact material properties will affect arc duration, contact hardness, heat generation from joule heating, and many other aspects which impact welding.

2.3 Electrical Contact Resistance: Fundamental Principles

The fundamentals of contact mechanics including deformation, constriction resistance, surface film effect on resistance, *a*-spot size, and the temperature of an electrically heated *a*-spot have been well documented by Hertz, Holm, and many others [32][33][34]. To begin explaining the fundamental theory, a frame of reference as used by Johnson is shown in Figure 12.

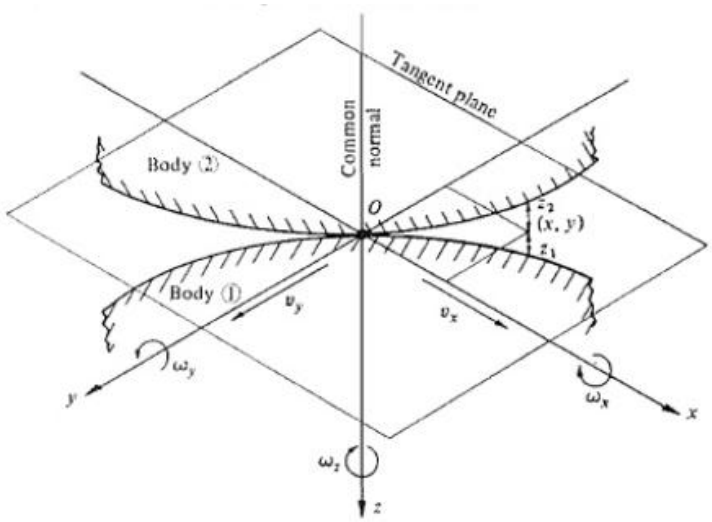

Figure 12: Reference Frame for Relay Contact Theory [34].

The initial point of contact is referred to as the zero point on the axis. This allows for equations to be formed explaining the material deformation under loading. Seen in Figure 13 is a depiction of two curved contacts and their deformation under a force L.

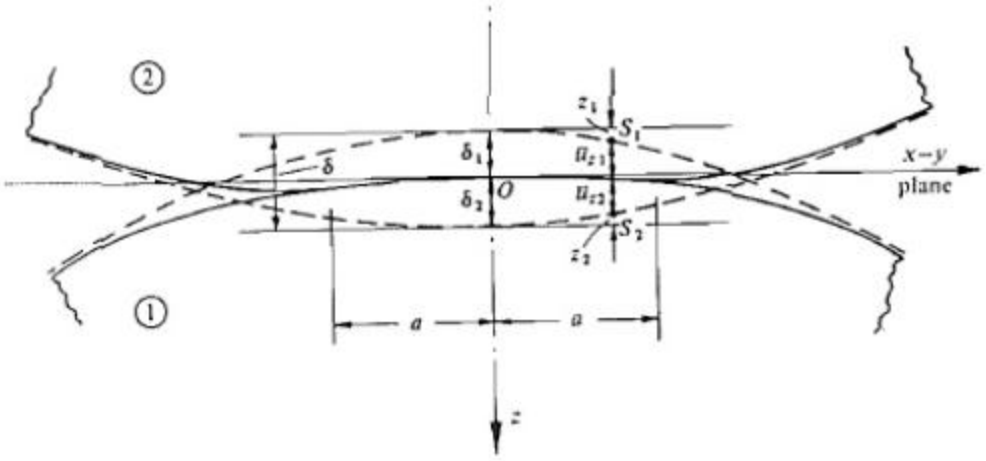

Figure 13: Cross-section after deformation.

The governing equations taken away from this are:

$$a = \left(\frac{3PR}{4E^*}\right)^{1/3} \tag{2.1}$$

$$\delta = \frac{a^2}{R} = \left(\frac{9P^2}{16RE^{*2}}\right)^{1/3} \tag{2.2}$$

$$p_0 = \frac{3P}{2\pi a^2} = \left(\frac{6PE^{*2}}{\pi^3 R^2}\right)^{1/3} \tag{2.3}$$

Where:

$$\frac{1}{R} = \left({}^{1}/_{R_1} + {}^{1}/_{R_2}\right) \tag{2.4}$$

$$\frac{1}{E^*} = \frac{1-v_1^2}{E_1} + \frac{1-v_2^2}{E_2} \tag{2.5}$$

Equation 2.1 gives the radius of the contact area, equation 2.2 gives the displacement at the x=0 position, equation 3 gives the max pressure, while equations 2.4 and 2.5 are supporting equations representing the relative curvature and effective modulus respectively.

2.4 Silver/ Tin Oxide as a Replacement to Ag/CdO

Electrical contact materials used in switching devices are commonly made from silver alloys because they exhibit excellent properties that minimize contact welding and arc erosion during operation. Comparisons of Ag-2Cu alloy, Ag/SnO_2 metal-oxide composites, and Ag-20Ni metal-metal composites found Ag/SnO_2 contacts to be very resistant to erosion and welding in lampload switching [35]. With growing environmental concerns over cadmium use and the passing of RoHS, Ag/SnO_2 has become a common replacement in cadmium-free contacts in many electrical power switching devices [36]. It is known from literature that $AgSnO_2$ contacts are better than AgCdO in terms of overall life and welding resistance [37][38]. In_2O_3 has been added for over 20 years because of the ability of indium to promote a uniform internally oxidized microstructure, which is particularly important in post oxidized contact manufacturing [39].

Internal oxidation of Ag/Sn can also be performed by In, Cu, or Bi. Hertz reported that the internal oxidized $Ag/(SnO_2+In_2O_3)10\%$ performed better than the same composition formed by powder metallurgy [40]. Work by others support the use of indium; however, powder metal Ag/SnO_2 with fine to medium oxide performed equally well [41]. Further studies by Witter and Chen showed that material transfer in $Ag/(SnO_2+In_2O_3)$ is reduced when oxide levels are increased from 10% to 14% [30]. The primary benefit of indium is in assisting the internal oxidation during powder metallurgy production. It also acts as a wetting aid to the tin oxide particles [1]. An example of the benefit of indium percentage can be seen though the drop in weld break force vs oxide % in silver tin indium oxide contacts as shown in Figure 14.

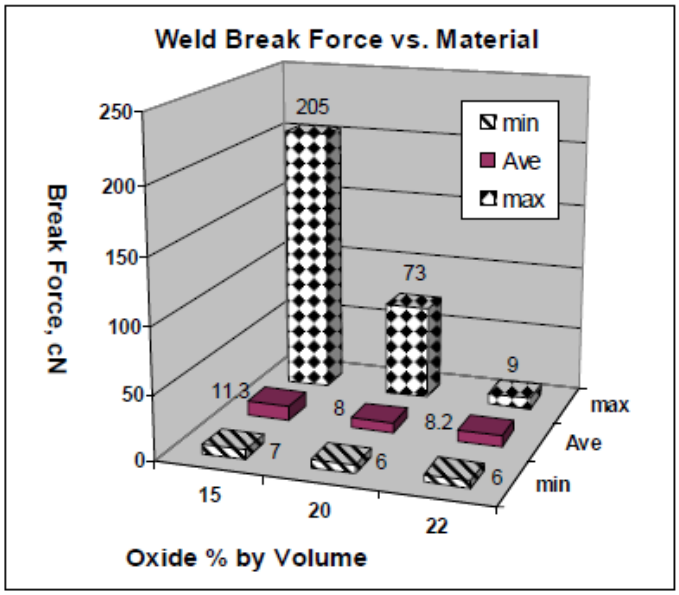

Figure 14: Weld break force vs. oxide % in silver tin indium oxide contacts tested for 16,000 operations of lamp load [42].

It is reported by Witter and Chen that increasing the oxide content of silver tin indium oxide from 15 to 22% significantly lowers the weld strength of both weak cold bond and strong short arc type welds [42]. Also, as the switching life of a device increases, the frequency and level of strong welds will increase as a result of lower contact force and higher incidence of short bounce arc welding. It should be noted that the results from this study apply to low and medium current devices and that mechanisms for high current may differ.

Lastly, while the amount of indium oxide present affects the contacts ability to internally oxidize, the amount of tin oxide relative to silver makes a big difference on contact performance as well. In a study by Mutzel, several materials (Table 5) were benchmarked for their performance in mechanical formability, anti-welding, contact resistance, and erosion and material migration behavior [43].

Table 5: Material Components [43].

material	additives	production method	granulo-metry
Ag-CdO	none	pre-ox.	fine
Ag-SnO_2 SP	none	p.m.	medium
Ag-SnO_2 SPW	WO_3	p.m.	medium
Ag-SnO_2 PMT1	Bi_2O_3, CuO	p.m.	coarse
Ag-SnO_2 VC	In_2O_3, CuO	p.m.	finest
Ag-SnO_2 POX1	In_2O_3	pre-ox.	fine

It was shown that after 500 operations, lower weld break forces were experienced by increasing the metal oxide content. The 86-14% $AgSnO_2$ outperformed the 88-12% as shown in Figure 15. The positive effects of CuO and Bi_2O_3 additives for powder metallurgical PMT materials can also be seen, where the additives work as wetting agents to keep the metal oxides in the liquid silver matrix during arcing. This keeps the viscosity much higher and reduces the amount of material loss.

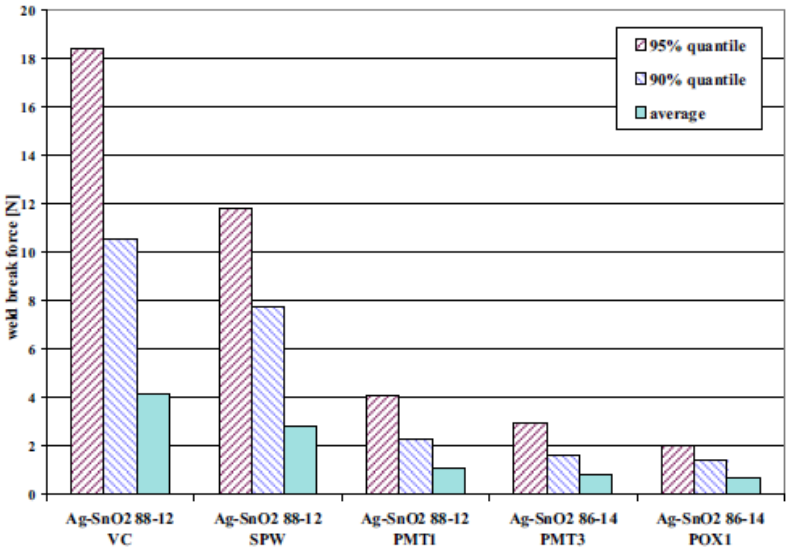

Figure 15: Weld break force quartiles of different Ag-SnO_2 compositions [43].

2.5 Electrical Testing

Relay life testing is an important aspect in determining the reliability of a particular type of relay. The aforementioned experiments which investigated the influence of contact material and relay dynamics all used different loads to study the parameter's effect on welding susceptibility and relay life. In Swingler's study on arc erosion, a resistive load arrangement was used with up to 42 VDC and 24A [13]. Another experiment by Teste studied the arc erosion phenomenon using a 3D profilometer by subjecting the relay contacts to 36VDC and current from 100-700A with a current pulse of 200ms [14]. Further testing by Rieder and Strof was performed from 40 to 45VDC at 1.2 to 2.4A in order to conduct relay life tests and to measure contact resistance after each cycle [44][45]. One unique test conducted by Leung includes an interruption test and a static gap test [1]. These tests are described in detail in previous papers [46]. The interruption test trips magnetically when a test current is applied and opens automatically one cm in the first half cycle (8.3ms) and is fully open at four cm in 23ms. The test makes 5 interruptions at 480V, 60Hz, and 1920A peak. Lastly, the static gap test uses a capacitor bank charged to 900V open circuit and produces 141 amps peak discharge where the contacts are mounted 1mm apart and the test simulates an arc breakdown across the gap. While there was extensive testing at the lower voltage levels such as 12VDC (the typical operating voltage of a car battery) up to 45VDC, little has been studied at higher voltages around 250V where some industrial and server equipment operate.

2.6 Experimental Selection

After careful review of the literature it was found that very little has been studied on the power conditions which result in a single cycle failure. Much of the attention has been on low voltage high current automotive relays, and most of it focuses on arc erosion degradation and not welding since relays are expected to last more than one cycle. For this reason, the interface between the one cycle failure and multiple cycle failure regions will be studied in more detail.

Three relay types of similar ratings were provided by the project sponsor in order to address manufacturer dependent reliability differences. The relay which had the susceptibility to latch up after one cycle was then studied under varying power conditions in order to better understand the power and energy required to weld the relay contacts. All three relays are of the $AgSnO_2$ type; however, percent composition is not uniform. This study will analyze the extent of degradation after testing at different power conditions, and then correlate it back to material characteristics including contact material, oxide content, hardness, sintered density, and surface roughness. Contact geometry will also be considered. The varying reliability will then be correlated back to these contact properties using a physics of failure approach.

Chapter 3: Preliminary Testing in the Standby Power Supply

This section covers the initial testing performed on the relays within a standby power supply (SPS). The purpose of this testing was to recreate the failure of the relay within its common application and to observe the relay while in operation by using a high-speed camera. In order to do so, wiring changes to the SPS and relay decapsulation was necessary to view the relay contacts.

3.1 SPS Preparation

In order to view the relays during operation, the SPS must first be opened to gain access to the PCBs. The SPS with the outer cover removed is shown in Figure 16 with the underside of the PCB exposed.

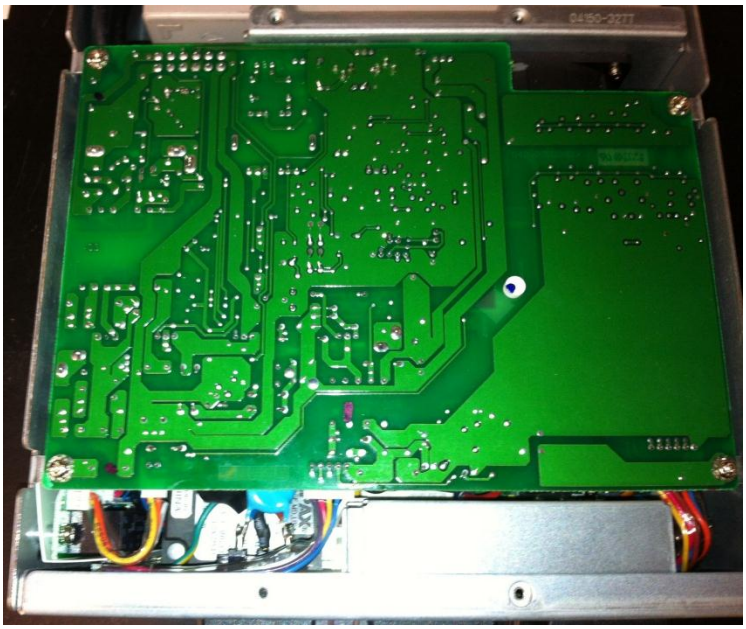

Figure 16: Underside of PCB when first opening SPS.

The next step was to remove the top PCB shown in Figure 16 to expose the rest of the electronics. The result of this step is shown in Figure 17.

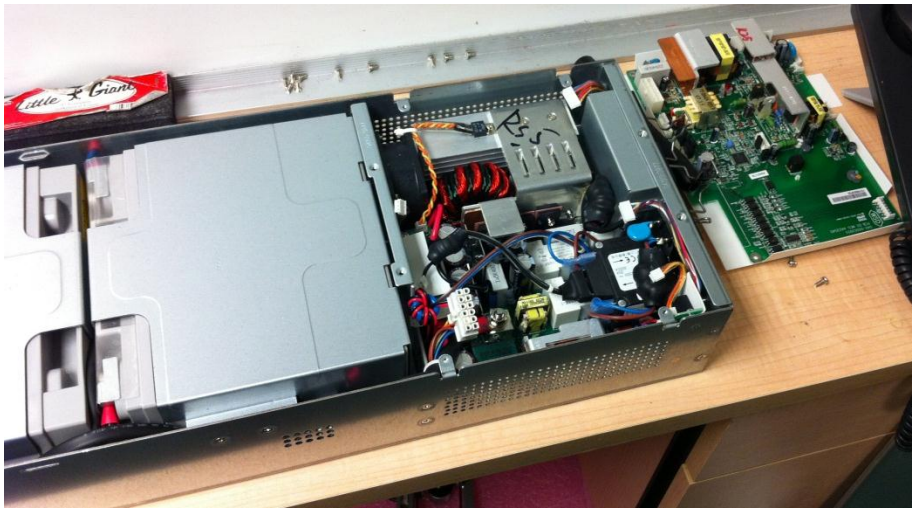

Figure 17: Removal of top PCB.

Next, the bottom PCB which supports the relays is removed from the SPS in order to get a clear line of sight. The bottom PCB is shown below in Figure 18 and identifies relays 102 and 103, the ones which experience failure. These two relays provide the switch path for DC output, whereas relay 101 is only included in the design to provide an additional spacing gap length in order to meet UL AC disconnect spacing requirements.

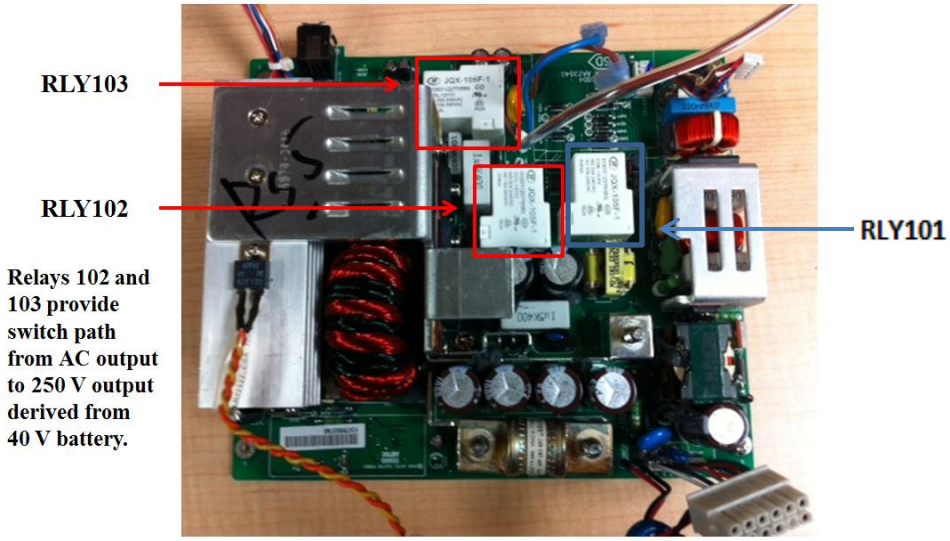

Figure 18: PCB with relays and power electronics.

After the boards were removed from the SPS, the wire leads needed to be extended in order to properly hookup the board. Instead of leads travelling vertically from one board to the next they now needed to travel the length of two boards to reach the same connection point. The wires were cut and resoldered to an additional length of wire as shown in Figure 19.

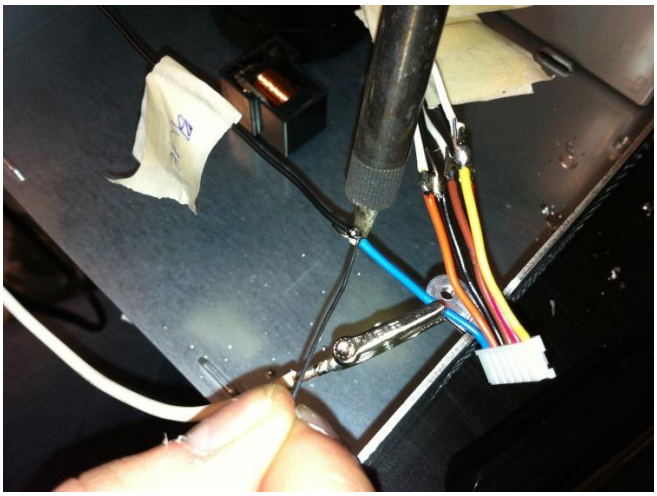

Figure 19: Soldering the pin connector to the additional wire lengths.

Each individual wire is insulated by shrink-wrap and then bundled together using a larger shrink-wrap in order to keep ribbon bundles organized. The ribbon wires were then connected to their respective terminals and the fan was positioned in order to maintain air flow over the large heat sink. A finished length of extension wire is shown on both the left and right side in Figure 20.

Figure 20: Fully reconnected SPS.

The last part of preparing the SPS for high speed cinematography was cutting open a window in the relay packaging in order to see the contact operation. As seen in Figure 1, the relay contacts are located in the top corner where the package protrudes out. To be more specific, the relay contacts are located where the two primary circuit pins, both NC and NO, are located as seen in Figure 31. To access them, the top side of the package must be cut away, and this step has been shown in Figure 21.

Figure 21: Opened relays on PCB.

After following these steps, the relays are now ready for investigation under the high speed camera.

3.2 Experimental Setup

A high speed camera was setup on a tripod overlooking the opened relays shown in Figure 21. The camera was capable of frame speeds up to 8300 fps at the settings chosen for this experiment. The SPS operates as follows: it provides AC bypass voltage when connected to the power main, and switches to a 250VDC backup when the power is interrupted. The output is limited at 2.2kW and the DC output is fixed at 250V, so in order to maximize the current, the resistance was optimized at 28.4Ω. Three variable 10Ω, 1000W rated ribwound resistors are used in series to dissipate the power generated by the SPS. The third resistor was configured at 8.4Ω by sliding a variable terminal closer or further away from the hookup terminal. An overview of the setup can be seen in Figure 22.

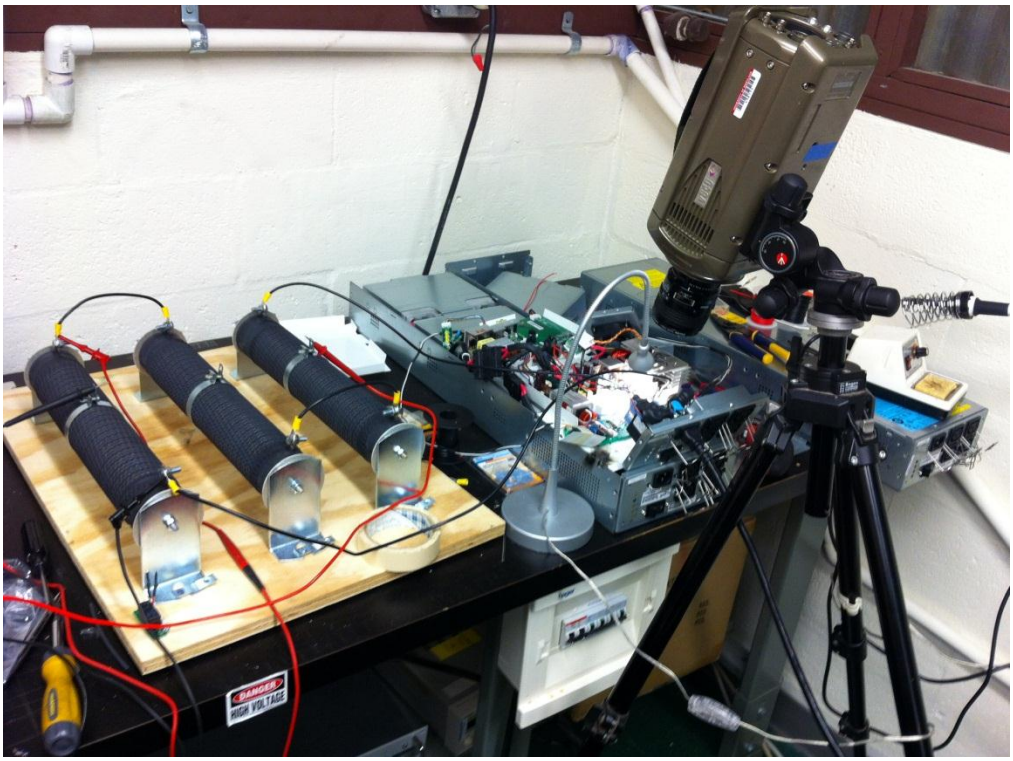

Figure 22: High speed camera setup.

To connect the resistor to the SPS, wires were made with a female disconnect at one end, and a ring terminal at the other end. The ring terminal was bolted to the terminal of the resistor while the female disconnect was connected directly to the V+ and V- on the SPS PCB.

It should also be noted that a large amount of light is necessary to record video at high speed - otherwise the camera is unable to track changes from frame to frame. In this experiment, a simple desk lamp is used to provide additional light to the relay contacts.

3.3 High Speed Video Clips

Videos of the relay contacts opening and closing were taken from 300 to 8300fps. The results shown are taken at the highest setting, 8300fps and are of relay 102. To simulate a power interruption, the AC line in was disconnected to the SPS. Upon doing so, it switches to the DC battery backup and the 250V DC output is derived from three 40V batteries. To then simulate a return to mains power, the AC line in is reconnected and the SPS makes the switchover back to normal operation. The following series of video frames show the DC backup return to AC switch first, followed by the AC to DC switchover.

3.3.1 Relay 102 switching from DC to AC, or NO to NC contact position.

In this series of video frames, relay 102 starts with the primary contact touching the normally open secondary contact (the down position). This occurs when the inductor coil is energized and represents the DC battery backup mode in the SPS. When the power returns to the SPS, the inductor coil is deenergized and the contact separates and returns to the normally closed, or the top position.

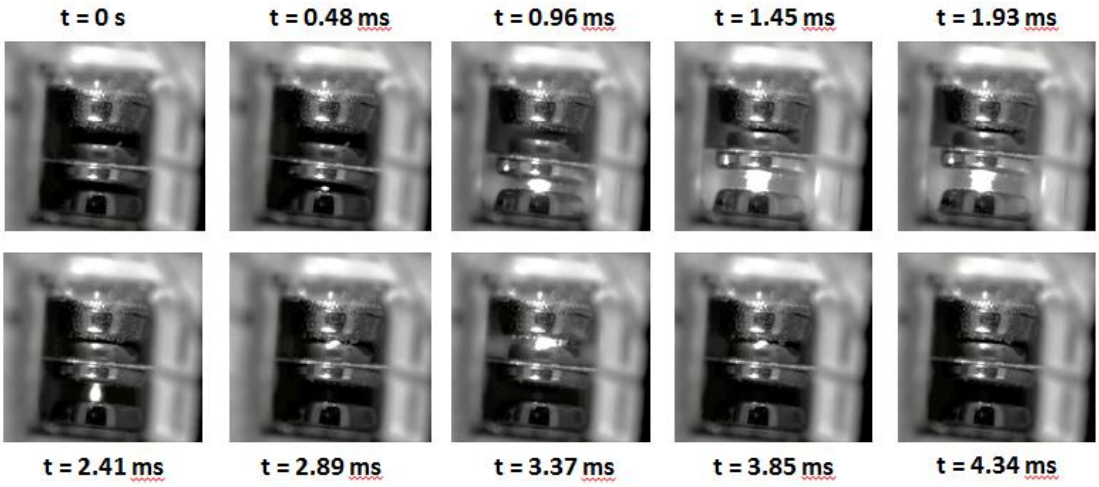

Figure 23: Relay 102 switching from NO to NC.

During the switchover from DC to AC, an arc is formed as the contacts begin to separate as shown in Figure 23. At frame 4, when t = 1.45 ms, the primary contact has fully reached the top position and is now in contact with the normally closed side; however, the arc is still in full formation. The arc persists 2.89ms into the switchover which is likely when the SPS internal circuitry turns off the DC backup and switches back to AC bypass. Interestingly, the primary contact recedes from the secondary contact after the AC switchover takes place, and one can see a small arc beginning to form at t = 2.89 ms and continue until t = 3.85 ms. During that time, the primary contact separates slightly from the secondary contact which is a phenomena that requires more study. Typically it is believed that the bounce leads to the arc formation.

3.3.2 Relay 102 switching from AC to DC, or NC to NO contact position.

In this series of video frames, relay 102 starts with the primary contact in contact with the normally closed secondary contact (the up position). This occurs when the inductor coil is deenergized and represents the AC bypass mode where most power goes straight to the load and some is diverted to maintain charge on the batteries. When the power is interrupted, the inductor coil is energized and the primary contact is pulled down to the normally open secondary contact. The 40V battery backup is stepped up and conditioned to 250VDC and is output through relay 102 and returns back to the SPS through relay 103 meaning they both see the same current.

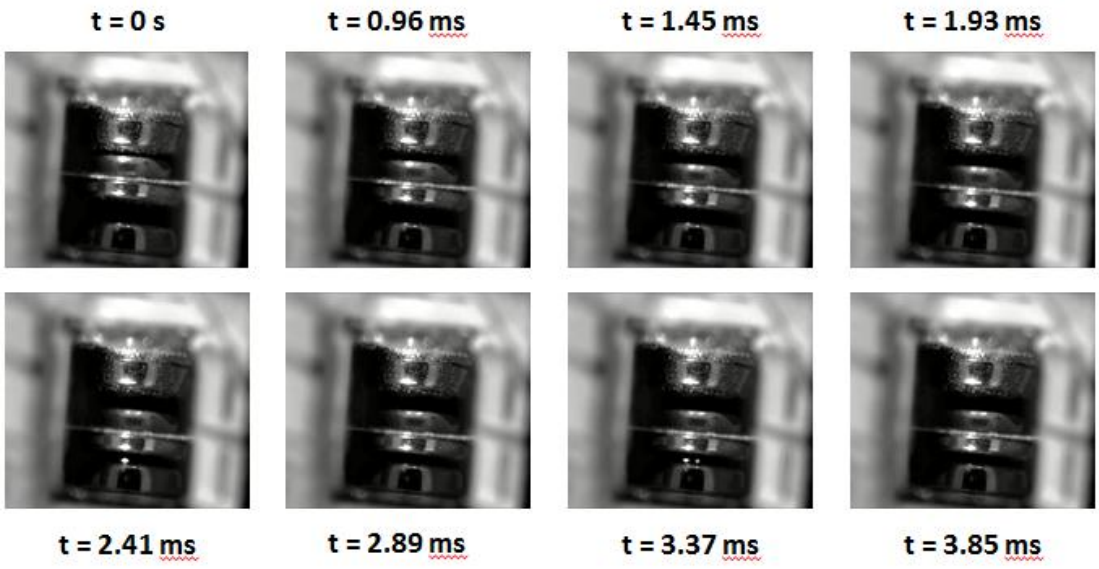

Figure 24: Relay 102 switching from NC to NO.

During the switch from AC to DC, the AC power is interrupted and there is no potential across the contact gap. As a result, no arc forms when the primary contact separates from the normally closed (NC) secondary contact. The primary contact finally makes contact with the (NO) secondary contact in the bottom position after 2ms, and a slight arc can be seen during the bounceback at 2.41ms in Figure 24. In-between the bounces, the primary contact again makes contact with the NO side and the arc extinguishes as seen at t = 2.89 ms. A second bounce is seen at t = 3.37 ms where a second arc is formed. The relay then settles after 3.85 ms when all bouncing and arcing is complete.

3.4 Discussion of Results

The videos provide an understanding of how the relay works within the SPS. The first video of the switchover from DC to AC catches the arc erosion process. A difference between this SPS application and other studies is the second arc and bounceback on the normally closed side after the initial arc extinguishes. This occurs after the primary

contact is already in contact with the secondary contact and no longer bouncing, suggesting that an arc can also cause a bounce or contact separation. In terms of arc erosion and arc formation, the sequence follows the studies by Teste and Swingler shown in Figure 12 & Figure 13. While the arc is an interesting phenomenon to observe, it is not likely to cause the weld failure observed in this device. Instead, it is believed that the relay failure in the SPS occurs during the switchover from interrupted AC to DC backup.

As shown in Figure 24, two distinct bounces and arcs occurred during the switchover to DC backup. Literature suggests that these short arcs and bounces are what result in stronger welds. While no relay failures were observed during the high speed video filming, it is believed that the load conditions used (purely resistive) did not match the load profile of the SPS application so the transient current values may not have been the same as those which result in failure. While it was not possible to obtain the particular device used to load the SPS, it was possible to recreate the transient conditions outside of the SPS. For this reason, it was determined that designing a standalone test circuit for relay failure outside of the standby power supply was the best approach in order to test for varying conditions that result in relay weld failure. The next section will describe how this automated circuit was setup and how it operates.

Chapter 4: Automated Test Circuit Setup and Sample Preparation

This chapter explains how the automated test circuit is setup and how relay samples are prepared.

4.1 Test Circuit Design

The test circuit must be able to charge a capacitor bank and discharge the energy into a relay quickly. Since relay life testing may require hundreds or thousands of cycles depending on the power and energy level, it is also a functional requirement for the test circuit to be automated. This requires the circuit to be able to identify when the relay has failed as well as to stop testing when this condition is met. To meet all of these design requirements, the test circuit shown below in Figure 25 is presented for relay failure testing.

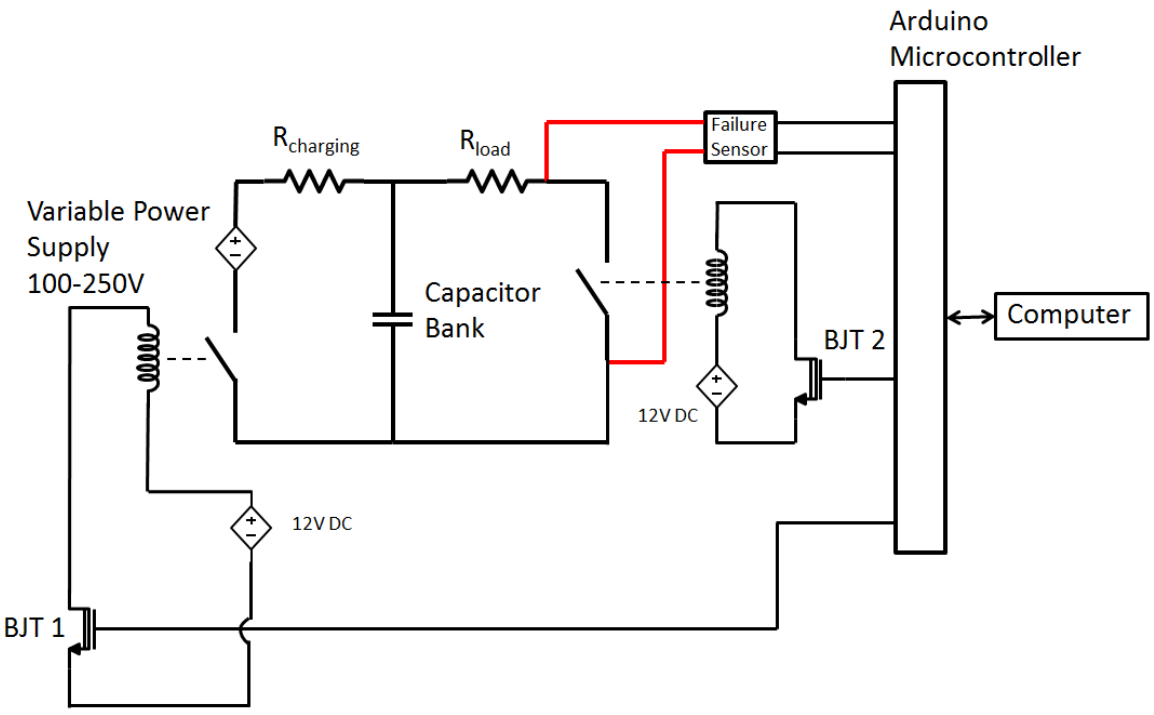

Figure 25: Automated relay test circuit.

The logic behind the design is simple: close the relay in the charging circuit by activating BJT 1. Once the capacitors are charged, the relay is opened by turning off BJT 1. To discharge the capacitors and test the sample relay, BJT 2 is turned on which closes the test relay. This discharges the capacitor across the relay and whatever load resistance is in the circuit. After the capacitor discharge, the test relay is deenergized by turning off BJT 2; if the failure sensor circuit recognizes that the relay returns to the normally closed (NC) position it knows that the relay did not fail and in turn repeats the loop until failure occurs. If the relay does not return to the NC position it means that the contacts have welded. When a weld condition is met, the circuit cycles BJT 2 on and off 5 times to see if the weld can be broken. If the weld is broken, it is considered an intermittent failure and the cycles to failure and coil cycles before the weld breaks are recorded. Testing then resumes until the sample fails again and the 5 cycle weld condition is met. When the circuit cycles the relay coil 5 times and it is still welded, the sample is considered permanently welded and testing is ended. This C++ code can be seen in the appendix. The next section will describe how the circuit diagram is wired and put into practice.

4.2 Circuit Construction

To build the automated test circuit, 12-gauge wire is used in order to allow for high currents. Smaller wire is used for the digital I/O of the Arduino and gator clips are used to hookup the relay inductor pins to the power supply. The circuit can be seen in its entirety in Figure 26 with the charging load resistor on the left with the ribwound resistors facing vertically, and the discharge load resistor on the right with the ribwound resistors facing horizontally. The vertical cylinders connected to wires are the capacitors and the PCB at the bottom left is the Arduino UNO board.

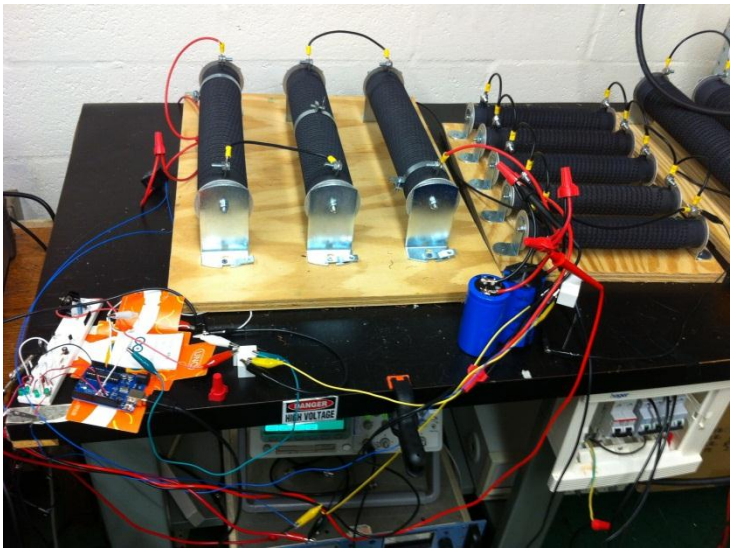

Figure 26: Automated test circuit.

4.2.1 Ribwound Resistors

Starting with the most basic component, the ribwound resistors are used because they are capable of dissipating a lot of power and withstanding very high currents. The charging resistor uses 3 - 10Ω resistors capable of dissipating 1kW each while the discharge circuit can use 5 - 0.5Ω 500W resistors in parallel to make an equivalent resistor of 0.1Ω. The resistors are mounted onto wood baseplates for stability and safety to prevent loose resistors from sliding around causing potential damage and injury from high voltage and currents. Ring terminals and bolts are used to connect one resistor to another, and as mentioned before the resistors can be wired in series or parallel to vary the resistance values.

4.2.2 Arduino UNO Microcontroller

An Arduino microcontroller is used to control the entire system including timing on when to charge and discharge capacitors, logical detection of relay failure, and communication with the computer to record cycles to failure data. The Arduino is shown on the next page in Figure 27.

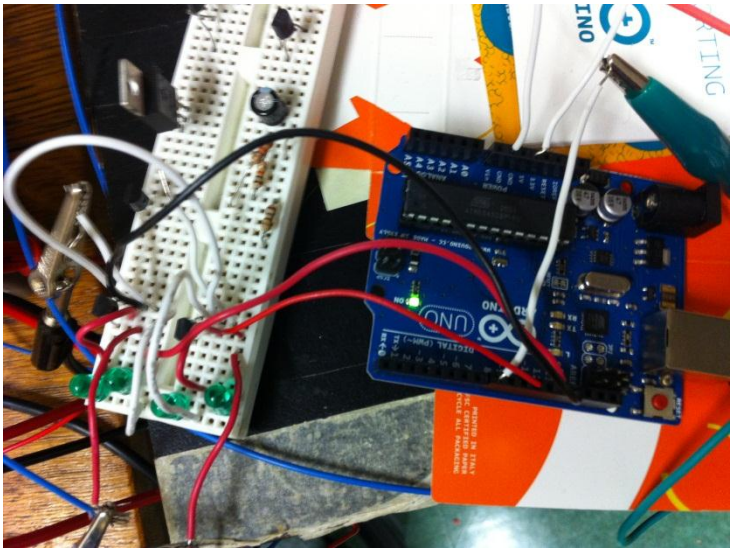

Figure 27: Arduino UNO.

The breadboard on the left in Figure 27 houses the BJT switches which use the 5V digital output from the Arduino to control the 12V circuit of the relay inductor coil which in turn controls a much higher voltage circuit up to 600V to charge and discharge the capacitors. LEDs are placed in parallel with the BJTs to serve as an indicator of when the charging relay is activated and when the test relay is being activated to discharge the capacitor.

4.2.3 Failure Sensing Method

Since detecting relay failure without visually opening the package is difficult, a simple but clever way of detecting whether the relay is in the normally open or closed position was derived. When the test relay is in the normally closed position, the +12VDC applied to the primary contact is output through the normally closed secondary contact which is connected to a supplemental relay's inductor coil. This means that supplemental relay is energized and the primary contact is touching the NO secondary contact meaning the Arduino digital input in port 8 is seeing a HIGH signal of +5VDC when the relay being tested is not failed. When the test relay does fail, the +12VDC does not reach the supplemental relay inductor coil so the Arduino digital input now sees a ground, or LOW

signal. This logic is easily written into an if statement in the C++ Arduino code seen in Appendix A. A circuit diagram showing the inputs and outputs for this failure sensing circuit can be seen below in Figure 28.

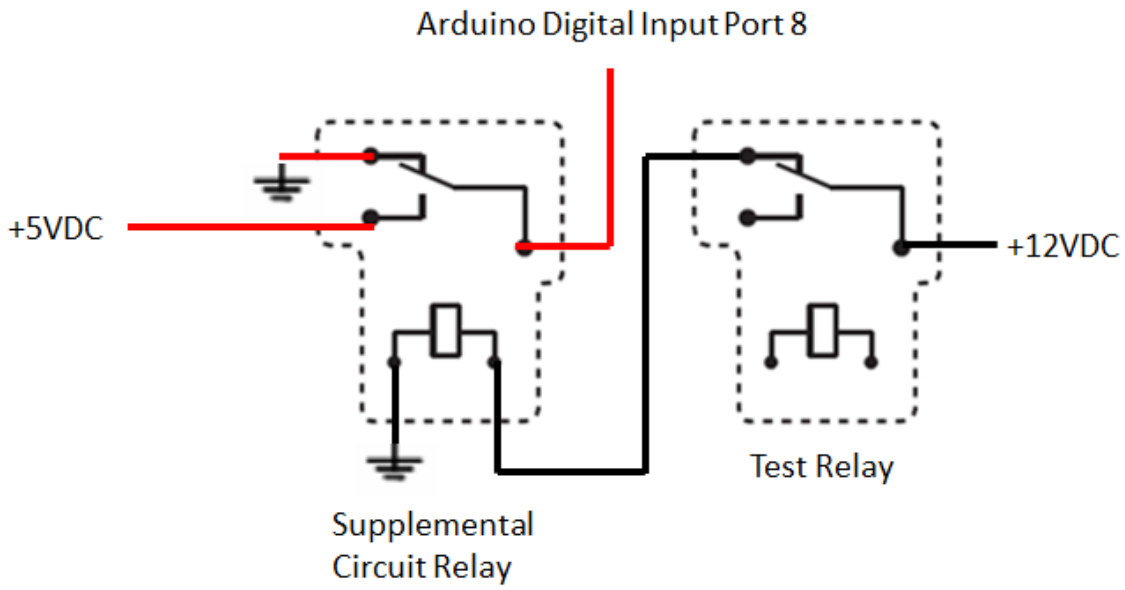

Figure 28: Failure sensing circuit.

4.2.4 Power Supplies and Curve Characterization

In order to power the relays and the capacitors, power supplies are needed. An Agilent B3630A 20V 0.5A DC power supply and an Agilent B3612A 60V 0.5A DC power supply were used to power the inductor coils of the charging relay, the test relay, and the failure circuit supplemental relay. Also used to measure voltage drops and resistance values is the HP digital multimeter model 34401 A. These three pieces of equipment are shown in Figure 29.

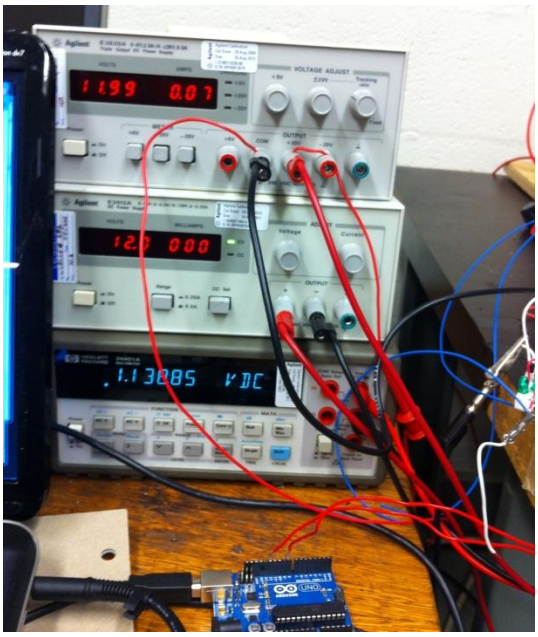

Figure 29: Low voltage power supplies and DMM.

In order to charge the capacitors, a high voltage TCR power supply capable of 600V and 2A is used. Lastly, to characterize trace curves, an Agilent 54624A Oscilloscope with 100 MHz resolution is used as shown in Figure 30. Because the voltage used during testing is outside the safe operating window of the oscilloscope, 10:1 reduction leads are used.

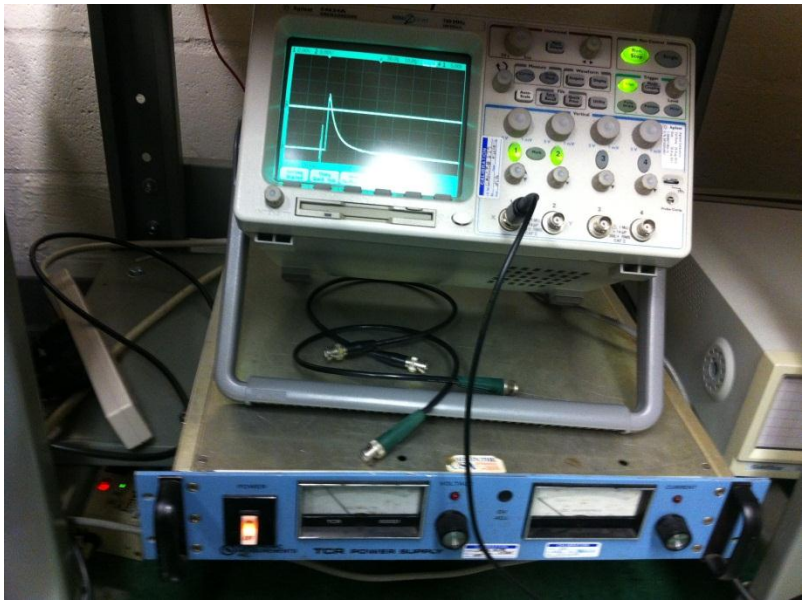

Figure 30: High voltage power supply and oscilloscope.

4.3 Relay Sample Preparation

The relays are SPDT type which means they have 5 pins total: 2 for the inductor coil circuit and 3 for the switching circuit where one input alternates between two outputs. The inputs can be seen below in Figure 31.

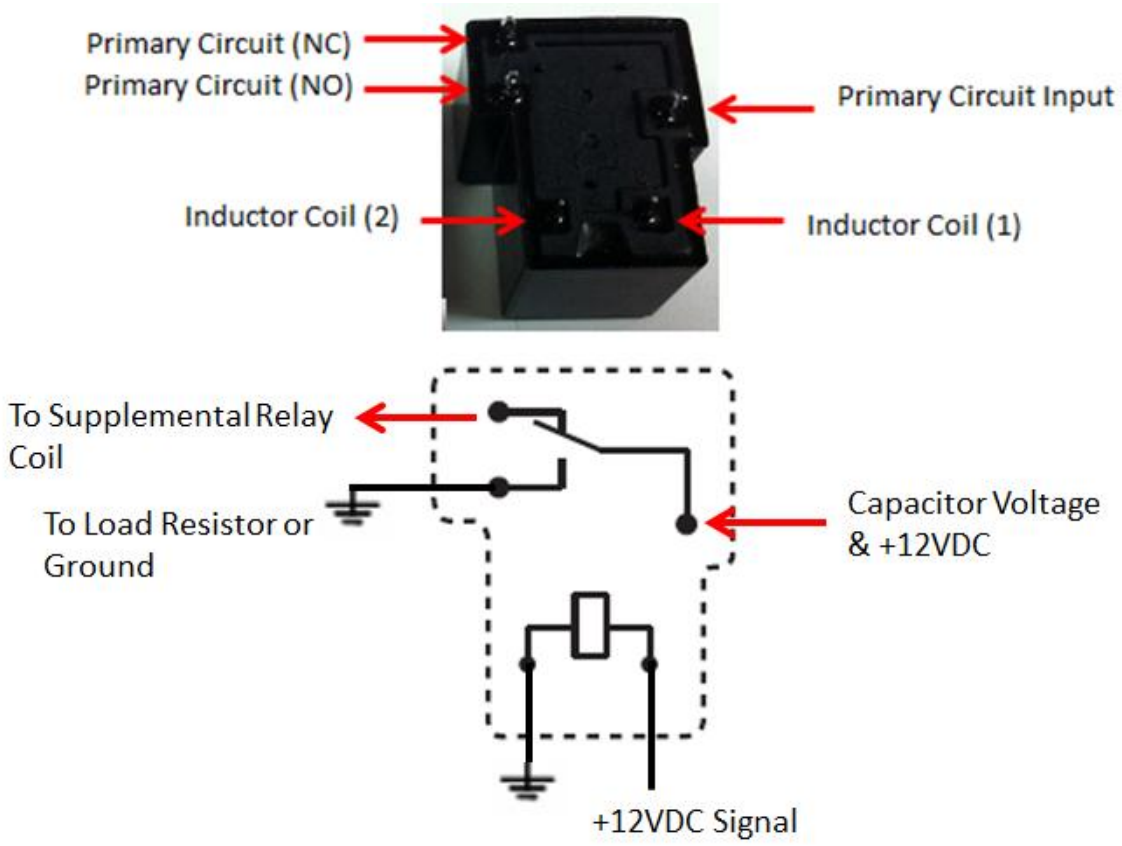

Figure 31: Relay pin layout.

Each relay has a 6 inch length of wire soldered to the primary circuit input and another to the primary circuit (NO) output. A 12-gauge wire is used in order to allow for high currents; during testing the leads are attached to the test circuit by using a twist-on wire connector. A +12VDC potential is applied to the primary circuit input which then goes to the supplemental relay coil of the failure sensing circuit by means of a gator clamp wire as previously described in section 4.2.3. Leads are connected to the test relay inductor

coil which is controlled by a BJT and the Arduino. Lastly, the wire that exits the normally open terminal is connected either to the load resistor or to the ground wire depending on the loading conditions desired.

4.4 Conclusion

A test circuit has been built which allows relays to be continuously cycled through a capacitor discharge until failure occurs. The circuit is run by an Arduino microcontroller which communicates with a computer and outputs the cycles to failure for both intermittent failures (failed to open but weld broke under 5 coil cycles) and permanent failures where the sample relay's coil is turned on and off five times and the contacts are still welded. This number was chosen arbitrarily where if the contacts separate after a few operations the weld is considered weak, whereas if the weld survives over 5 coil cycles it is considered a strong weld and thus permanent. This circuit was used to test the relays at the power conditions stated in the proceeding section.

Chapter 5: Comparison of Relay Reliability

This chapter covers the second part of the experiment: a comparison of manufacturer dependent relay reliability. A constant power test at 250V is used starting at 10μF and increased up to 70μF. The number of cycles each relay lasts is recorded for each energy level and reliability is compared. For the equations on RC circuit theory, see Appendix B which describes the power and energy levels seen by the relay.

5.1 Constant Power Test

The constant power test was derived in order to recreate the transient load conditions on the relay within the SPS. It is known that the DC output is 250V and a design engineer associated with the SPS indicated that an inrush current of 600A into an EMI filter capacitor on the load side may weld the contacts. This EMI filter was believed to be 10μF in capacitance; however, the true value was not provided. For this reason, multiple 10μF film capacitors were purchased (Panasonic JS251106-BA) and the capacitance level was stepped up at 10μF intervals until failure was observed. To be clear, samples of each relay were limited so the group size of samples tested at each energy level is quite small.

5.2 Constant Power Results

The cycles to failure at each point are recorded versus the capacitance level. The capacitance level can be related to the total energy by equation B.6 in Appendix B. It was shown that relay A performed the worst, and failed after one cycle at 70 μF while relays B and C performed better respectively and did not fail at one cycle until higher energies of 90 and >100μF respectively. It can be seen from Figure 32 that as expected, each relay type decreases in cycles to failure (CTF) as the energy / capacitance goes up. Analysis of this phenomenon is provided in the next section.

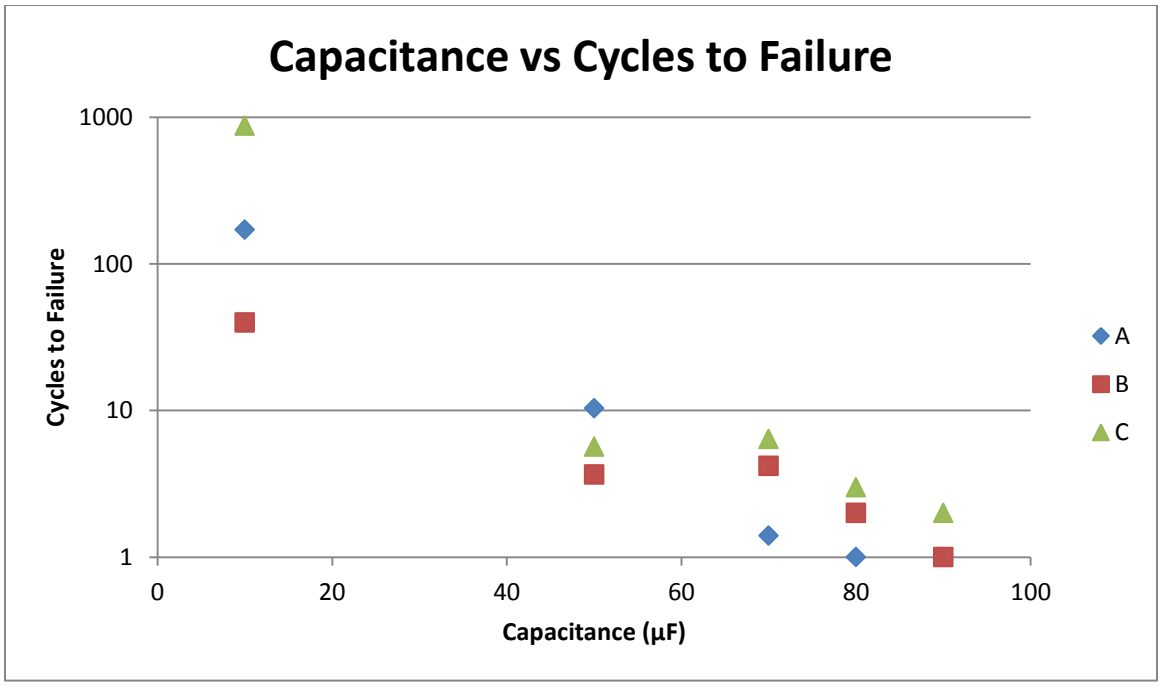

Figure 32: Constant Power Test - Capacitance vs. Average CTF.

Table 6: Constant Power Test Results.

Capacitance (µF)	10			50			70			80			90		
Energy to Relay (J)	0.15625			0.78125			1.09375			1.25			1.40625		
Relay Type	A	B	C	A	B	C	A	B	C	A	B	C	A	B	C
Average	170	39.75	871.67	10.33	3.67	5.67	1.4	4.2	6.4	1	2	3	1	1	2
Median	54	34	696	6	4	6	1	3	3	1	2	3	1	1	2
Variance	254.00	44.59	400.52	7.51	0.58	3.51	0.89	3.42	6.77	-	-	-	-	-	-
Sample Size	4	4	3	3	3	3	5	5	5	1	1	1	1	1	1

Table 6 shows the test results in table format. Relay A had an average life of 170 cycles at 10µF, but a median of only 54 cycles because one relay in the group lasted a few hundred cycles. Likewise, sometimes a relay fails relatively quickly even at low energy levels, again affecting the average. For this reason, it is better to fit the median of the samples to a curve to account for such a high variance. It can be seen that relay C outperforms relays A and B at 10 µF, while there is no significant statistical difference between the relays at 50 µF. At the transition to the one cycle to failure region, it was shown that relay A fails the earliest at 70µF, whereas relays B and C consistently lasted for multiple cycles at that energy level. It should be noted that small sample sizes were

used in this study (5 or less) since the total number of relays provided for the batch of interest were limited in number and to acquire more from the manufacturer may have resulted in relays from a different production batch being mixed into the original samples. Relays from a different batch may produce signicantly different results so it was determined that it was not beneficial to add more samples that originate from outside of the original supply chain.

Table 7: Test Parameter Power and Energy Levels.

Voltage:	Capacitance:	Total Energy:	Energy to Relay	Total Power:	Power to Relay:	Resistance:	Time Constant
(Volts)	(micro Farads)	Joules	Joules	Watts	Watts	Ohms	Micro Seconds
250	10	0.3125	0.15625	3,125,000	1,562,500	0	0.1
250	50	1.5625	0.78125	3,125,000	1,562,500	0	0.5
250	70	2.1875	1.09375	3,125,000	1,562,500	0	0.7
250	80	2.5	1.25	3,125,000	1,562,500	0	0.8
250	90	2.8125	1.40625	3,125,000	1,562,500	0	0.9
250	100	3.125	1.5625	3,125,000	1,562,500	0	1

It should also be noted that not all of the energy and power from the capacitor is delivered to the relay. Any resistance besides the contact acts as a voltage divider circuit; so in order to determine the total resistance from connections and wires, the total resistance was measured using the HP DMM. It was determined that the total resistance was 0.01Ω, with 0.005Ω of this coming from the relay contacts, and the other 0.005Ω coming from the wire and connectors. With zero load resistance, as was the case in this test, the calculation for power and energy from the capacitor to the relay contacts is simple: the power and energy is halved. When external load resistance is added as is the case in later tests, the formula becomes more complex and reflects the ratio of contact resistance to total circuit resistance as shown in Appendix B. Since power is only dependent on voltage and resistance, it remains constant for each of the test parameters whereas total energy to the relay varies as a function of capacitance as shown in Table 7.

5.3 Discussion and Analysis of Results

It has been shown that relay A is most likely to fail on the first cycle at a lower total energy discharge than relays B and C. When the cycles to failure are plotted against the energy dissipated in the relay contacts, one can see the results follow a power law model of degradation as shown in Figure 33 & Figure 34.

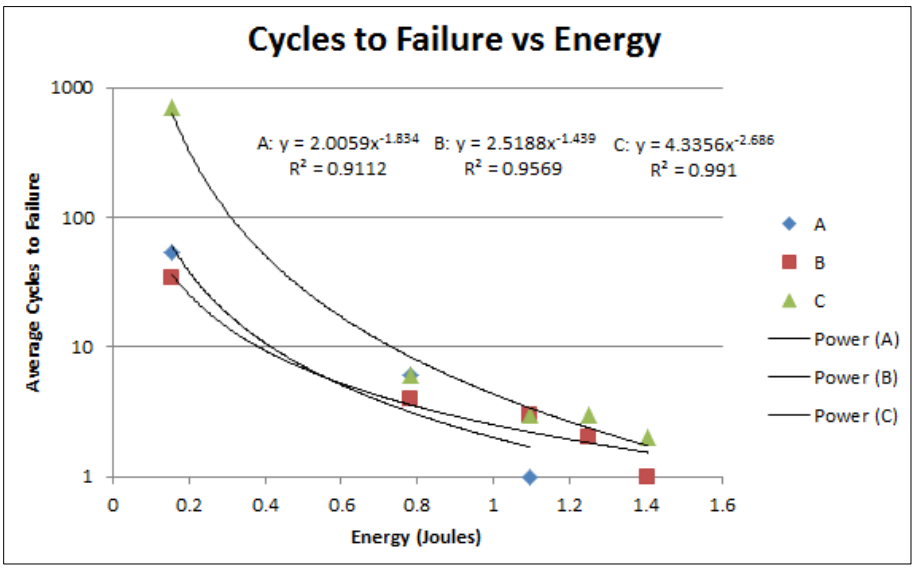

Figure 33: CTF vs. Energy semi-log scale.

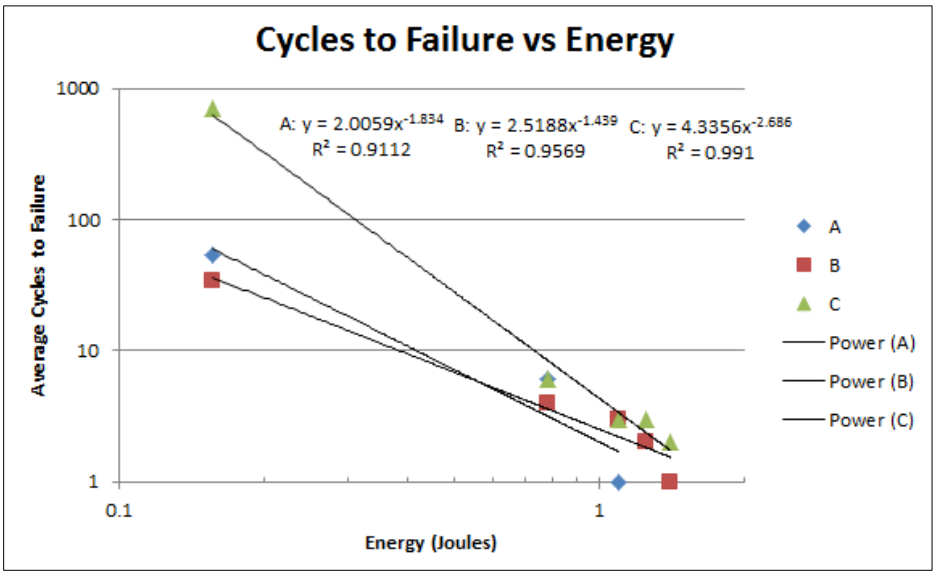

Figure 34: CTF vs. Energy log-log scale.

While the exponential time-to-failure (TF) model for stress was considered and is also a good curve fit for the data recorded, it is clear that at the 0.15J energy level corresponding to 10μF, the model begins to significantly underestimate the CTF. The exponential model does not match the failure behavior at low energy levels because the model is more conservative than the power-law model. Experimentally, the relays exhibited a higher TF sensitivity at the lowest energy levels which is not representative of the exponential model. For this reason, one would expect the difference in CTF between an exponential model theory and the experimental results to increase for low energies much more than the power-law. On the other hand, for the same reason that an exponential model is conservative at low energies, it will cross the one cycle to failure threshold at a smaller energy level than the power-law model, which may be a better projection at higher energies as shown in Figure 35. The power-law tends to overshoot the energy value that leads to one cycle failure because it approaches zero more slowly than an exponential function; however, while the exponential model predicts the single cycle failure energy value more accurately, it is still an invalid TF model because it does not match the CTF behavior at low energy and high cycle values.

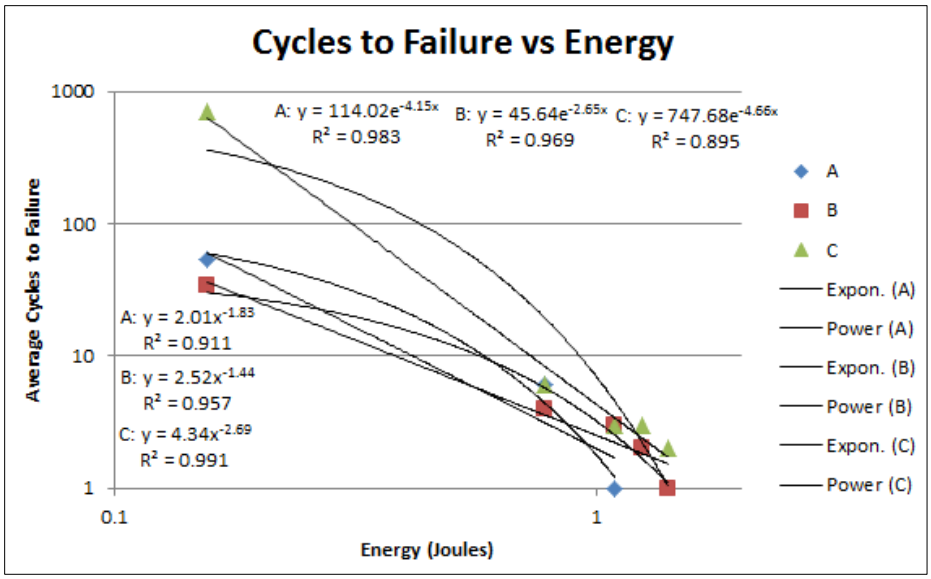

Figure 35: Power-Law vs. Exponential Comparison.

A power law time-to-failure model is given by equation 5.1 and an exponential time-to-failure equation is given in 5.2 [47]. A_0 and B_0 are material/device dependent prefactors that vary based on relay properties, material, and manufacturing process. The generalized stress is represented as ξ, n is the power-law exponent, γ is the exponential stress parameter, Q is the activation energy, K_B is Boltzmann's constant (8.62×10^{-5}eV/K) and T is temperature in Kelvin.

$$TF = A_0(\xi)^{-n}\exp(\frac{Q}{K_B T}) \tag{5.1}$$

$$TF = B_0 exp(-\gamma * \xi)\ \exp(\frac{Q}{K_B T}) \tag{5.2}$$

Since the temperature is held constant in all of the test conditions and is not a variable within the scope of this project, the $\exp(Q/K_B T)$ term is absorbed into A_0 and B_0. To calculate n and γ, one can use equations 5.3 and 5.4.

$$n = -\left[\frac{\partial lnTF}{\partial ln\xi}\right]_T \tag{5.3}$$

$$\gamma = -\left[\frac{\partial lnTF}{\partial \xi}\right]_T \tag{5.4}$$

The results from the data analysis are shown below in Table 8.

Table 8: Power and Exponential Law Constants.

	$A_0exp(Q/K_BT)$	n	$B_0exp(Q/K_BT)$	γ
A	114	4.2	2	1.8
B	45.6	2.7	2.5	1.4
C	747.7	4.7	4.3	2.7

What Table 8 shows is an empirical way of comparing the performance of each relay type. The intercept of the y = 1 value represents the energy required to achieve the single cycle weld condition and is based off of both the prefactor value and the slope n. It can be said that C > B > A with respect to single cycle weld behavior. Taking a look at the slope value n shows the sensitivity of each relay type to energy level with respect to failure time. This parameter shows that C > A > B for low energy high cycle failure. From this analysis, it can be determined that characteristics of relay C are desirable for both low and high energy cycling conditions, whereas the characteristics of relay A are undesirable for high energy conditions just like the characteristics of relay B are unsuitable for low energy cycling.

5.4 Conclusion

The manufacturer dependence of relay reliability has been shown in this chapter where relay A is most likely to fail at high energy levels on the first cycle at much lower levels (1.1J / 70μF) than relay B and C (1.4J / 90μF). Likewise, relay C survived much longer (696 cycles) at low energy levels (0.15J / 10μF) compared to both A and B (54 and 34 cycles). It was also shown that while keeping the power constant and referring to the total energy seen by the relay contacts as stress (ξ), the time-to-failure can be described by a power-law relationship. The power-law failure model showed a better representation of relay response to energy levels than other models, and it also gave a better estimate of cycles to failure at low energy levels where the CTF is very high; however, it had a tendency to overestimate the energy level at which one cycle failure occurred. The exponential model is more conservative, so for that reason it always underestimated the CTF at low energy levels and did not model the behavior at low energy very well; however, it did give a more accurate projection of the energy level at which one cycle failure occurred. Now that the reliability is shown to be manufacturer dependent, it is now necessary to investigate the characteristics of the relay which lead to these differences. The next chapter will address the manufacturer dependent differences by assessing material properties and design variations that make a relay more susceptible to welding failure. Using a physics of failure approach, the cause for relays A and B to perform poorly compared to C at low energy levels, and relays B and C to perform better than A at high energy levels will be addressed.

Chapter 6: Physics of Failure Analysis of Manufacturer Dependent Relay Reliability

This chapter addresses the material type and design differences between the three relays studied which result in manufacturer dependent relay reliability. The relays are examined using optical and scanning electron microscopy for evidence of arcing, welding, erosion, and other degradation mechanisms. The incidence and extent of degradation is then correlated to material characteristics including contact material, oxide content, hardness, sintered density, and surface roughness. Contact geometry and its effect on current density are also considered. Destructive and non-destructive techniques including wavelength dispersive spectrometry (WDS), x-ray diffraction (XRD), light optical microscopy and scanning electron microscopy (SEM) are used to conduct this relay characterization.

6.1 Relays Investigated in This Study

There were three relays investigated in this study, all of the SPDT type rated for 20A in the NO position.

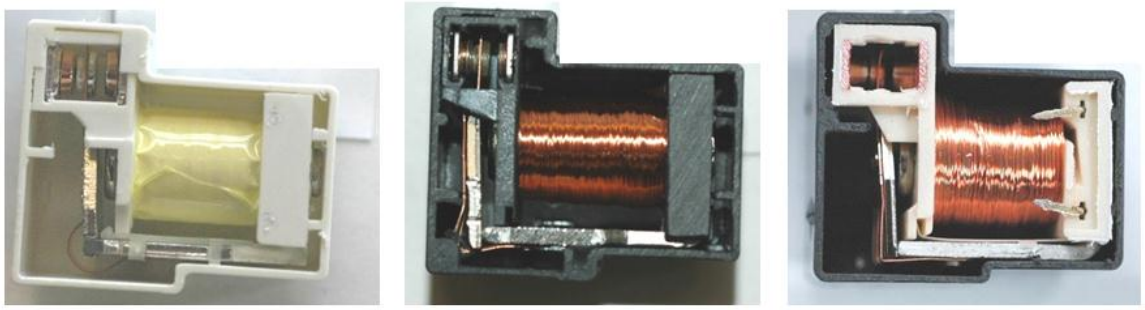

Figure 36: Relay A, B, and C from left to right.

Each relay is powered by a 12VDC electromagnetic coil. Relay A is rated for 240VAC whereas relays B and C are rated for 250 VAC. The reason for voltage rating differences

is unknown; however, it was shown in the previous chapter that relay A is more likely to weld at lower energy levels than relays B and C. This manufacturer dependent difference in reliability is the focus of this section and each property of the relay will be addressed based on its relationship to weld tendency.

6.2 Contact Size

To begin the relay contact comparison, each of the relays was decapsulated and the contacts removed in order to analyze material and design differences. The relay contact diameters were determined by using a ruler to measure the contacts shown in Figure 37 as well as by distance measurement using an optical microscope and image processing of the cross-sectioned contacts shown in the figures used in the next section (6.3) on contact geometry. The results are shown in Table 9 where relay A had the largest contact diameters which would lead one to believe it has a lower current density. At the same time, relay B and C have similar main contact diameters while relay C has the smallest secondary contact diameter of 3.2 mm. Since it is the relay curvature instead that determines current density and not the contact diameter, the curvature of the contacts is investigated next.

Figure 37: Relay contacts A (left), B (middle), and C (right).

Table 9: Contact diameter.

Relay	Main Contact Diameter (mm)	Secondary Contact Diameter (mm)
A	4.9	4.6
B	4.1	4.0
C	4.0	3.2

6.3 Contact Geometry

The radius of curvature is of particular interest because it determines the contact area and affects current density as seen from equations 2.1 and 2.4 where the effective radius of the contact area is based on the radius of curvature of both the primary and secondary contact. To determine the radius, the relay contacts were cross-sectioned and then photographed using optical microscopy. The photo was then input to MATLAB and points were selected along the edge of the contact curvature. These points then went into an algorithm that determines a best fit radius of curvature, then plots the radius based on the center point and radius determined by the program. The graphing verifies that the curve corresponds to the provided input points and more importantly the relay contact itself. The code for this program is provided in Appendix C and the results can be seen below in Table 10. Based on theory from equation 2.1, and assuming P and E are equal, one determines that relay B should have a contact area 270% larger than relay A, and relay C should have a contact area 350% larger than relay A. The actual measured contact areas are shown in the next section.

Table 10: Contact radius of curvature.

	A	B	C
Main Contact (NC)	10.9	7	10.4
Main Contact (NO)	9.8	9.3	10.5
Secondary Contact	13.3	flat	flat

The cross-sectioned contacts and curvature output is shown in the next six figures.

Relay A:

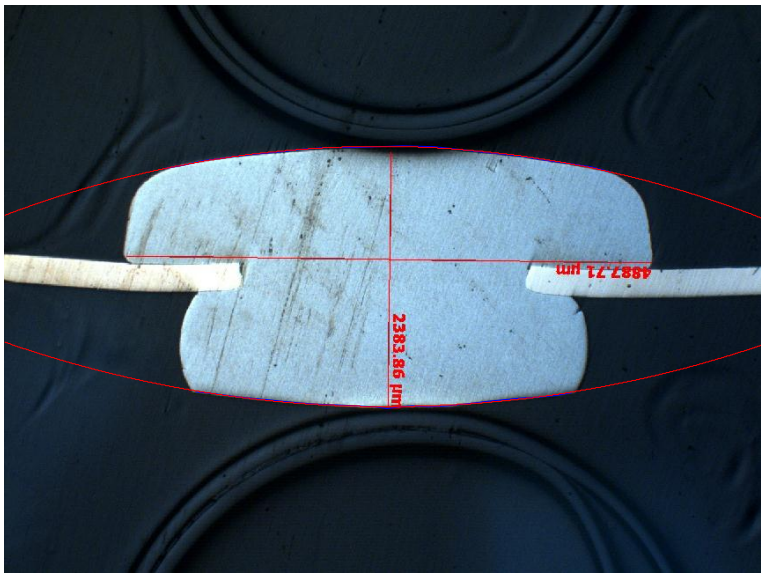

Figure 38: Relay A main contact where NO is the top side and NC is the bottom side.

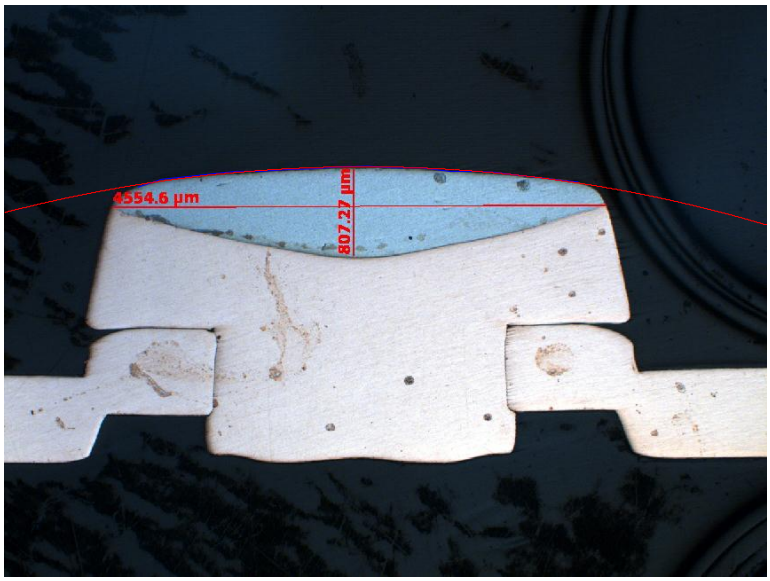

Figure 39: Relay A secondary contact.

Relay B:

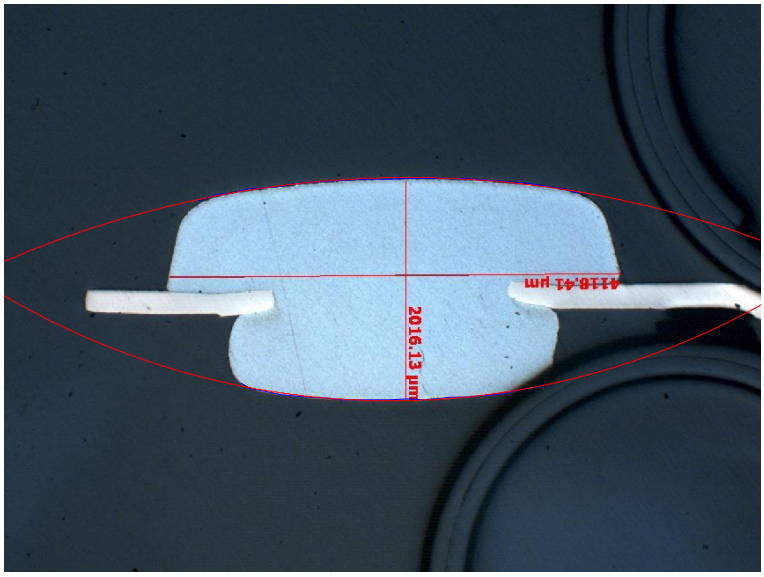

Figure 40: Relay B main contact with NO side on top and NC on bottom.

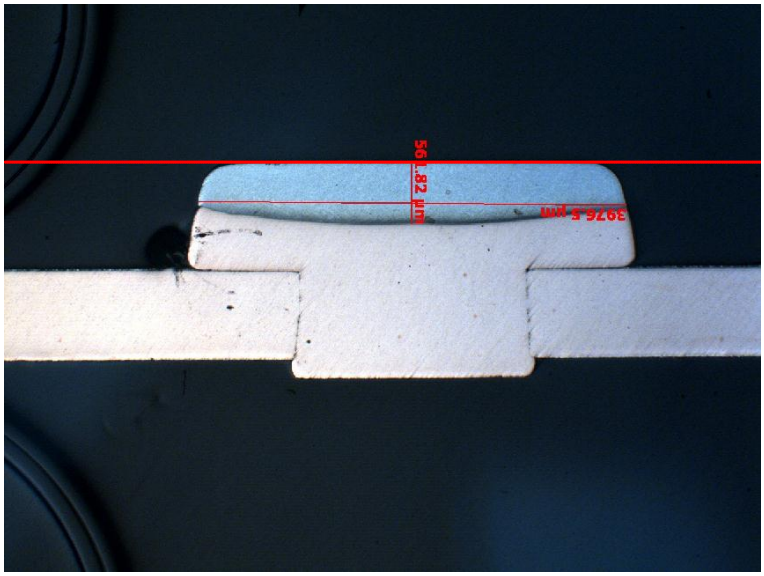

Figure 41: Relay B secondary contact.

Relay C:

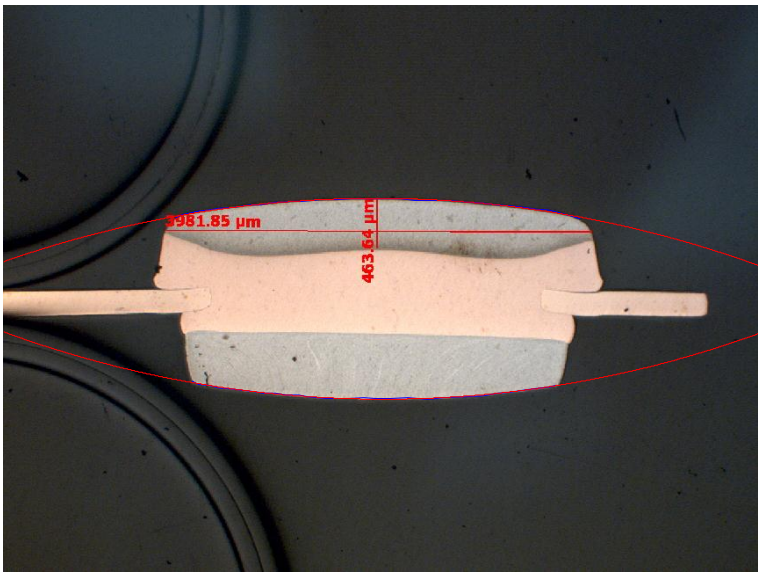

Figure 42: Relay C main contact with the NO side on top and NC on bottom.

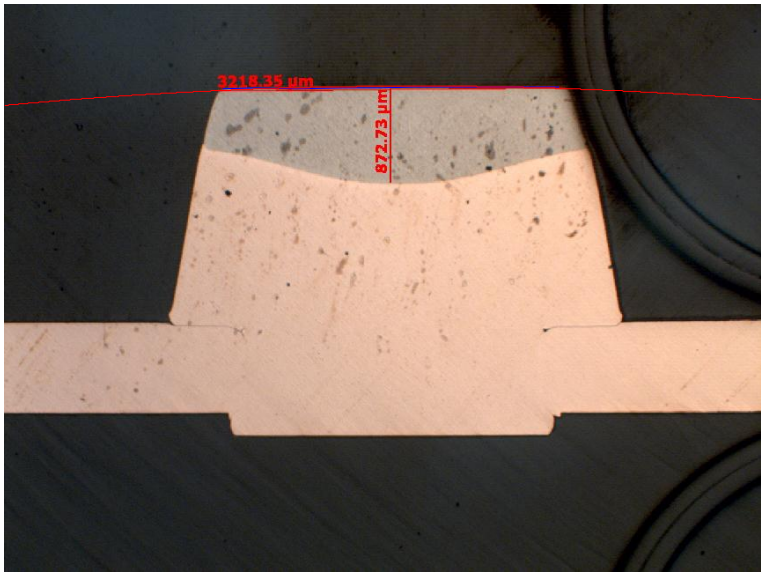

Figure 43: Relay C secondary contact.

Some differences to note among the main contacts are relays A and B are solid silver/tin oxide as seen in Figure 38 and Figure 40 whereas relay C is silver/tin oxide embedded on a copper interlayer shown in Figure 42. The main point to take away is that relay A has a

round secondary contact shown in Figure 39 whereas both relays B and C (Figure 41Figure 43) have flat secondary contacts which increase their contact area and reduce their current density, making them less susceptible to welding.

6.4 Contact Area

To measure the contact area, Ultra Low Fujifilm Prescale® Tactile Pressure Indicating Sensor Film was used with a pressure rating of 28-85psi/2-6kg/cm^2. The film was placed between the primary contact and secondary contact on the normally open side, and then a +12VDC potential was applied across the inductor coil to switch the relay. The film then leaves a red mark wherever pressure is applied, with a darker red indicating a greater pressure. The results from this study are shown below in Figure 44.

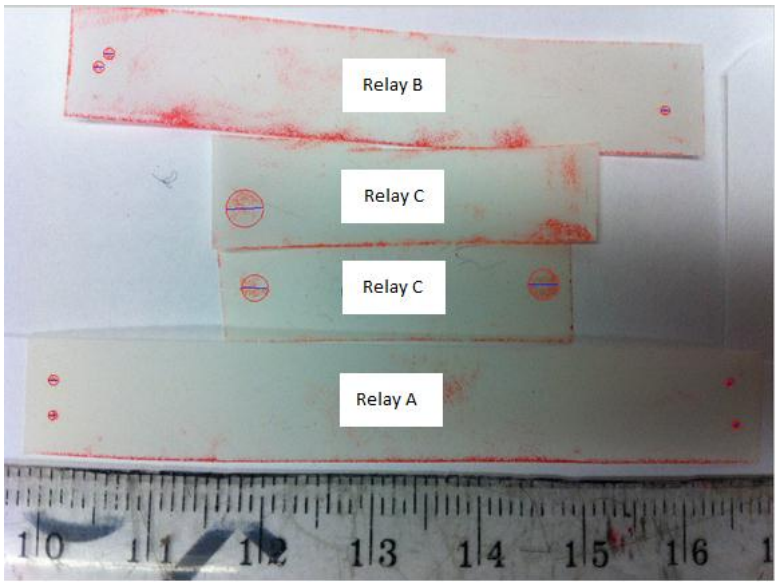

Figure 44: Pressure film results.

A MATLAB image processing code was written in order to determine the contact diameter and area shown on the pressure film. The code can be found in Appendix D, but, in short, one selects the edge of the contact area in order to determine the diameter.

The program then plots the circle and area corresponding to the input points in order to verify that the output matches up with the actual contact area on the pressure paper. The results are shown below in Table 11 where three runs of the same image are used in order to minimize the error from user input. Multiple samples were used to account for variability within the relay type, and the average of each is taken. The averages are shown in Table 12 where relay A had the smallest contact area, relay B had 125% more contact area than A, and relay C had 1377% more than relay A. It should be noted that because the area was so great for relay C, the pressure film did not record the contact area because a similar force over a much greater area greatly reduces the contact pressure. For this reason, an external force was applied to the contact in order for the film to register a high enough pressure to show the contact area; however, by doing so more deformation may have occurred resulting in an overestimated contact area. Nonetheless, a conservative estimate still says that relay C contact area is significantly greater than relay A and B.

Table 11: Results from MATLAB code.

	Trial 1	Trial 2	Trial 3	Row Average	Relay Average
A1	0.211	0.4772	0.541	0.4097	
A2	0.2896	0.4055	0.417	0.3707	
A3	0.4219	0.3304	0.3734	0.3752	
A4	0.4137	0.4055	0.4469	0.4220	0.3944
B1	0.457	0.5139	0.4996	0.4902	
B2	0.2896	0.5139	0.4583	0.4206	
B3	0.331	0.4038	0.4979	0.4109	0.4406
C1	1.4481	1.7269	1.7031	1.6260	
C2	1.324	1.2119	1.5441	1.3600	
C3	1.2826	1.3949	1.5357	1.4044	1.4635

Table 12: Contact radius and area.

Relay	Radius (mm)	Area (mm^2)	% Different
A	0.39	0.49	
B	0.44	0.61	125%
C	1.46	6.73	1377%

Contact area will greatly affect the current density which in turn has an effect on joule heating. A smaller contact area results in a higher susceptibility of welding as more heat is generated and the contacts are more likely to melt during operation. Contact area can also impact the relay resistance if a constriction is imposed.

6.5 Contact Resistance

Contact geometry and material have an effect on contact resistance where the resistivity is based on the bulk material properties, the constriction effect, and a possible film buildup on the contact. The contact resistance was measured using a 4-point probe and the averaged results can be seen below in Table 13.

Table 13: Contact resistance.

	Average (mΩ)	Stdev
A	4.8	0.412
B	3.6	0.821
C	3.6	1.384

Relay A had the highest resistance of 4.8mΩ whereas relays B and C had an average resistance of 3.6mΩ. Relay A is 134% more resistive than B and C, which again results in more joule heating at similar current levels. This makes relay A more susceptible to welding and matches the results presented in chapter 5.

6.6 Contact Material

All of the contacts are of the Ag/SnO_2 type; however, the composition of each varies by manufacturer. In order to determine the material type and percentage of each additive, energy dispersive spectrometry (EDS), wavelength dispersive spectrometry (WDS), and x-ray diffraction (XRD) are used. Because tin and indium have very similar K_α values of 25keV and 24keV respectively, EDS had difficulty distinguishing between the two elements. Figure 45 shows the point used in EDS analysis for relay C, and Table 15 lists the element weight% and atomic%. It can be seen that the listed Ag content is much less than that stated in the datasheet, and the EDS did not detect indium.

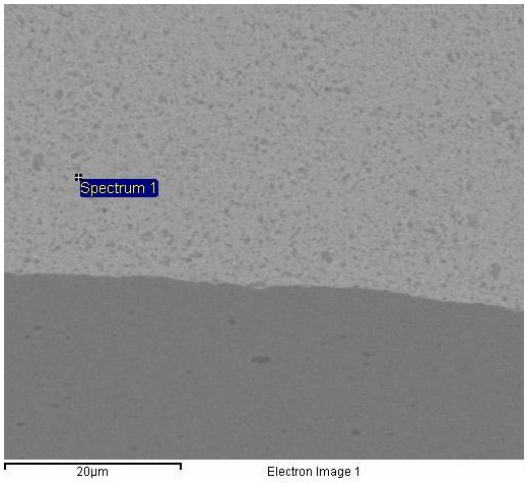

Figure 45: SEM image of Cu / AgSnO2 interface and EDS analysis point in relay C.

Table 14: Element type and % weight from EDS analyis.

Element	Weight%	Atomic%
O K	11.56	46.86
Cu K	1.59	1.62
Ag L	74.32	44.67
Sn L	12.53	6.85
Totals	100.00	

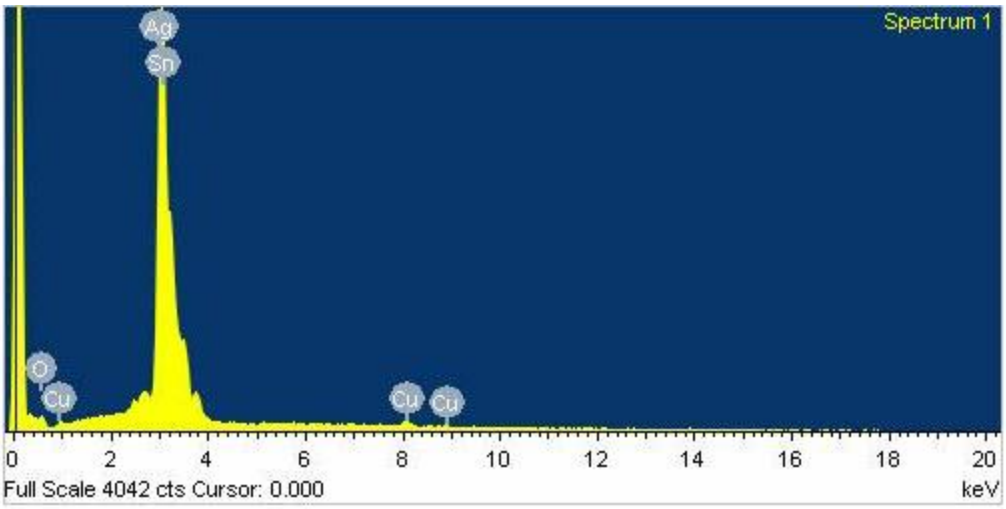

Figure 46: Ka peaks in EDS analysis of relay C.

Figure 46 shows the energy peaks that were detected, further illustrating how difficult it is for EDS to distinguish between In and Sn. Also, EDS cannot differentiate between metals and metal oxides. For this reason, XRD is used because it is capable of distinguishing elements based on their crystal structure by observing the scattered intensity of an X-ray beam after it hits a sample and reflects/absorbs/reemits the energy as a function of incident angle, scattered angle, polarization, and wavelength (energy). One problem with XRD is many elements and molecules have the same crystal structure, so one must know what they are looking for in order to get reasonable results with XRD. The initial results from XRD are shown in Table 15 which indicates the presence of Ag, SnO_2, and In_2O_3. A small amount of CdO was found in relay A only.

Table 15: XRD results in phase weight %.

	Intensity from Data column K x 100				Relative content calculated using *				Normilized content - Phase weight %			
	Ag1+Ag2	SnO2	CdO2	In2O3	Ag1+Ag2	SnO2	CdO2	In2O3	Ag1+Ag2	SnO2	CdO2	In2O3
Relay A main contact	86.1	2.0	0.4	0.0	30.36	0.40	0.04	0.00	98.6%	1.3%	0.1%	0%
Relay A secondary contact	141.8	10.1	1.5	0.6	50.00	2.00	0.15	0.40	95.1%	3.8%	0.3%	0.8%
Relay B main contact	118.2	5.6	0.0	2.4	41.68	1.11	0.00	1.60	93.9%	2.5%	0%	3.6%
Relay B secondary contact	111.8	4.3	0.0	2.5	39.42	0.85	0.00	1.67	94.0%	2.0%	0%	4.0%
Relay C main contact	123.9	0.9	0.0	3.0	43.69	0.18	0.00	2.00	95.3%	0.4%	0%	4.4%
Relay C secondary contact	104.5	1.7	0.0	2.6	36.85	0.34	0.00	1.73	94.7%	0.9%	0%	4.5%
* Relative content from XRD for Sample#2					50	2	0.15	0.40				
					2.836	5.05	10	1.5				

Again, the percentages of silver seem much higher than the suggested ASTM values of 92 silver/8 tin oxide, 90/10, and 88/12 [48]. For this reason, EPMA (WDS) is used to get accurate weight percentages since the electron probe microanalyzer has a library of calibration samples to attain much more accurate results. An electron microprobe JEOL JXA-8900 Superprobe was used as shown below in Figure 47.

Figure 47: EPMA used in material analysis.

In the WDS results, it was shown that the Ag content of all relays ranged from 83% to 87.3% and the total oxide percentage ranged from 12.4% to 16.1%. What is most interesting is relay A contains the most amount of tin oxide while the secondary contact of relay B contains the least. Also seen from Table 16 is relay A has very little indium

oxide present whereas relay C has the most in its primary contact and relay B has a significant amount in both its primary and secondary contacts.

Table 16: WDS average weight %.

	Ag	SnO2	In2O3	Cu	Total
Relay A main contact	83.0	16.0	0.1	0.1	99.2
Relay A secondary contact	83.0	14.3	1.6	0.1	99.0
Relay B main contact	84.0	10.5	4.5	0.0	99.0
Relay B secondary contact	85.5	8.9	4.2	0.1	98.7
Relay C main contact	83.7	10.9	5.2	0.1	99.9
Relay C secondary contact	87.3	12.3	0.1	0.0	99.8

As stated in the literature review, the primary benefit of indium is in assisting the internal oxidation during powder metallurgy production. It also acts as a wetting aid to the tin oxide particles, and the benefit of indium percentage can be seen though a drop in weld break force vs. oxide % in silver tin indium oxide contacts. What the material analysis shows is that while relay A has a high amount of oxide %, without the indium oxide to spread the tin oxide throughout the silver the contacts behave poorly during switching and are more susceptible to welding than contacts with higher levels of indium oxide. Relay B has an intermediate level of indium oxide %, and as shown in the constant power testing it performed between relays A and C. Lastly, relay C has the highest indium percentage and a high total oxide percentage of 16.1 % in its main contact, making it favorable for the conditions tested since it is more resistant to arc erosion and material transfer. While other factors are also important in determining a relay's susceptibility to weld, the indium and tin oxide percentages have a great effect on contact erosion and welding behavior.

6.7 Contact and Spring Hardness

The contact and spring hardness were measured for each relay using a microindenter. It was found that relay A has a soft main contact hardness and a higher spring hardness – the latter causes the spring to be more stiff. Relay B also has a soft contact hardness and a very high spring hardness. Lastly, relay C differs and has a higher contact hardness and softer spring hardness. The results are tabulated and shown below in Table 17.

Table 17: Contact and spring hardness.

	Main Contact Hardness	Spring Hardness
Relay A	117±2 HV0.1	217±4 HV0.1
Relay B	120±8 HV0.1	267±15 HV0.1
Relay C	135±4 HV0.1	197±2 HV0.1

The importance of contact and spring hardness is as follows: the contact hardness affects the amount of bounce when the contact closes. A higher hardness equates to a higher bounce whereas a softer contact will absorb more of the energy and not bounce as high. Furthermore, a higher spring constant will result in a higher opposition force to the magnetic inductor coil which results in a lower net closing force and reduced closing velocity. Based on this, a relay with a soft contact and hard spring will bounce at a lower amplitude than a relay with a harder contact and softer spring. To relate this to welding, it has been shown that short arcs are more susceptible to cause welds whereas long, slow arcs are less likely to cause welding. Relays A and B had softer contacts and higher spring hardness than relay C, and relay C demonstrated superior reliability at both low and high energy levels when compared to A and B.

6.8 Failure Analysis

Upon failure of the samples used in the constant power test, the relays were decapsulated and epoxied in order to investigate the weld region. Using the SEM, images were taken of the relays which were tested at 250V at 10μF, 50μF, and 70μF capacitance levels; however, a welded cross-section of 10μF was not obtained since the weld broke apart during decapsulation because the weld strength was much weaker than at higher energy levels.

6.8.1 10μF

This section shows the erosion damage and weld spots for the relays that welded under 10μF conditions. In order to get a baseline comparison of the degradation, unused contacts were examined and can be seen below in Figure 48.

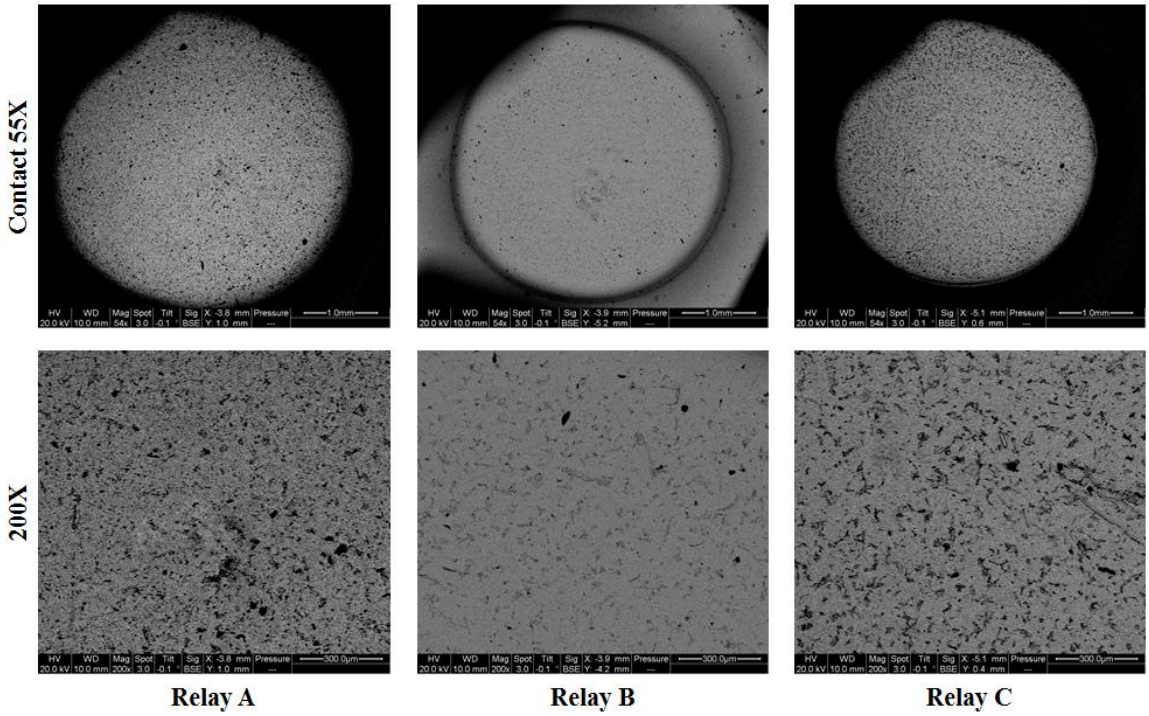

Figure 48: New/unused contact images.

One can see that relay A and C are more porous than relay B as seen by the dark spots in the 200X zoom images. After welding, it is clear that the surface of the contact changes drastically. Figure 49 shows the main and secondary contacts after welding. The most noticeable difference is the size in splash area; relays A and B have splash regions slightly less than 1mm, whereas relay C has a splash diameter of about 3mm, roughly taking up the entire face of the contact. It is known that arc erosion degradation is a function of cycles, so while relays A and B survived under 100 cycles before welding resulting in a small erosion splash spot, relay C survived over 1000 cycles and thus underwent more arc erosion.

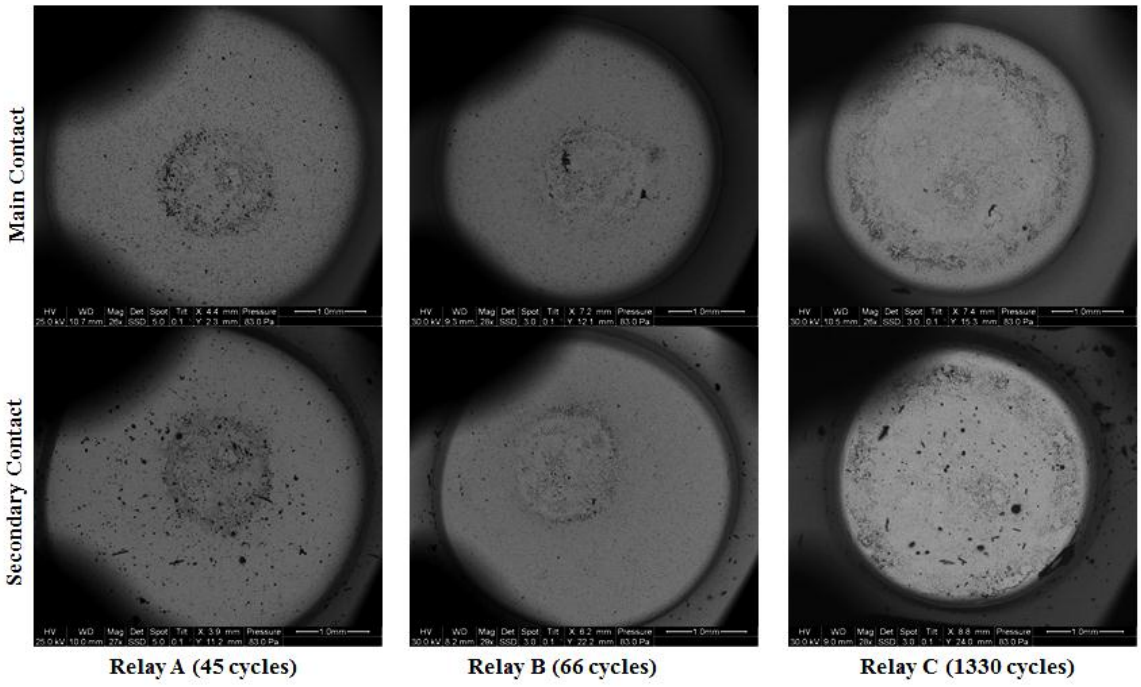

Figure 49: Main and secondary contact after welding.

It is interesting to note that while relay C underwent more cycles and arc erosion, it did not weld until a high number of cycles. This can be described as follows: long arcs from a high contact bounce melt the silver on the contact surface. When the contact returns to

the closed position, the closing velocity is much higher than for a short bounce, and the high closing force displaces the molten silver away from the contact point radially, resulting in arc erosion splash. This is the case in relay C where the splash region is very large – remember that relay C has hard contacts and a soft spring resulting in high amplitude bounces and greater closing velocity. Since the silver is displaced before it has a chance to solidify, the likelihood of welding is much lower. On the other hand, short arcs are more damaging because the closing velocity is much less because of the shorter amplitude, so less silver is displaced from the contact area upon closure and when it solidifies welding occurs. The weld region can be seen in the top row of images in Figure 50 and the splash area boundary can be seen in the bottom row. The pips and craters in the contact spots are visible and a large weld region in relay C stands out.

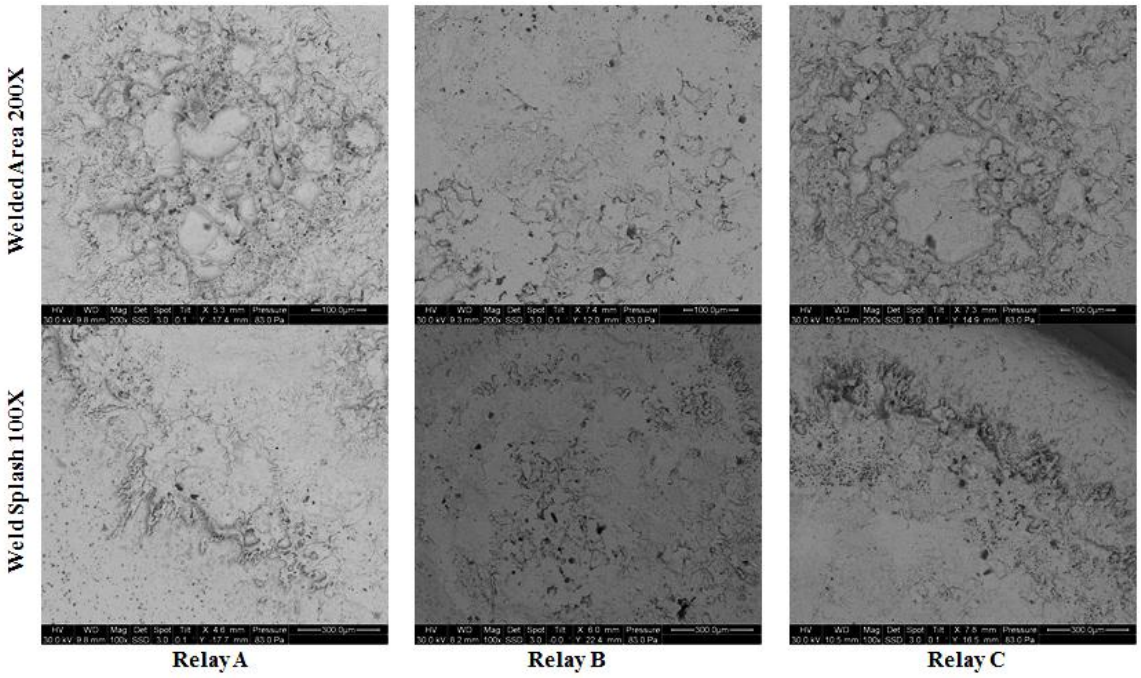

Figure 50: Weld region and splash area.

6.8.2 50μF

This section shows the welded samples at 50μF after they were epoxied and cross-sectioned. Figure 51 shows an overview of each of the relay contacts at 2.5X as well as a 10X overview of the weld interface. One can see that relay A has the longest weld length of about 1.4mm, relay B is in the middle at 1.0mm, and relay C has the smallest weld length at around 400μm.

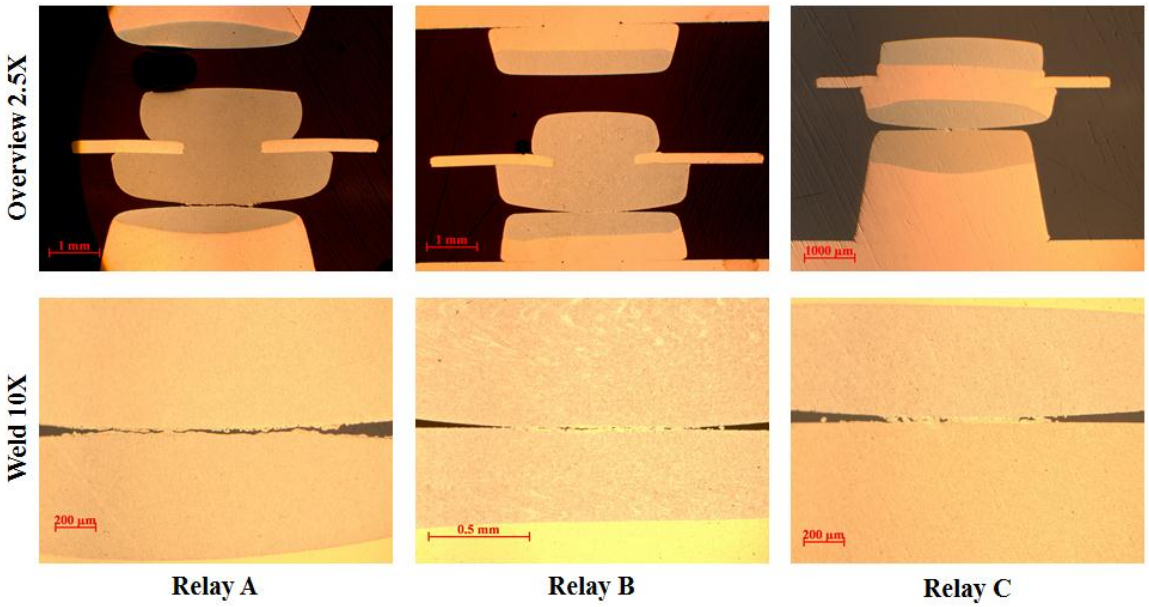

Figure 51: Overview of weld section.

Other differences to note are the uniformity of the weld: relay A has a less uniform weld with many voids, whereas relay C has a very solid weld with no gaps. Relay B is in-between the two where it is mostly uniform but has some small gaps at the interface between the main and secondary contact. These results can be seen in Figure 52 on the next page. Also notable is the color change at the weld interface, suggesting a change in material composition compared to the bulk contact material. In order to investigate this, a

line scan using EPMA was run perpendicular to the weld and will be discussed later in this chapter.

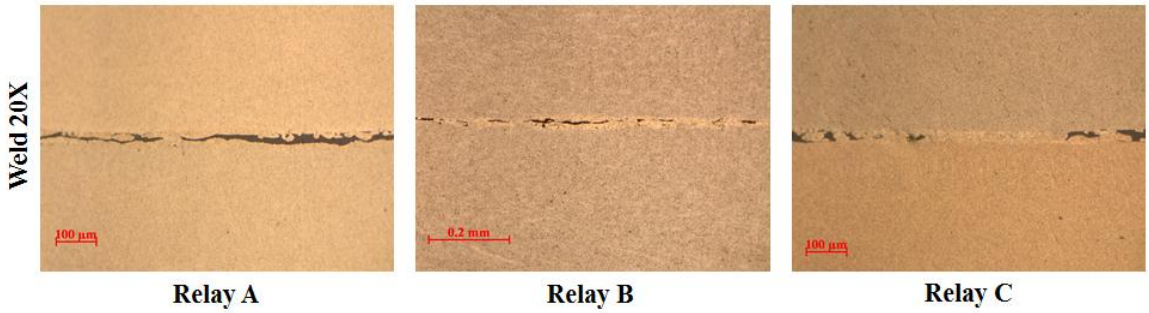

Figure 52: Close up of weld at 20X.

6.8.3 70µF

The last group of photos taken using the optical microscope shows the weld at 70µF. These load conditions were great enough to result in first cycle welding where 80% of the relays in group A failed after one cycle, and at least one relay in groups B and C failed in one cycle as well. The overview of the weld is shown below in Figure 53.

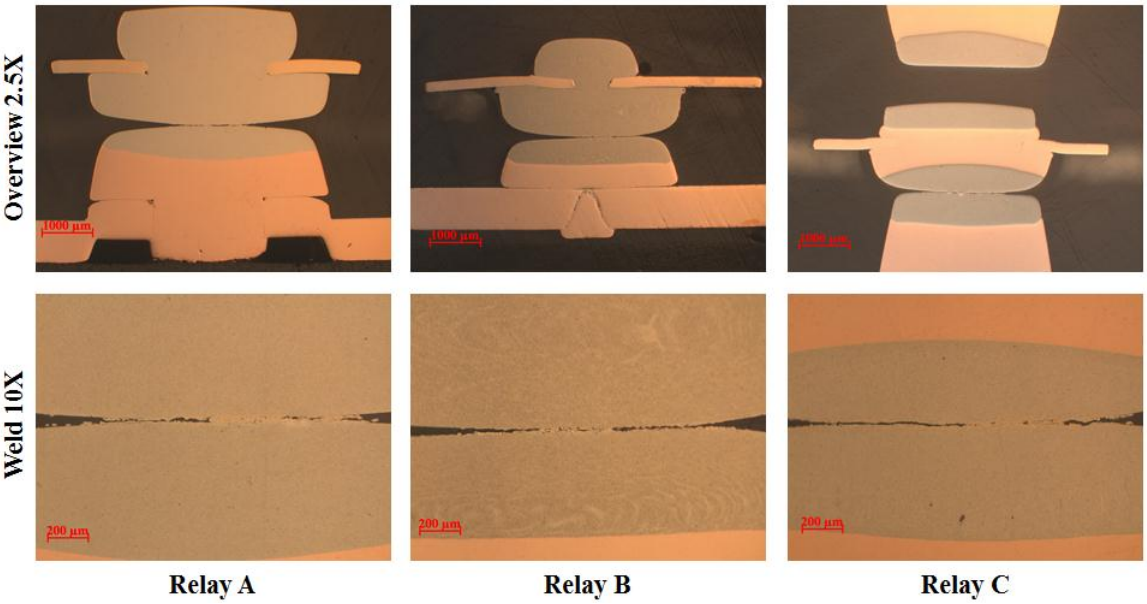

Figure 53: Contact and weld overview.

Compared to the welds at 50µF, it is evident that the weld length has increased due to the higher amount of energy and longer arc duration that comes with the additional 20µF at the 70µF test conditions. The weld in relays A and B is about 1.4mm in length, and the weld in relay C has increased to 1.6mm.

Other notable comparisons include the uniformity of the welds – now that there is enough energy to melt enough silver to form a stronger weld, relay A now sees a more uniform weld than at lower energy levels. Relay B is more uniform but still with some voids, and relay C is similar in uniformity to 50µF conditions. This can be seen in Figure 54 below which gives a close-up 100X image of the weld. Due to surface roughness, not all points were in contact during contact make operation, likewise the melted silver does not form a perfect connection between the primary and secondary contacts. Instead, small voids are present as evident in the 100X image in Figure 54.

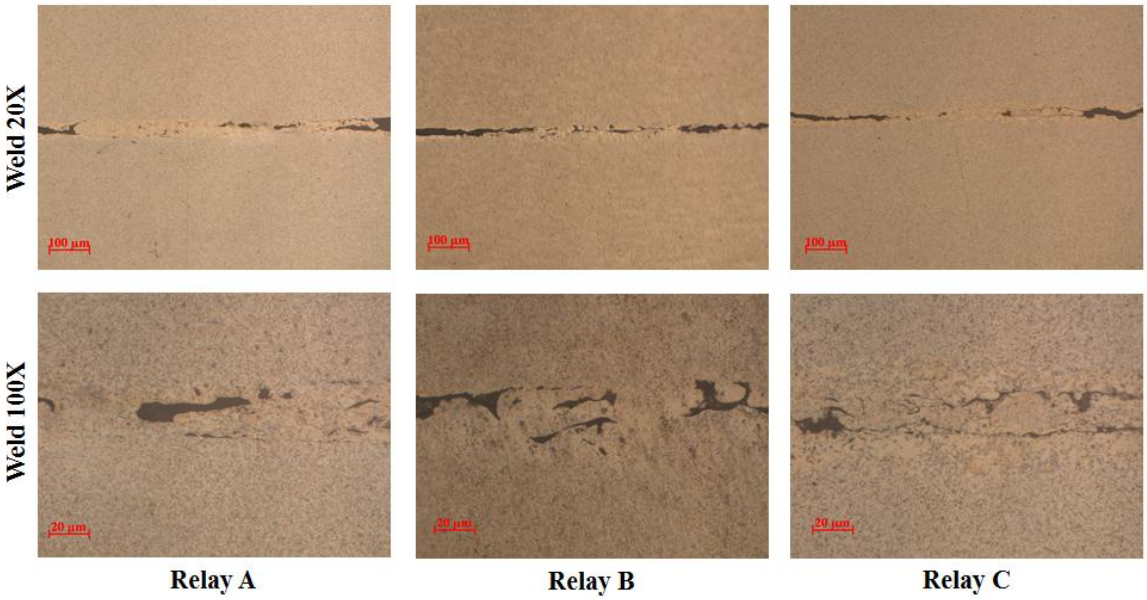

Figure 54: Weld interface at 20X and 100X.

6.8.4 EPMA Line Scan Across Weld Interface

Silver has a lower melting temperature of around 960°C compared to tin oxide which melts around 1630°C. For this reason, the silver melts to form the weld region. During an EPMA line scan, it was shown that the content of silver was significantly less at the weld interface, which can be seen in Table 18 and Table 20. The interface in relay B was much harder to detect (Table 19); however, some points reached peak total metal oxide levels of 19% - far higher than the average of 15% for the primary contact and 13.1% for the secondary. Likewise, relay A saw a peak of 22.8% metal oxide and a minimum of 76.4% Ag compared to averages of 16 and 83% respectively. Lastly, relay C had a peak metal oxide content of 23.2% and a minimum value of silver of 75.7% compared to averages of 16.1% and 83.7%. This shows that the silver is melting at the weld spot and is being forced away from the center of the weld upon closure of the contacts. The arc erosion from the 10μF case verifies this theory.

Table 18: EPMA line scan of relay A weld region.

Cu	In2O3	Ag	SnO2	Total	Comment
1.56	0.06	80.44	16.53	98.59	Line 1
2.48	0.07	79.41	17.21	99.17	Line 2
0.88	0.07	82.15	16.96	100.05	Line 3
1.49	0.07	81.65	15.82	99.03	Line 4
4.30	0.11	77.75	16.84	99.00	Line 5
1.22	0.09	75.34	22.70	99.35	Line 6
1.42	0.07	79.46	18.39	99.33	Line 7
2.43	0.11	80.78	15.75	99.08	Line 8
1.39	0.07	80.09	18.13	99.68	Line 9
0.81	0.10	76.84	22.74	100.49	Line 10
0.69	0.37	78.80	16.63	96.49	Line 11
1.89	1.29	80.34	15.25	98.77	Line 12
2.10	1.67	80.43	14.64	98.84	Line 13
1.19	1.76	77.66	15.03	95.63	Line 14
1.49	1.27	80.00	17.73	100.49	Line 15
1.51	1.31	78.85	15.64	97.31	Line 16
1.36	1.12	78.55	18.13	99.16	Line 17
7.12	0.86	76.83	16.68	101.48	Line 18
1.35	1.51	79.47	17.54	99.87	Line 19
1.95	1.58	82.01	12.99	98.53	Line 20

Table 19: EPMA line scan of relay B weld region.

Cu	In2O3	Ag	SnO2	Total	Comment
0.00	4.90	83.27	10.92	99.09	Line 1
0.01	3.38	86.61	9.24	99.24	Line 2
0.00	4.30	84.02	10.34	98.65	Line 3
0.16	4.38	84.28	9.46	98.29	Line 4
0.00	6.87	80.39	11.99	99.25	Line 5
0.00	3.67	84.00	9.14	96.81	Line 6
0.00	4.05	85.86	7.91	97.82	Line 7
0.00	4.32	84.48	10.98	99.78	Line 8
0.15	4.92	84.49	10.06	99.62	Line 9
0.11	4.98	83.24	11.14	99.47	Line 10
0.00	3.24	86.16	6.34	95.75	Line 11
0.18	3.16	88.04	7.11	98.50	Line 12
0.15	6.75	81.30	10.44	98.63	Line 13
0.00	3.41	86.12	8.89	98.42	Line 14
0.00	2.96	88.92	6.46	98.34	Line 15

Table 20: EPMA line scan of relay C weld region.

Cu	In2O3	Ag	SnO2	Total	Comment
0.15	7.12	81.42	11.77	100.46	Line 1
0.03	4.75	84.15	10.89	99.82	Line 2
0.16	5.12	82.67	11.44	99.39	Line 3
0.11	5.94	81.93	11.79	99.77	Line 4
0.00	5.09	83.97	10.04	99.11	Line 5
0.25	3.91	84.90	9.27	98.33	Line 6
0.02	5.13	83.39	11.08	99.62	Line 7
0.02	5.15	84.27	11.13	100.58	Line 8
0.01	5.14	83.47	12.10	100.72	Line 9
0.00	4.26	84.59	9.88	98.73	Line 10
0.07	7.03	75.72	16.18	98.99	Line 11
0.20	7.30	77.28	14.52	99.30	Line 12
0.00	0.41	85.37	14.37	100.14	Line 13
0.00	0.11	86.26	13.75	100.12	Line 14
0.00	0.10	90.58	7.37	98.05	Line 15
0.06	0.07	87.22	12.09	99.45	Line 16
0.04	0.05	88.81	10.37	99.27	Line 17
0.09	0.09	86.90	12.71	99.79	Line 18
0.00	0.13	87.52	11.94	99.59	Line 19
0.08	0.07	85.90	14.62	100.68	Line 20

6.9 Correlations to Welding

After the material analysis and relay characterization, one can begin to explain the manufacturer dependent reliability differences between relays by correlating the characteristics and their effect on the susceptibility of welding. Based on the parameters covered in this chapter, the following influences have been determined:

- Relay cycles to failure correlate to capacitance (energy level).
- Higher cycles to failure result in rougher contact surface profile and more material splash (arc erosion).

- Contact diameter is not as important to welding as contact interface area and radius of curvature.
- Contacts with less curvature increase the interface area (a-spot) and decrease the current density improving the weld resistance.
    - Relay A had the smallest contact area and a curved secondary contact.
    - Relays B and C had flat secondary contacts resulting in more contact area.
- Contacts with lower electrical resistance decrease Joule heating at the contact interface thus improving weld resistance.
    - Relay A contacts are 34% more resistive than relays B and C.
- Higher concentrations of indium oxide appear to improve relay reliability.
    - Very low concentrations in relay A.
    - Higher levels in relays B and C.
- Contacts with higher hardness create a larger bounceback – this long arc is less likely to cause a weld than a short arc.
    - Relay A and B have softer contact hardness and higher spring hardness causing a short bounce.
    - Relay C has a harder contact hardness and soft spring hardness resulting in longer bounces.
- Variation in data is based on the randomness of the number of contact spots, spot size, volume of melted pool, and the cooling rate of melted pool.

6.10 Conclusion

In this chapter, the influence of contact geometry, interface area, resistance, material composition, and hardness on welding susceptibility has been shown. Correlations based on these results have been made to explain the manufacturer dependent relay reliability which suggest that relay A has certain characteristics that make it less reliable than relay C. To reiterate what has been found, contact geometry affects the contact interface area (a-spot) and thus influences susceptibility to welding. A larger contact area has a lower current density and in turn experiences less Joule heating. Also, a higher contact resistance will result in more heat generated under similar currents during Joule heating – again making a relay more susceptible to weld. Relay A had rounded secondary contacts which made the contact area much smaller than those of relays B and C. Furthermore, relay A was 34% more resistive than B and C. Beyond geometry, the material composition of the relays is very important to reliability, where it has been shown that higher concentrations of indium oxide appear to improve relay reliability. This is because indium assists the internal oxidation during powder metallurgy production and also reduces the weld break force as oxide levels are increased in silver tin indium oxide contacts. Material studies show that relay A has the least amount of indium oxide present while B and C have much higher values. Lastly, it was demonstrated that relays with a higher contact hardness and softer spring hardness are likely to have longer bounces which result in arcs with a higher closing velocity. From these conditions, any melted silver is forced away from the contact area upon closure (arc erosion splash) and is less likely to weld than a short amplitude bounce with a short arc duration. Relays A and B had softer contacts and harder springs which result in a lower amplitude bounce and short arc duration. When the silver melts, it is not squeezed out from between the contacts

nearly as much as a higher amplitude bounce with a faster closing velocity, so instead the silver has time to cool and solidify. This results in a greater likelihood of welding and stronger weld strengths than longer arc durations. From these correlations, one can explain why relay A was the first to reach the one cycle to failure region and relays B and C had greater reliability. More so, the analysis gives understanding to why relay C was capable of withstanding many more cycles at lower capacitance values than relays A and B.

Chapter 7: One Cycle Weld Failure Interface

The final focus of this research is the investigation of one cycle weld failure. No previous study has been performed on the electrical load parameters that result in relay weld failure on the first cycle. This is of importance because it is a failure mode that has been documented in standby power supplies. In order to investigate this failure mode further, the test setup was modified to change total power and energy levels by varying voltage, resistance, and capacitance. This chapter presents the test methodology and results; and concludes with a discussion of the results.

7.1 Test Methodology

The purpose of this test is to find the boundary in power and energy space between single cycle weld failure and multiple cycle weld failure for relay A. During the constant power test, this interface occurred at 70μF or 1.09J of energy to the relay. This testing was performed at 250V, so in order to increase the total energy one must increase the voltage or capacitance as shown in equation 7.1. Furthermore, to increase power one must increase voltage or decrease total resistance, but since most testing was done with no external load resistors, reducing the total resistance below just the contact and wire resistance was not an option.

$$W_{total} = \frac{1}{2} C V^2 \tag{7.1}$$

$$P_{avg} = \frac{V^2}{2R_{total}} \tag{7.2}$$

Assuming $R_{contacts} = 0.005\Omega$ and $R_{wires} = 0.005\Omega$

$$W_{contacts} = \frac{1}{2} CV^2 \frac{R_{contacts}}{R_{wires} + R_{load} + R_{contacts}} \quad (7.3)$$

$$P_{contacts} = \frac{V^2}{2R_{total}} \frac{R_{contacts}}{R_{wires} + R_{load} + R_{contacts}} \quad (7.4)$$

Equations 7.3 and 7.4 show the energy and power going to the contacts, not to be confused with the total energy and power of the circuit shown in equations 7.1 and 7.2. Since the circuit consists of a few components in series, the current remains the same and for this reason it acts as a voltage divider circuit. The power and energy are both proportional to the contact resistance, which for relay A is about 5mΩ, and the total resistance which includes the relay contacts, wires, and any external load resistors.

Knowing that at 250V and 70μF relay A failed at one cycle, one would expect if power went up, the total energy required to make the relay fail would likely go down or stay constant. Conversely, if the power goes down one would expect a longer pulse duration and a greater amount of energy would be required to weld the relay. For this reason, one set of points was tested at 100V with a 0.11Ω resistor in the load to reduce the power while increasing the energy seen by the relay. This group is shown by the red squares in Figure 55. Additional testing was done at 350V and 450V with the thought that less energy would be required; however, more test points were added to 450V after the one CTF region was not reached. The 350V and 450V test points are shown by green triangles and blue Xs respectively. Lastly, the other test points correspond to the 100V capacitor at different voltages – the uppermost point is at 100V and the bottom left one corresponds to 16V. A detailed list of all test point information can be seen in Table 21.

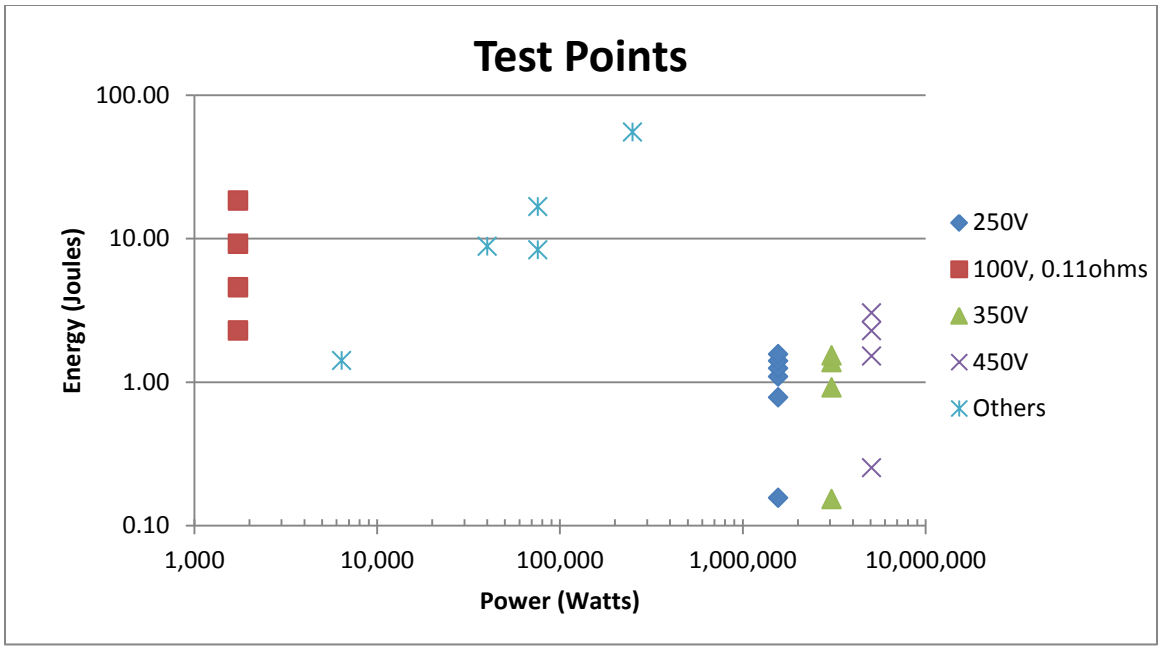

Figure 55: Test points used in one cycle to failure testing.

Table 21: Test point parameters used in one cycle failure testing.

Voltage:	Capacitance:	Total Energy:	Energy to Relay	Total Power:	Power to Relay:	Resistance:	Time Constant
(Volts)	(micro Farads)	Joules	Joules	Watts	Watts	Ohms	Micro Seconds
250	10	0.31	0.16	3,125,000	1,562,500	0	0.1
250	50	1.56	0.78	3,125,000	1,562,500	0	0.5
250	70	2.19	1.09	3,125,000	1,562,500	0	0.7
250	80	2.50	1.25	3,125,000	1,562,500	0	0.8
250	90	2.81	1.41	3,125,000	1,562,500	0	0.9
250	100	3.13	1.56	3,125,000	1,562,500	0	1
100	11000	55	2.29	41,667	1,736	0.11	1320
100	22000	110	4.58	41,667	1,736	0.11	2640
100	44000	220	9.17	41,667	1,736	0.11	5280
100	88000	440	18.33	41,667	1,736	0.11	10560
350	5	0.31	0.15	6,125,000	3,062,500	0	0.05
350	30	1.84	0.92	6,125,000	3,062,500	0	0.3
350	45	2.76	1.38	6,125,000	3,062,500	0	0.45
350	50	3.06	1.53	6,125,000	3,062,500	0	0.5
450	5	0.51	0.25	10,125,000	5,062,500	0	0.05
450	30	3.04	1.52	10,125,000	5,062,500	0	0.3
450	45	4.56	2.28	10,125,000	5,062,500	0	0.45
450	60	6.08	3.04	10,125,000	5,062,500	0	0.6
55	22000	33.28	16.64	151,250	75,625	0	220
16	22000	2.82	1.41	12,800	6,400	0	220
100	22000	110.00	55.00	500,000	250,000	0	220
40	22000	17.60	8.80	80,000	40,000	0	220
55	11000	16.64	8.32	151,250	75,625	0	110

7.2 Test Results

The same points are shown below in Figure 56 indicating their cycles to failure.

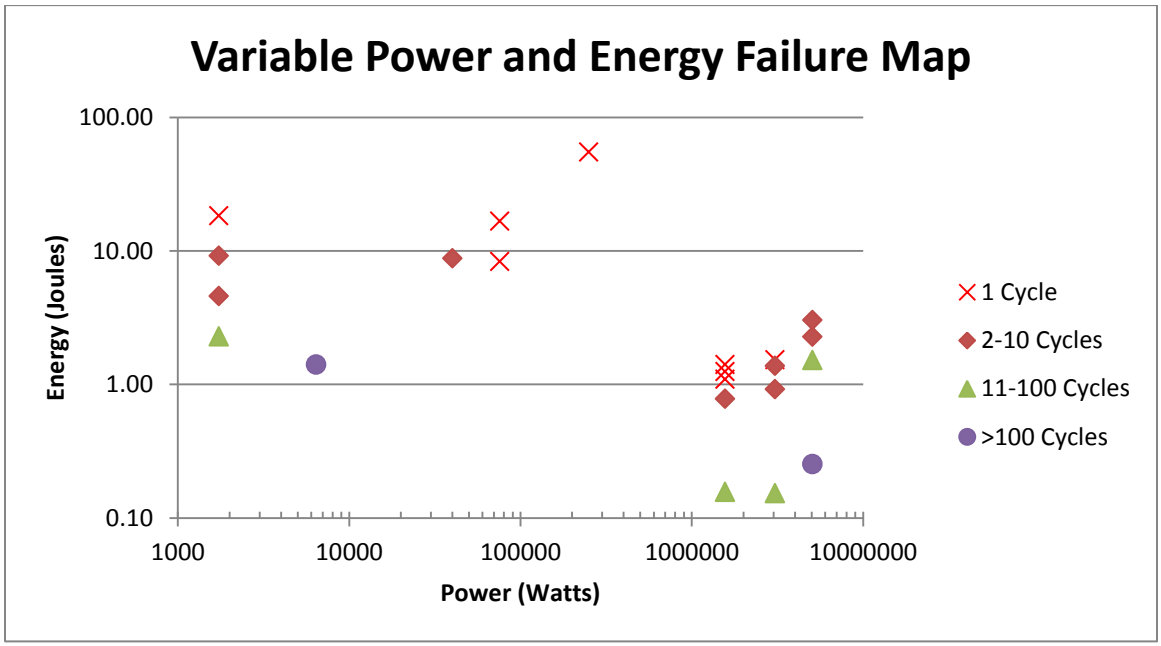

Figure 56: Variable Power and Energy Failure Region Map.

From Figure 56, one can see that as power was increased from the 250V test condition with a power of 1.5MW up to 350V with a power of 3MW, the energy required for a single cycle failure went up. Furthermore, at 450V or 5MW, relay A did not fail at the same energy conditions which caused it to fail on the first cycle at lower power levels. The test points between 2kW and 1MW were conducted with the 100V, 22000µF capacitor by varying the voltage to get different power and energy levels. The red diamond at 40kW is close to the 1 CTF interface and corresponds to 40V. First cycle failure was seen at 55V, or 75kW. Interestingly, when the total energy was halved to 8.32J by halving the capacitance, first cycle failures were still experienced. By adding a resistor into the circuit as is the case with the lowest power level at 1.7kW, first cycle welding was not experienced until a total capacitance of 88,000µF was used, equating to

440J in the total circuit, 18.33J of which actually make it to the relay. The results for each group are broken down and explained as a constant power test at different power levels. At the end of this section, test points of similar energy are compared to understand the relationship between power, energy, and cycles to failure.

7.2.1 250V Test –1.5MW Power

The results of relay A from the multiple relay reliability comparison are shown again to serve as a baseline comparison to the other test points. It can be seen from Figure 57 that the CTF goes down as a function of total energy, and the system closely matches an exponential curve for high energies and CTF below 10. The exponential curve more accurately predicts the energy level at single cycle failure because it is more conservative than the power-law model; however, a power-law model is more accurate in predicting higher cycle degradation failure and is an overall better fit when looking at failure behavior over a wide energy range.

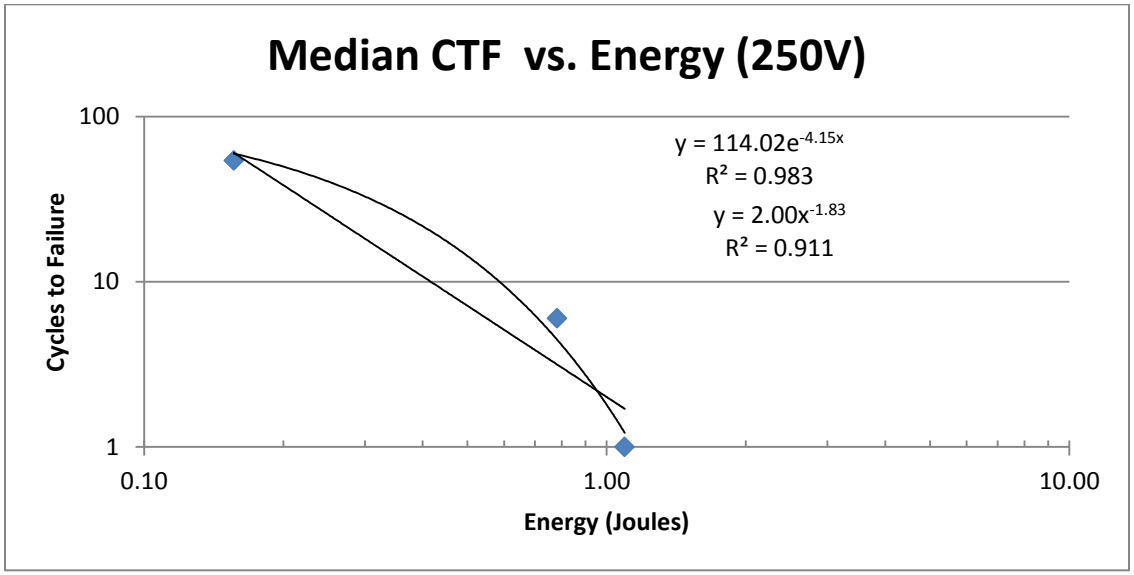

Figure 57: CTF vs. Energy for 250V, 1.5MW.

At 1.5MW, first cycle failure was seen at 1.1 Joules of energy.

7.2.2 350V – 3.0MW

By raising the voltage to 350V, the power is substantially increased to 3.0MW. Again, at energy levels of 0.15J, 50 or more cycles are required to fail the relay. In fact, the CTF at this level went up compared to the 1.5MW test condition. This is likely due to a smaller time constant because the 250V test used a 10µF capacitor and the 350V test used a 5µF capacitor to reach the same energy level of 0.15J. This equates to the time constant dropping from 0.9µs to 0.45µs. Also seen in Figure 58 the relays begin to consistently fail after the first cycle when the energy reaches 1.5J which equates to 50µF. Again, the curve can be fit to an exponential model; however, the γ value, or exponential stress parameter, is different than at 2.5MW / 250V suggesting a power level effect on this parameter.

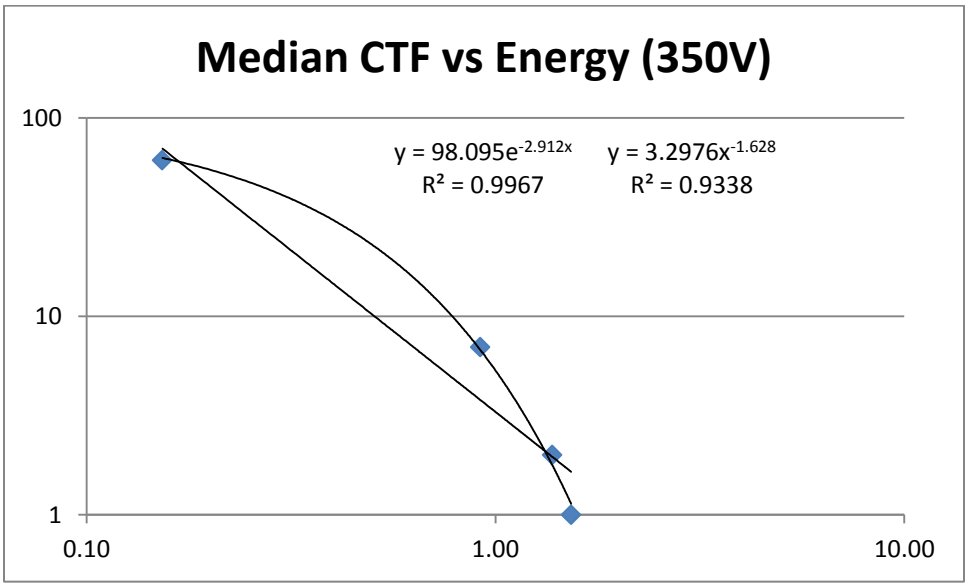

Figure 58: CTF vs. Energy for 350V, 3.0 MW.

7.2.3 450V – 5MW

Continuing to an even higher power level of 5MW, one can see the curve trends more towards a power-law model than exponential since the CTF is around 10 cycles or more

at each energy level test. As shown in Figure 59, at the exponential slope, one would expect the single cycle failure energy level to be around 4J; however, using the power-law model one would expect energy of 10J to fail relay A on the first cycle. Since the voltage is much higher, less capacitance is required to achieve equal energy at lower power levels because voltage has a squared effect on total energy while capacitance has a linear effect. This means that for similar energy levels, the pulse duration is much less at high power levels and this may have an effect on welding since the arc time greatly affects the amount of silver melted at the contact surface.

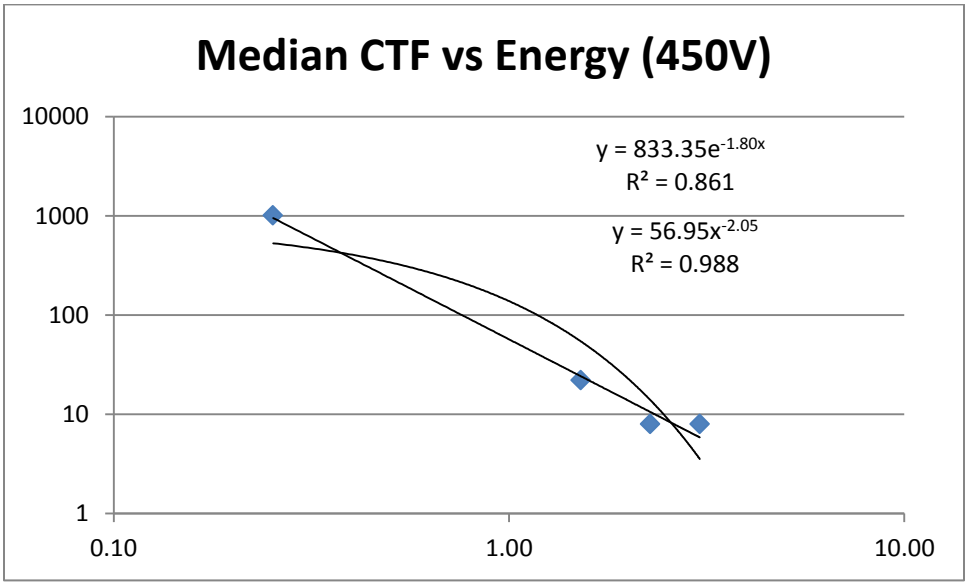

Figure 59: CTF vs. Energy for 450V, 5.0MW.

7.2.4 100V 0.11Ω – 1.7kW

At the lower end of the power spectrum, one would expect the cycles to failure to be much greater, even at high energy levels. At 2.29J, relays survived up to about 100 cycles – at much greater power levels a total energy of only 0.3J had similar results. While the curve does not fit either a power-law or exponential model as well as other tests (Figure

60), this may be an effect of adding a load resistor to reduce the power level as well as the use of electrolytic capacitors instead of film capacitors which were used in every other test (film capacitors are not cost effectively available in such high capacitances of 22,000-88,000μF). Despite this, one can still determine the one cycle failure interface lies between 20J and 30J depending on whether the exponential or power-law model is used as a predictor. It should be noted that one sample did fail after the first cycle at 18.33J, and all samples failed in five or less cycles, so the first cycle failure region is very close to that condition.

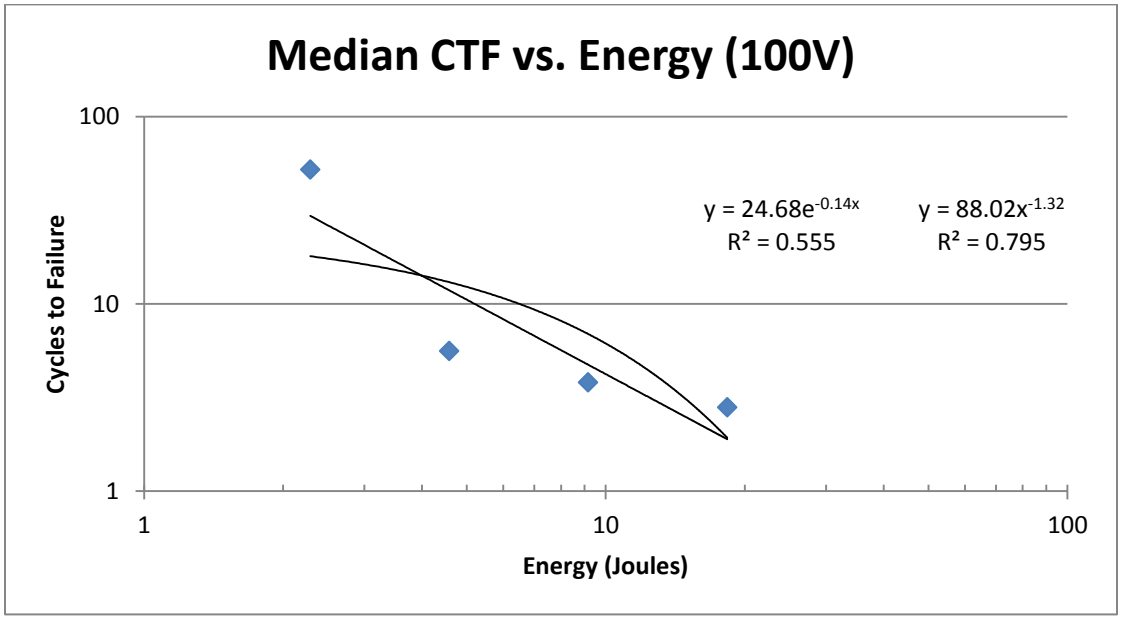

Figure 60: CTF vs. Energy for 100V, 0.11Ω, 1.7kW.

7.2.5 Constant Energy

Since many test points correspond to the same energy, it is important to look at the cycles to failure and its relationship to power while holding energy constant. The results of this can be seen below in Figure 61 and correspond to energies around 1.4J.

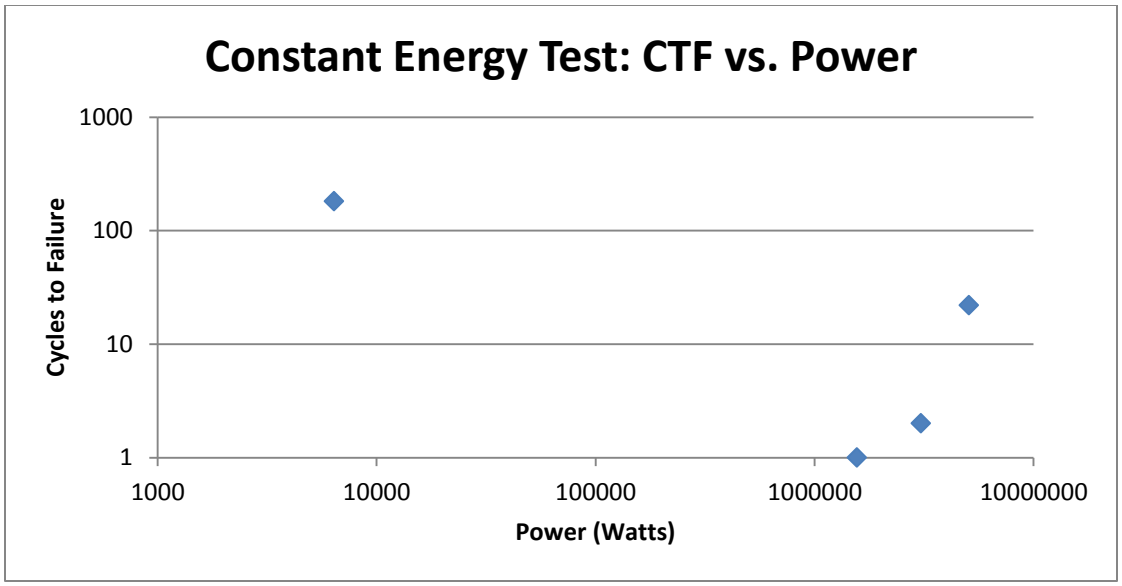

Figure 61: Constant energy CTF vs. Power.

What Figure 61 tells us is that from low power levels up to a certain point (1.5MW in this case) the cycles to failure will go down as energy is maintained and power is increased. Then the relays reach an optimal point where at power levels above it, the cycles to failure increase again because the power levels are so great the pulse durations shorten and are less likely to cause welding. In order to melt the silver at the contact surface, the arc must raise the material temperature above its melting temperature; however if the impulse is so great and short in duration, not all of the energy and heat may go to the relay surface and could be lost by sustaining the arc. While some surface material may melt, failure only occurs when the weld strength is greater than the spring force. This constant energy test tells us that the pulse duration, which is related to power when at a constant energy, plays a role in the cycles to failure and energy is not the only important variable. Since there is a large gap in the middle of this chart, more test points would be necessary to get a better representation of the CTF vs. Power relationship.

7.2.6 Power-Law Model Comparison

It has been observed that the slope of the power-law has a downward trend as the power level increases. A comparison of the slope can be seen below in Table 22 where the exponent increases from 1.32 at 1.7kW up to 2.05 at 5.0MW.

Table 22: Power-law slope vs. test voltage and power.

Voltage	Power	n
100V	1.7kW	1.32
250V	1.5MW	1.83
350V	2.5MW	1.63
450V	5.0MW	2.05

Physically this means that the sensitivity of CTF to energy goes up when the voltage and power goes up. N is a dimensionless parameter and is simply a power-law exponent, but the trend shows that at low power levels, a small difference in energy does not create as great a difference in probability of failure when compared to higher power levels. At the higher power levels, an equal increase in energy results in a much greater change in probability of failure. This is likely a result of the intensity of the stress increasing with respect to power and not just energy.

7.3 Conclusion

This constitutes only an initial investigation into the power and energy relationship to first cycle failure. It is obvious that total energy dissipated in the relay shows a strong relationship to cycles to failure where a higher capacitance results in longer pulse duration, more energy dissipated in the contacts, and a higher likelihood of single cycle weld failure. The one cycle failure region begins at a high energy level for low power just above the minimum power level necessary to cause significant erosion damage. The energy then trends down as power goes up until a minimum point is reached in which the pulse duration is so short that a longer pulse duration is required to fail the relay. This trend can be seen in Figure 56 where three regions are shown: 1) One Cycle Failure Region – The energy boundary between one cycle and multiple cycle failure where above this boundary one cycle failure will occur at this energy level and above; 2) 2-10 CTF Region – A region close to one cycle failure where the conditions are severely damaging and approach single cycle failure; and 3) >10 CTF Region where the lower the energy and pulse duration seen by the contacts, the more cycles the relay is likely to survive. What one can take away from this information is the farther (lower) in energy one gets from the single cycle failure interface, the more cycles a relay is likely to survive.

It is also shown that total energy is not the only important variable in terms of weld failure – varying the power influences the amount of energy and pulse duration necessary to achieve a single cycle failure. At 1.4J, the CTF trends down to single cycle failure at 250V / 1.5MW, after which the CTF trends up as power continues to rise. This is believed to be a result of reduced time constants (pulse duration) at higher power levels / lower capacitance values which lower the amount of silver that is effectively melted on

each make operation. Since weld strength is based on melted pool size among other variables, and the weld strength must be stronger than the restoring spring for weld failure to occur, it is shown that the CTF goes up at higher power levels above the minimum point at 250V / 1.5MW. The pulse duration at these power conditions and above are so short at the same energy that causes single cycle failure at 250V / 1.5MW that it is not sufficient to melt enough silver to cause welding on the first discharge.

Also shown was the increase in sensitivity to energy as the power increases. This shows that degradation is accelerated when both power and energy are increased and that there is an interaction between power and energy that can be correlated to an absolute stress level. As power increased, the slope of the power-law model increased as well indicating a small increase in energy at greater power levels will have a greater effect on contact life than at low power levels. More testing is necessary to get a deeper understanding of the influence of both power and energy on the stress level; however, it has been shown that considering energy as a stress at a constant power level follows a power-law failure model. Further study is needed to understand why the total energy necessary to cause one cycle failure goes down as power increases, reaches a minimum point, and then increases again at much higher power levels.

Chapter 8: Conclusions and Contributions

8.1 Conclusions

The research presented in this thesis allows conclusions to be drawn concerning the material and design characteristics and their effect on relay reliability, the manufacturer dependence on relay reliability and how it correlates to the material and design characteristics, and lastly the influence of both power and energy on relay switching life. In the first part of this research, material characteristics including contact material, oxide content, hardness, contact geometry, and electrical resistance were investigated. It was assumed that larger diameter relays and those with larger radii of curvature would result in less current density, less Joule heating, and a reduced likelihood of welding. The same can be said about relays with a lower electrical resistance. It was also believed that increasing the oxide percentage would increase the relay reliability by reducing the weld strength and decreasing the susceptibility of welding. Due to contact geometry and the lack of indium oxide, relay A was expected to perform poorly and relays B and C the best. The observed characteristics were then correlated to previous literature and checked by performing comparison testing on the three relay types.

The three relay types were then tested at varying power and energy using an automated test circuit. The results from this demonstrated that relays A and B perform poorly compared to C at low energy levels, and relays B and C perform better than A at high energy levels. Testing showed that relay cycles to failure correlate to capacitance (energy level). Larger numbers of cycles to failure result in a rougher contact surface profile and more material splash (arc erosion). This was experienced by relay C which significantly outlasted A and B at low energy conditions. Testing also demonstrated that contact

diameter is not as important to welding as contact interface area and radius of curvature, where contacts with less curvature (B and C) increase the interface area (a-spot) and decrease the current density improving the weld resistance. Relay A had the smallest contact area and a curved secondary contact while relays B and C had flat secondary contacts resulting in more contact area. Also shown was contacts with lower electrical resistance decrease Joule heating at the contact interface and improve weld resistance - relay A contacts are 34% more resistive than relays B and C. The most important parameters to relay reliability and the resistance to welding are the amount of total oxides and the concentration of indium oxide in the relay material. Higher concentrations of indium oxide appear to improve relay reliability where very low concentrations were found in relay A and much higher levels were present in relays B and C. The last finding from electrical testing and failure analysis was that contacts with higher hardness create a larger bounceback, and this long arc is less likely to cause a weld than a short arc. Relay A and B have softer contact hardness and higher spring hardness causing a short bounce whereas relay C has a harder contact hardness and soft spring hardness resulting in longer bounces. These parameters which are manufacturer specific were shown by electrical testing to influence the reliability of relays. Next, additional electrical testing was performed on relay A with varying power and energy to better understand the conditions which result in one cycle failure.

The final portion of the research showed the interaction of power on cycles to failure when energy is considered the stress in a power-law model. It was shown that the slope of the power-law model increases with increasing power meaning the sensitivity to energy goes up as power increases. This occurs because adding 2J of energy at 5MW is

much more damaging to the relay contacts than at lower power levels of 1.7kW. Also found was the one cycle to failure map for varying power levels. This map shows a region where single cycle failure is likely to occur and a safe operating region can be deduced from this map. Most interesting is the minimum point observed at the constant energy test where at first there is a decrease in energy required to initiate a first cycle failure as power increases followed by an increase in energy as the power becomes so great that the pulse duration becomes too short. This begins to give an insight into the power and energy dependence of welding, but shows that the interaction is a complex relationship which must be studied further to gain more understanding. Nonetheless, one can still take away from the experiment that pulse duration is an important parameter which affects the amount of silver melted on the contact surface and in turn plays a significant role in the melted pool size and weld strength. The information found in this research will better assist in future modeling of relay contacts in greatly varying load conditions where the underlying power and energy conditions can then be related back to current, voltage, and pulse duration.

8.2 Contributions

This work added many contributions to the high power relay reliability field. It:

- Developed a scheme for evaluating reliability of relays based on material and design parameters.
- Presented a safe operating area map based on power and energy to avoid one cycle weld failure.
- Introduced a relationship between electrical power and power-law exponent (stress/energy sensitivity to CTF) – also characterized as a power effect on CTF stress dependence.

8.3 Future Works

While this thesis presents many new ideas on the influence of power and energy on relay life, there are many more topics that need to be investigated. First, the contribution of each parameter to the overall susceptibility to weld must be determined. The influence of contact geometry must be decoupled from the influence of material composition. As such, the first future study of importance is an experiment that holds geometry constant and varies the material composition with respect to indium oxide content. This would give an empirical influence factor of the % content of indium oxide while keeping all other factors constant. Secondly, a full mathematical analysis of design factors required for first cycle welding must be conducted. This includes the latent heat, pulse duration, melted material mass, power, and temperature required on the contact surface to induce first cycle weld failure. Once the calculations have been deduced, an additional test that maintains contact material while varying contact geometry is required. This will verify

the calculations and quantify the contribution of geometry on the likelihood of welding. Lastly, a test setup that evaluates the surface profile evolution as a function of cycles would be extremely beneficial in determining metrics for degradation. This then makes it possible to further explain what parameters change over time that make a relay more likely to weld with an increase in cycles.

Appendix A: Automated Test Circuit Arduino C++ Code

```
int charge = 13;      // select the pin for the LED
int relay = 11;
int input = 8;
int Iteration = 0;
int Cycles = 0;
int i = 1;
int n = 0;
int chargetime = 7500; //Time required to charge capacitors
int dischargetime = 3000; //Time that test relay remains in contact
boolean fail = LOW;

void setup() {
  // declare charge and relay as an OUTPUT:
  pinMode(charge, OUTPUT);
  pinMode(relay, OUTPUT);
  pinMode(input, INPUT);
  Serial.begin(19200);
}

void loop() {

  delay(3000);

while (n <= 5000){

  fail = digitalRead(input);

while (fail == HIGH && n <=5000) {

  // turn the charging relay on
  digitalWrite(charge, HIGH);
  // stop the program for said milliseconds:
  delay(chargetime);
  // turn the charging circuit off:
  digitalWrite(charge, LOW);
  delay(300);
  // turn the relay off:
  digitalWrite(relay, HIGH);
  delay(dischargetime);
  // turn the relay off:
  digitalWrite(relay, LOW);

  n++;
  Iteration = n;
  Serial.print("Cycles = ");
```

```
  Serial.println(Iteration);
  delay(1000);
  fail = digitalRead(input);

  }

  if (fail == LOW)
  {
    Serial.print("Cycles to Failure = ");
    Serial.println(Iteration);
    i = 1;

    while (i <= 5){
      digitalWrite(relay, HIGH);
      delay(1000);
      digitalWrite(relay, LOW);
      delay(2000);
      fail = digitalRead(input);

      if (fail == HIGH) {
        Cycles = i;
        Serial.print("Coil Cycles = ");
        Serial.println(Cycles);
        i = 6;
      }

      if (i == 5) {
        Cycles = 5;
        Serial.print("Test Over Coil Cycles = ");
        Serial.println(Cycles);
        n=10000;
      }
      i++;
   }
  }

}
}
```

Appendix B: RC Circuit Theory

This section describes how the power and energy equations are derived for RC circuits. The equations are then used to determine power and energy levels based off of capacitance and voltage values.

$$P(t) = I(t)V(t) \tag{B.1}$$

$$I = C\frac{dV}{dt} \tag{B.2}$$

$$P(t) = CV\frac{dV}{dt} \tag{B.3}$$

$$W = \int_0^t P(t)dt \tag{B.4}$$

$$W = \int_0^t CV\frac{dV}{dt}dt \tag{B.5}$$

$$W = \int_0^{V(t)} CV\,dV \tag{B.6}$$

$$W = \frac{1}{2}CV^2 \tag{B.7}$$

$$p_{avg} = \frac{\Delta W}{\Delta t} = \frac{w(t)}{\tau} = \frac{\frac{1}{2}CV^2}{RC} = \frac{V^2}{2R} \tag{B.8}$$

The derivation of work is seen in equations B.4 through B.7 using the fundamental power equation (B.1) and the current equation for a capacitor (B.2). Equations B.1 and B.2 are combined to form the power equation for a RC circuit. The total energy stored in the relay is given by equation B.7; however, due to resistances resulting in a voltage dividing circuit, not all of the power and energy reaches the contact.

Appendix C: MATLAB Code for Contact Radius of Curvature Image Analysis

```
imshow(A) %A is the default name for an image uploaded of contact
            cross-section.
[x,y]=ginput;
hold on
plot(x,y)
mx = mean(x); my = mean(y)
X = x - mx; Y = y - my; % Get differences from means
dx2 = mean(X.^2); dy2 = mean(Y.^2); % Get variances
t = [X,Y]\(X.^2-dx2+Y.^2-dy2)/2; % Solve least mean squares problem
a0 = t(1); b0 = t(2); % t is the 2 x 1 solution array [a0;b0]
r = sqrt(dx2+dy2+a0^2+b0^2); % Calculate the radius
a = a0 + mx; b = b0 + my; % Locate the circle's center
curv = 1/r; % Get the curvature
[h,k]=ginput(2);
length=sqrt((h(1)-h(2))^2+(k(1)-k(2))^2);
length
scale=input('Length of Scale');
radius=r/length*scale %In millimeters

%plot results

start=a-r;
finish=a+r;
circlex=start:.5:finish;
circley=sqrt(r^2-(circlex-a).^2)+b;
hold on
plot(circlex,circley,'r')
circleyy=-sqrt(r^2-(circlex-a).^2)+b;
hold on
plot(circlex,circleyy,'r')
```

Appendix D: MATLAB Code for Contact Area Image Analysis

```
imshow(ContactArea)

[h,k]=ginput(2);
length=sqrt((h(1)-h(2))^2+(k(1)-k(2))^2);
length
```

```
scale=input('Length of Scale');

n=10;
for i=1:n
    [x,y]=ginput(2);
    hold on
    plot(x,y)
    r = (sqrt((x(1)-x(2))^2+(y(1)-y(2))^2))/2;
    a = x(1)+(x(2)-x(1))/2; b = y(1)+(y(2)-y(1))/2; % Locate the
circle's center
    start=a-r;
    finish=a+r;
    circlex=start:.25:finish;
    circley=sqrt(r^2-(circlex-a).^2)+b;
    hold on
    plot(circlex,circley,'r')
    circleyy=-sqrt(r^2-(circlex-a).^2)+b;
    hold on
    plot(circlex,circleyy,'r')
    eval(['radius' num2str(i) ' = r/length*scale']) %In millimeters
end
```

Appendix E: XRD Material Analysis Raw Data

Sample Name	Phase	Obs. Max	d (Obs. Max)	FWHM	Chord Mid.	I. Breadth	Gravity C.	d (Gravity C.)	Raw Area	Net Area
		2-Theta °	Angstrom	2-Theta °	2-Theta °	2-Theta °	2-Theta °	Angstrom	Cps x 2-Theta °	Cps x 2-Theta °
SAMPLE #1	SnO2	26.597	3.348670	0.22	26.59	0.304	26.579	3.3509	0.078	0.020
SAMPLE #2	SnO2	26.582	3.350510	0.21	26.59	0.246	26.585	3.3501	0.163	0.101
SAMPLE #3	SnO2	26.558	3.353480	0.23	26.56	0.273	26.568	3.3523	0.114	0.056
SAMPLE #4	SnO2	26.568	3.352260	0.22	26.57	0.263	26.575	3.3514	0.102	0.043
SAMPLE #5	SnO2	26.547	3.354840	0.27	26.56	0.320	26.557	3.3536	0.067	0.009
SAMPLE #6	SnO2	26.551	3.354400	0.24	26.56	0.281	26.550	3.3545	0.073	0.017
SAMPLE #1	Ag1	38.108	2.359520	0.32	38.11	0.406	38.094	2.3604	0.582	0.472
SAMPLE #2	Ag1	38.108	2.359500	0.30	38.11	0.382	38.105	2.3597	1.097	0.967
SAMPLE #3	Ag1	38.121	2.358700	0.29	38.13	0.364	38.119	2.3588	0.951	0.831
SAMPLE #4	Ag1	38.134	2.357930	0.30	38.14	0.379	38.134	2.3579	0.894	0.776
SAMPLE #5	Ag1	38.087	2.360730	0.32	38.09	0.412	38.067	2.3620	0.607	0.484
SAMPLE #6	Ag1	38.115	2.359100	0.36	38.12	0.468	38.109	2.3595	0.710	0.587
SAMPLE #1	Ag2	44.268	2.044420	0.42	44.26	0.533	44.244	2.0455	0.492	0.389
SAMPLE #2	Ag2	44.245	2.045420	0.40	44.24	0.514	44.228	2.0462	0.566	0.451
SAMPLE #3	Ag2	44.275	2.044100	0.36	44.28	0.472	44.278	2.0440	0.464	0.351
SAMPLE #4	Ag2	44.286	2.043600	0.38	44.29	0.511	44.285	2.0437	0.452	0.342
SAMPLE #5	Ag2	44.242	2.045560	0.38	44.24	0.480	44.217	2.0466	0.882	0.755
SAMPLE #6	Ag2	44.226	2.046260	0.42	44.22	0.558	44.210	2.0469	0.581	0.458
SAMPLE #1	CdO2	28.981	3.078430	0.20	28.97	0.266	28.982	3.0783	0.041	0.004
SAMPLE #2	CdO2	29.029	3.073450	0.21	29.03	0.248	29.030	3.0733	0.053	0.015
SAMPLE #3										
SAMPLE #4										
SAMPLE #5										
SAMPLE #6										
SAMPLE #1										
SAMPLE #2	In2O3	30.569	2.921990	0.23	30.57	0.219	30.645	2.9149	0.074	0.006
SAMPLE #3	In2O3	30.694	2.910360	0.40	30.70	0.417	30.730	2.9071	0.093	0.024
SAMPLE #4	In2O3	30.718	2.908200	0.39	30.73	0.427	30.736	2.9066	0.090	0.025
SAMPLE #5	In2O3	30.449	2.933260	0.45	30.47	0.520	30.474	2.9309	0.104	0.030
SAMPLE #6	In2O3	30.500	2.928470	0.58	30.56	0.641	30.558	2.9230	0.094	0.026

Appendix F: One Cycle Weld Interface Test Results

Table 23: 100V 1.7kW Test Results.

Capacitance	11000	22000	44000	88000
Energy	2.29	4.58	9.17	18.33
Sample 1	73	16	6	3
Sample 2	91	4	3	5
Sample 3	3	1	6	2
Sample 4	19	2	2	3
Sample 5	74	5	2	1
Average	52	5.6	3.8	2.8
Median	73	4	3	3
STDEV	38.52	6.02	2.05	1.48

Table 24: 350V 3.0MW Test Results.

Capacitance	5	30	45	50
Energy	0.15	0.92	1.38	1.53
Sample 1	958	3	1	1
Sample 2	61	5	4	24
Sample 3	33	55	2	1
Sample 4	52	7	3	4
Sample 5	2710	23	2	1
Average	762.8	18.6	2.4	6.2
Median	61	7	2	1
STDEV	1157.59	21.84	1.14	10.03

Table 25: 450V 5.0 MW Test Results.

Capacitance	5	30	45	60
Energy	0.25	1.52	2.28	3.04
Sample 1	842	19	11	21
Sample 2	1007	42	1	8
Sample 3	2088	22	4	6
Sample 4	1231	3	8	22
Sample 5	810	53	12	8
Average	1195.6	27.8	7.2	13
Median	1007	22	8	8
STDEV	526.05	19.77	4.66	7.81

References

[1] Chi Leung; Streicher, E.; Fitzgerald, D.; Cook, J.; , "High Current Erosion of Ag/SnO2 Contacts and Evaluation of Indium Effects in Oxide Properties," *Electrical contacts - 2006, proceedings of the fifty-second ieee holm conference on* , vol., no., pp.143-150, 25-27 Sept. 2006.

[2] ASTM Standard B781, 1993 (2012), "Standard Guide for Silver-Cadmium Oxide Contact Material," ASTM International, West Conshohocken, PA, 2012, DOI: 10.1520/B0781-93AR12, www.astm.org.

[3] "Types of Relays," http://www.ia.omron.com/data_pdf/guide/36/generalrelay_tg_e_3_1_3-4%28classifications%29.pdf, pp. 1.

[4] Storr, W., "Electronic Tutorial about Electrical Relays," pp.5, 2012.

[5] Gurevich, V., "Electrical Relays: Principles and Applications," London - New York: CRC Press, 2005.

[6] National Instruments, "How to Choose the Right Relay," www.ni.com/white-paper/2774/en, pp.2, 2 April 2012.

[7] Kian, S., "Identify Terminal Pins of A Relay Without Reference to Datasheet," Cytron Technologies, http://tutorial.cytron.com.my/2012/08/01/identify-terminal-pins-of-a-relay-without-reference-to-datasheet-2/, 1 Aug. 2012.

[8] TE Connectivity (formerly Tyco Electronics), "Contact Systems," http://relays.te.com/schrack/pdf/C0_v4bg_4.pdf pp. 41.

[9] Panasonic, "Relay Technical Information," http://www.panasonic-electric-works.com/peweu/en/downloads/ds_x61_en_relay_technical_information.pdf, pp. 12, Aug. 2012.

[10] A. R. Neuhaus, W. F. Rieder, M. Hammerschmidt, "Influence of Electrical and Mechanical Parameters on Contact Welding in Low Power Switches," IEEE Transactions on Components and Packaging Technologies, Vol. 27, No. 1, March 2004.

[11] M. Sampson, "Tin (and Other Metal) Whisker Induced Failures," NASA, http://nepp.nasa.gov/whisker/failures/index.htm, 3 Aug. 2009.

[12] C. Stevens , "Relay Failures Induced by the Growth of Tin Whiskers. A Case Study," The Foxboro Company, 1999. http://nepp.nasa.gov/whisker/reference/tech_papers/stevens2001-relay-failures-induced-by-tin-whiskers.pdf.

[13] Swingler J., and Sumption A.: "Arc Erosion of $AgSnO_2$ Electrical Contacts at Different Stages of a Break Operation", *Rare Metals*, 2010, 29, pp. 248-254.

[14] Teste P., Andlauer R., Leblanc T.: "General properties of high current switching under 36 V DC for Ag and AgSnO2 contacts", *IET Science, Measurement & Technology*, 2010, 4, pp. 156-168.

[15] Picker Components, "Contact Arc Phenomenon." www.pickercomponents.com/pdf/application note/Contact_ARC_Phenomenon.pdf.

[16] Clare, "Advantages of Solid-State Relays over Electro-Mechanical Relays." Specification: AN-145-R01.1, http://www.clare.com/home/pdfs.nsf/www/an-145.pdf/$file/an-145.pdf, pp.6, 17 May 2007.

[17] Jemaa, N.B.; Nedelec, L.; Benhenda, S.; Neveu, J.; , "Anodic and cathodic erosion of Ag, Ag alloys and Ag-MeO contact materials in energy range below 10 joules,".

Proceedings of the Forty-Second IEEE Holm Conference on Electrical Contacts, 1996. Joint with the 18th International Conference on Electrical Contacts, vol., no., pp.70-74, 16-20 Sept. 1996.

[18] J.W. McBride, S.M.A. Sharkh, "The Effect of Contact Opening Velocity and the Moment of Contact Opening on the AC Erosion of Ag/CdO Contact," *IEEE Transactions on Components, Packaging,* and Manufacturing Technology, Part A, vol. 17, No. 1, pp. 2-7, March 1994.

[19] Tong Weiming, Liang Huimin, Wang Yuhong, and Liu Maokai, "Effect of Contact Breakaway Muzzle Velocity on Contact Breakaway in Direct Circuit," *Journal of Harbin Institute of Technology. Harbin,* vol. 33, No. 3, pp.414-418, June 2001.

[20] N.B. Jemma, "Break arc duration and contact erosion in automotive application," *IEEE Trans. On C.P.M.T.,* Part A, vol. 19, No. 1, pp. 82-86, March 1996.

[21] Swingler, J.; McBride, J.W.; , "The erosion and arc characteristics of Ag/CdO and Ag/SnO_2 contact materials under DC break conditions," *Components, Packaging, and Manufacturing Technology, Part A, IEEE Transactions on* , vol.19, no.3, pp.404-415, Sep 1996.

[22] Utsumi T., "Theoretical and Experimental Investigations of the Dynamic Molten Bridge," *IEEE Trans. Parts Mater. Packag.*, 1969, PMP-5 (1): 62.

[23] Chen Z.K., "Material Transfer and Contact Resistance Deterioration in Light Duty Electrical Contacts," [Dissertation], Keio University, 1995.

[24] Nakagawa, Y.; Yoshioka, Y.; , "Theoretical Calculation of the Process of Contact Arc Erosion Using a One-Dimensional Contact Model," *Components, Hybrids, and Manufacturing Technology, IEEE Transactions on* , vol.1, no.1, pp. 99- 102, Mar 1978.

[25] Swingler, J.; McBride, J.W., "Modeling of energy transport in arcing electrical contacts to determine mass loss," *Components, Packaging, and Manufacturing Technology, Part A, IEEE Transactions on* , vol.21, no.1, pp.54-60, Mar 1998.

[26] Pons, F.; Cherkaoui, M., "An Electrical Arc Erosion Model Valid for High Current: Vaporization and Splash Erosion," *Electrical Contacts, 2008. Proceedings of the 54th IEEE Holm Conference on* , vol., no., pp.9-14, 27-29 Oct. 2008.

[27] Llang Huimin; Ma Guangcheng; Cai Ling; Xie Yong; Xie Guoqiang; , "Research on the relationship between contact breakaway initial velocity and arc duration [relays]," *Electrical Contacts, 2003. Proceedings of the Forty-Ninth IEEE Holm Conference on* , vol., no., pp. 204- 210, 8-10 Sept. 2003.

[28] G. Witter and Z.K. Chen, "Dynamic Welding Resistance of Silver and Silver Metal Oxides," *19th ICEC*, Nuremberg, Germany, pp. 355-359, 1998.

[29] Z.K. Chen and G. Witter, "Dynamic Welding of Silver Contacts Under Different Mechanical Bounce Conditions," in *Proc. 45th IEEE Holm Conf. Elect. Contacts,* Chicago, IL, pp. 1-8, 1999.

[30] Witter, G.; Chen, Z.; , "A comparison of silver tin indium oxide contact materials using a new model switch that simulates operation of an automotive relay," *Electrical Contacts, 2004. Proceedings of the 50th IEEE Holm Conference on Electrical Contacts and the 22nd International Conference on Electrical Contacts* , vol., no., pp. 382- 387, 20-23 Sept. 2004.

[31] Zhao L., Zhang H., and Hasegawa M.: "Random Occurrence of Contact Welding in Electrical Endurance Tests," *IEICE TRANS. ELECTRON*, Vol. E94-C, No. 9, 2011.

[32] Holm, Ragnar, and Else Holm. *Electric Contacts: Theory and Application*. Berlin: Springer-Verlag, 1967.
[33] Hertz, H.H., *Hertz's Miscellaneous Papers,* MacMillian, London, Chaps. 5-6, 1896.
[34] Johnson, K. L. *Contact Mechanics*. Cambridge [Cambridgeshire]: Cambridge University Press, 1985.
[35] Leung, C., and Lee, A., "Electric Contact Materials and Their Erosion in Automotive DC Relays," *Proc. 37th IEEE Holm Conf. on Elec. Contacts*, Chicago, pp. 114-121, 1991.
[36] Directive 2002/95/EC on the restriction of the use of certain hazardous substances in electrical and electronic equipment. Official Journal of the European Union. Jan 2003.
[37] Nilsson, O.; Hauner, F.; Jeannot, D.; , "Replacement of AgCdO by $AgSnO_2$ in DC contactors," *Electrical Contacts, 2004. Proceedings of the 50th IEEE Holm Conference on Electrical Contacts and the 22nd International Conference on Electrical Contacts* , vol., no., pp. 70- 74, 20-23 Sept. 2004.
[38] F. Hauner, D. Jeannot, and K. McNeilly, "Advanced AgSnO2 Contact Materials with High Total Oxide Content", Proc. 21st ICEC, September 9-12, Zürich 2002, pp. 452-456.
[39] Y. Shen, W. Cote & L. Gould, "A Historic Review of Ag-MeO Materials" 32nd Holm Conference, 1986, p71-76.
[40] K. Herz & E. Sauter, "Erosion, Welding and Contact Resistance Characteristics of Several Powder Metallurgical Silver Contact Materials," 3OthHolm 1984, p215-231.
[41] Rong Mingzhe & Wang Qiping, "Effects of Additives on the AgSnO2 contacts erosion behavior," 3 thHolm 1993, p33-36.
[42] Chen, Z.K.; Witter, G.J.; , "A Study of Dynamic Welding of Electrical Contacts with Emphasis on the Effects of Oxide Content for Silver Tin Indium Oxide Contacts," *Electrical Contacts (HOLM), 2010 Proceedings of the 56th IEEE Holm Conference on* , vol., no., pp.1-6, 4-7 Oct. 2010.
[43] Mutzel, Timo; Niederreuther, Ralf; , "Advanced silver-tin oxide contact materials for relay application," *Electrical Contacts (ICEC 2012), 26th International Conference on* , vol., no., pp.194-199, 14-17 May 2012.
[44] Rieder, W.F.; Strof, T.W.; , "Relay life tests with contact resistance measurement after each operation," *Components, Hybrids, and Manufacturing Technology, IEEE Transactions on* , vol.14, no.1, pp.109-112, Mar 1991.
[45] Rieder, W.F.; Strof, T.W.; , "Reliability of commercial relays during life tests at low electrical contact load," *Components, Hybrids, and Manufacturing Technology, IEEE Transactions on* , vol.15, no.2, pp.166-171, Apr 1992.
[46] S. Allen & E. Streicher, "The Effect of Microstructure on the Electrical Performance of Ag-WC-C Contact Materials", 44th IEEE Holm Conference, Arlington, VA, October 1998, p276-285.
[47] McPherson, J. W. *Reliability Physics and Engineering*. New York: Springer, 2010.
[48] ASTM Standard B844, 1998 (2010), "Standard Guide for Silver-Tin Oxide Contact Material," ASTM International, West Conshohocken, PA, 2012, DOI: 10.1520/B0844-98R10, www.astm.org.